

365067

PB247932


PHILCO-FORD TMLV TR-0037A

RA-OR&D-75-21A

PB

CONCEPTUAL DESIGN AND ANALYSIS OF
THE TRACKED MAGNETICALLY LEVITATED VEHICLE
TECHNOLOGY PROGRAM (TMLV) - REPULSION SCHEME
VOLUME II - APPENDICES A - F



February 1975

FINAL REPORT
DOT-FR-40024 (Task I)

Document is available to the public through the
National Technical Information Service,
Springfield, Virginia 22151

Prepared for:

Department of Transportation



Federal Railroad Administration
Office of Research, Development and Demonstrations
Washington, D.C. 20590

REPRODUCED BY: **NTIS**
U.S. Department of Commerce
National Technical Information Service
Springfield, Virginia 22161

NOTICES

The United States Government does not endorse products or manufacturers. Trade or manufacturers' names appear herein solely because they are considered essential to the object of this report.

This document is disseminated under the sponsorship of the Department of Transportation in the interest of information exchange. The United States Government assumes no liability for its contents or use thereof.

1. Report No. FRA-OR&D-75-21A	2. Government Accession No.	3. Recipient's Catalog No. PB247932	
4. Title and Subtitle Conceptual Design and Analysis of the Tracked Magnetically Levitated Vehicle Technology Program (TMLV) - Repulsion Scheme; Volume II - Appendices A - F		5. Report Date February 1975	6. Performing Organization Code
7. Author(s)	8. Performing Organization Report No. Philco-Ford Report TMLV-37A		
9. Performing Organization Name and Address Ford Motor Co. Scientific Research Staff P.O. Box 2053, Dearborn, Michigan 48121 and Aeronutronic Div.; Philco-Ford Corp. Ford Road, Newport Beach, Ca 92663		10. Work Unit No. (TRAIS)	11. Contract or Grant No. DOT-FR-40024
12. Sponsoring Agency Name and Address U.S. Department of Transportation Federal Railroad Administration 400 7th Street, S.W., Room 5416A Washington, D.C. 20590		13. Type of Report and Period Covered Final Report for Period of June 1974 to January 1975	
15. Supplementary Notes		14. Sponsoring Agency Code	
<p>16. Abstract</p> <p>This report summarizes the studies of a program to establish the technology of magnetic suspension for ultimate use in a passenger-carrying high-speed ground transportation (HSGT) system - at speeds on the order of 134 m/s (300 mph). Magnetic Levitation (MAGLEV) is one of the advanced vehicle suspension concepts considered as alternatives to conventional transportation modes in the short-haul regime. These advanced systems have the potential of alleviating the heavy traffic congestion prediction for the highly populated regions of the U.S. in the 1985-1995 period. The national energy shortage has intensified the search for more energy-efficient and cost-effective transportation modes.</p> <p>This volume presents some details of the mathematical analysis associated with the MAGLEV vehicle dynamics and control (i.e., ride quality) in Appendices A through D; the noise or acoustic characteristics associated with the baseline Hamilton Standard Q-fan air propulsion system (Appendix E); and the Raytheon final report for the linear synchronous motor (LSM) studies (Appendix F).</p> <p style="text-align: right;">PRICES SUBJECT TO CHANGE</p>			
17. Key Words High Speed Ground Transportation, Magnetic Levitation, Vehicle Dynamics, Ride Quality, High Speed Vehicle Design, Superconducting Magnets, Guideway and Systems Analysis		18. Distribution Statement Document is available to the public through the National Technical Information Service, Springfield, Virginia 22151	
19. Security Classif. (of this report) Unclassified	20. Security Classif. (of this page) Unclassified	21. No. of Pages 	22. Price 

PREFACE

The study documented in this second volume of the MAGLEV Final Report was conducted by Ford Motor Co. under contract to the U.S. Department of Transportation (DOT), Federal Railroad Administration, Office of Research, Development and Demonstrations. The DOT Program Manager was Dr. John T. Harding. Additional support was provided by Mr. Arnold Gross of DOT and Dr. Roger Katz of MITRE Corp.

Overall program management and levitation magnet design were the responsibility of the Ford Scientific Research Staff. Vehicle and guideway conceptual designs and overall systems analysis were the responsibility of the Aeronutronic Division of Philco-Ford Corp. Dr. John R. Reitz of the Ford Motor Company was the Program Manager.

This volume contains Appendices A through F of the report "Conceptual Design and Analysis of the Tracked Magnetically Levitated Vehicle Technology Program (TMLV) - Repulsion Scheme", DOT Report No. FRA-ORD&D-75-21, February 1975. The three volumes of this report document the work done to define a conceptual Revenue MAGLEV; a potential system for High Speed Ground Transportation (HSGT) applicable to the heavily-traveled Northeast and California corridors for the 1985-1995 time frame.

The work described in this volume was under the overall direction of Mr. Robert L. Pons, the Deputy Program Manager for Systems at Philco-Ford. Dr. D. A. Rodriguez was in charge of the vehicle dynamics and control work reported in Appendices A through D. Mr. T. B. Clark of Philco-Ford was in

charge of the Hamilton Standard work (Appendix E); and the Raytheon work (Appendix F), along with Dr. Rodriguez.

The individual authors of the Appendices were:

- Appendices A, C, and D Dr. C. C. Wan, Philco-Ford
- Appendix B Dr. C. C. Wan and
Mr. L. C. Sutherland,
Philco-Ford
- Appendix E Mr. B. S. Gatzert, Hamilton
Standard Div. of United
Aircraft Corp.
- Appendix F Dr. C. H. Tang and
Mr. W. J. Harrold, Raytheon
Co., Equipment Division

The editors of this volume were Mr. T. B. Clark and Dr. D. A. Rodriguez.

TABLE OF CONTENTS

APPENDIX .	PAGE
A	MAGNETIC FORCE MODELING A-1
A.1	Description of the Algorithm A-2
A.2	Definition of Forces and Moments on a Rectangular Coil Moving in an L-Shaped Guideway A-4
A.3	Force and Moment Coefficients for a Typical MAGLEV Vehicle Levitation Coil A-6
B	MATHEMATICAL REPRESENTATION OF VEHICLE CHARACTERISTICS B-1
B.1	Vehicle Coordinate System B-1
B.2	Local Coordinate System for Levitation Coils B-3
B.3	Equations of Motion B-5
B.4	Incorporation of Control Function B-9
B.5	One and Two Degree-of-Freedom Dynamic Models B-10
C	STABILITY ANALYSIS AND GAIN SELECTION C-1
C.1	Delineation of Control Parameters C-1
C.2	Formulation of the Characteristic Equation C-2
C.3	Expansion of the Characteristic Determinant C-5
C.4	Gain Selection C-7
C.5	Results for Heave/Pitch Mode Without Signal Filtering C-7
D	FREQUENCY RESPONSE SOLUTION TECHNIQUES D-1
D.1	Frequency Response Calculations D-1
D.2	Decomposition of Guideway Irregularities D-1
D.3	Unit Solution D-2
D.4	Control Current Commands and Power Requirement D-4
D.5	Generation of Response and Ride Quality Data D-4

TABLE OF CONTENTS (Continued)

APPENDIX		PAGE
E	Q-FAN PROPULSION SYSTEM ACOUSTIC CHARACTERIZATION	E-1
	E.1 Fan Source Noise	E-1
	E.2 Engine Source Noise	E-3
	E.3 Fan Noise Suppression	E-3
	E.4 Engine Noise Suppression	E-5
	E.5 Summary	E-5
F	FINAL REPORT FOR LINEAR SYNCHRONOUS MOTOR STUDIES	F-1
	1. Introduction	F-5
	2. Summary of Results	F-9
	3. TMLV Requirements	F-11
	4. LSM System Considerations	F-13
	5. Design Analysis	F-17
	6. Hybrid LSM Design	F-49
	7. On Detailed LSM Design Problems	F-58
	8. Conclusions and Recommendations	F-62

APPENDIX A

MAGNETIC FORCE MODELING

By C. C. Wan

Mathematical techniques employed for calculating the forces and moments on a current-carrying coil moving over a non-magnetic conducting medium are described in this appendix. Forces and moments calculated by the method described herein are presented in terms of deviations from a nominal configuration for use in linear analyses of stability and ride quality. Calculated results for off-nominal conditions are also presented graphically for use in nonlinear studies.

Forces and moments acting on a coil moving at a fixed distance above a non-magnetic conducting medium are generated by the interaction between current in the coil and an eddy current field created in the medium during the passage of the coil. Exact solutions for a coil moving at a constant speed over a thin conducting sheet and for a coil moving at a constant speed over a thick slab have been given, respectively, by Reitz (Reference A-1) and by Reitz and Davis (Reference A-2). Experimental results confirming these theoretical calculations have been presented by Borcherts and Davis (Reference A-3). These experimental results also provided verification of simplified formulations for predicting forces to account for edge effects and corner effects. In particular, it was noted that the drag force component for more complex conducting surface geometry, such as an L-shaped corner, can be adequately correlated with the sum of force components normal to the two conducting surfaces in the same manner as in the case of an infinite conducting plane.

Thus, it has become possible to formulate an algorithm for predicting forces and moment on a moving coil which obviates the need for detailed analyses of time history of field variations. Forces and moments predicted on this basis are adequate for studies of the motion of a vehicle using

magnetic coils for levitation. However, they will not, in general, be suitable for design analyses of propulsion devices such as SLIM and LSM.

Detailed comments on the computational algorithm and its application to L-shaped guideway elements are presented in the following paragraphs.* Specific results are presented for the baseline MAGLEV coil and guideway configuration. Preliminary values were used for such parameters as the longitudinal distance between coils, the position of the vehicle center of gravity, and the vehicle weight. These parameters were subsequently modified for the baseline conceptual vehicle, however, the values chosen adequately demonstrate the force modeling technique.

A.1 DESCRIPTION OF THE ALGORITHM

The procedure for determining forces and moment on a single rectangular coil moving at a constant speed at a fixed distance with respect to a thin, non-magnetic conducting guideway element consists of the following steps:

- (a) Determine the mutual inductance between the coil and its image with respect to the surface of the conducting guideway element. All three images must be taken into consideration when the cross section of the conducting guideway element has the shape of a rectangular corner. When the cross section of the conducting guideway element is a part of a circle, an inversion transformation may be used to accomplish this step.
- (b) Forces and moments acting on a coil moving at infinite speed are given exactly by appropriate spatial derivatives of the mutual inductance, M , as formulated under (a) above, multiplied by the product of current intensity, I_1 , in the coil and eddy current intensity, I_2 , in the image coils; i.e.,

$$F_n = I_1 I_2 \quad f_n = -I_1 I_2 \left(\frac{\partial M}{\partial n} \right) \quad (n: \text{normal vector})$$

$$M_\phi = I_1 I_2 \quad m = -I_1 I_2 \left(\frac{\partial M}{\partial \phi} \right) \quad (\phi: \text{direction of axis of rotation})$$

*Forces and moments for a rectangular coil over a circular guideway are presented in Philco-Ford Technical Report TMLV-022, August 1974.

where f_n and m may be interpreted as coefficients related only to geometrical parameters, independent of the current in the coil.

- (c) Evaluate the effects of finite speed on force characteristics for a coil of identical geometrical configuration at the same normal separation between the plane of the coil and an infinite conducting sheet of the same thickness and material as the actual guideway element, using the method described in Reference A-1. Results of this calculation provide variations in both lift and drag force components as a function of forward speed. The lift force coefficient, $f_{L\infty}$, calculated by the method of Reference A-1 is identical to that calculated for the coil using the derivative formulation described under (b).

- (d) At a particular forward speed, two dimensionless ratios are formed:

$$f_L/f_{L\infty} \quad \text{and} \quad f_L/f_D$$

It is assumed that these two ratios will also apply to guideway element configurations which are different from an infinite plane. This assumption is the only one introduced in this algorithm to facilitate force modeling for levitation coils.

- (e) Forces and moments acting on an actual coil at finite speeds over an actual guideway element are products of their values evaluated at infinite speed according to (b), and the $f_L/f_{L\infty}$ ratio for that speed. The magnetically-induced drag force component is given by dividing the sum of all normal force components relative to the actual guideway surfaces, corrected for finite speed, by the f_L/f_D ratio evaluated at that speed.

A.2 DEFINITION OF FORCES AND MOMENTS ON A RECTANGULAR COIL MOVING IN AN L-SHAPED GUIDEWAY

The baseline guideway configuration selected for the program consists of two L-shaped corners with the vertical elements located between the horizontal elements. The baseline vehicle has four identical levitation coils and four identical control coils. Since it is appropriate to neglect the coupling effects of individual coil sets on each other, it is sufficient for analytical purposes to define only one set of force and moment coefficients. The geometry of the coil and guideway configuration is shown in Figure A-1. The coil dimensions correspond to the centerline geometry of the winding, and a local coordinate system is employed. Forces and displacements in a direction away from the conducting surfaces are taken to be positive; with the local Y-direction normal to the vertical leg of the L and the local Z-direction normal to the horizontal leg of the L. The local X-axis forms a right-handed set with the Y- and the Z-axes. The following quantities are basic to the force model used for the present study:

- F_L, f_L Lift force* acting at the center of the main coil, always normal to the horizontal guideway surface
- F_G, f_G Lateral force* acting at the center of the main coil, always normal to the vertical guideway surface
- L Rolling moment about the longitudinal axis of the main coil
- A Width of the main coil, based on centerline dimensions of the winding
- B Length of the main coil, based on centerline dimensions of the winding
- h Nominal coil elevation above the horizontal guideway surface when the plane of the coil is parallel to the horizontal guideway surface ($\phi = 0$)
- h' Nominal coil separation from the vertical guideway surface to the centerline of the near-side winding when the plane of the coil is parallel to the horizontal guideway surface ($\phi = 0$)

*Upper and lower case "F" is used interchangeably for these forces.

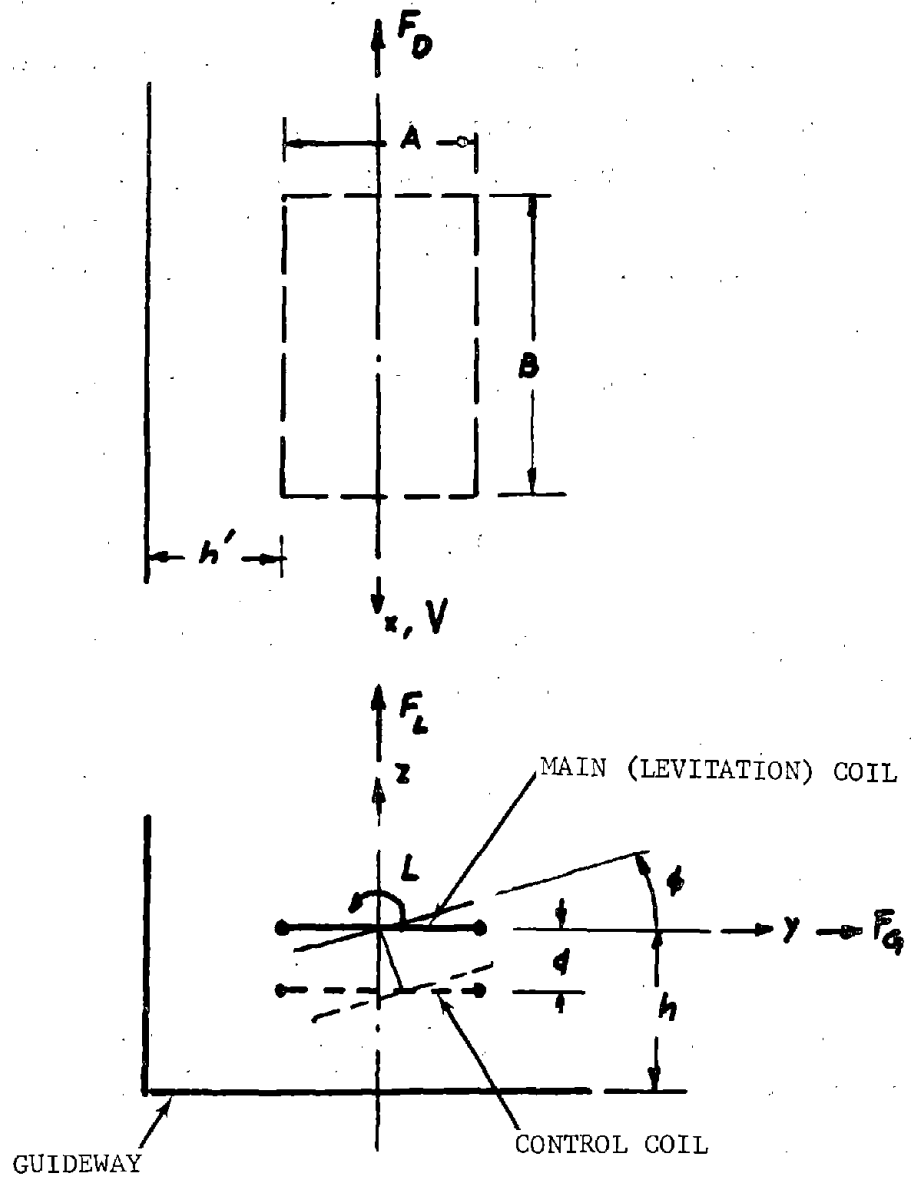


FIGURE A-1. GEOMETRY OF A RECTANGULAR COIL OVER AN L-SHAPED TRACK

- φ Roll angle of the coil, or angle of inclination of the plane of the coil relative to the horizontal guideway surface
- d Separation between the main coil and the control coil

The centerline dimensions of the control coil are taken to be identical to those of the main coil for the present study, although this is not mandatory. The control coil, however, is rigidly connected to the dewar of the main coil, and these two coils move as an integral part of the vehicle for studies of vehicle dynamics.

A.3 FORCE AND MOMENT COEFFICIENTS FOR A TYPICAL MAGLEV VEHICLE LEVITATION COIL

Both the main coil and the control coil for the MAGLEV vehicle have a width of 0.5 m and an overall length of 3.0 m. The main coil is located at a nominal elevation (h) of 0.3 m and a nominal lateral separation (h') of 0.3 m. The control coil is located 0.1 m below the main coil. The four identical coil sets are located near each corner of the vehicle, and are symmetrically placed about the longitudinal centerline of the vehicle. The centerline to centerline distance between the left side and the right side coils is 1.93 m. The centers of the front coils are 9.00 m* forward of the nominal vehicle center of gravity, and the centers of the rear coils are 7.65 m* aft of the nominal vehicle center of gravity (the magnet "wheel" base = 16.65 m*). All main coils are located 1.21 m* below the nominal vehicle center of gravity.

The L-shaped guideway elements are made of 1100-H14 aluminum alloy sheet of 2.54 cm thickness. The nominal design cruise speed is 134 m/s (300 mph), and a preliminary gross weight of the vehicle of 444.8 kN (100,000 lb) has been used.

The effect of vehicle speed on lift and drag coefficients is shown in Figure A-2 for an infinite conducting sheet of 2.54 cm thickness. The two dimensionless ratios at a speed of 134 m/s and h = 0.3 m are:

$$\left(\frac{f_L}{f_D}\right)_{134} = 61.505$$

*These values are based on the preliminary vehicle design, and have subsequently been modified for the baseline configuration.

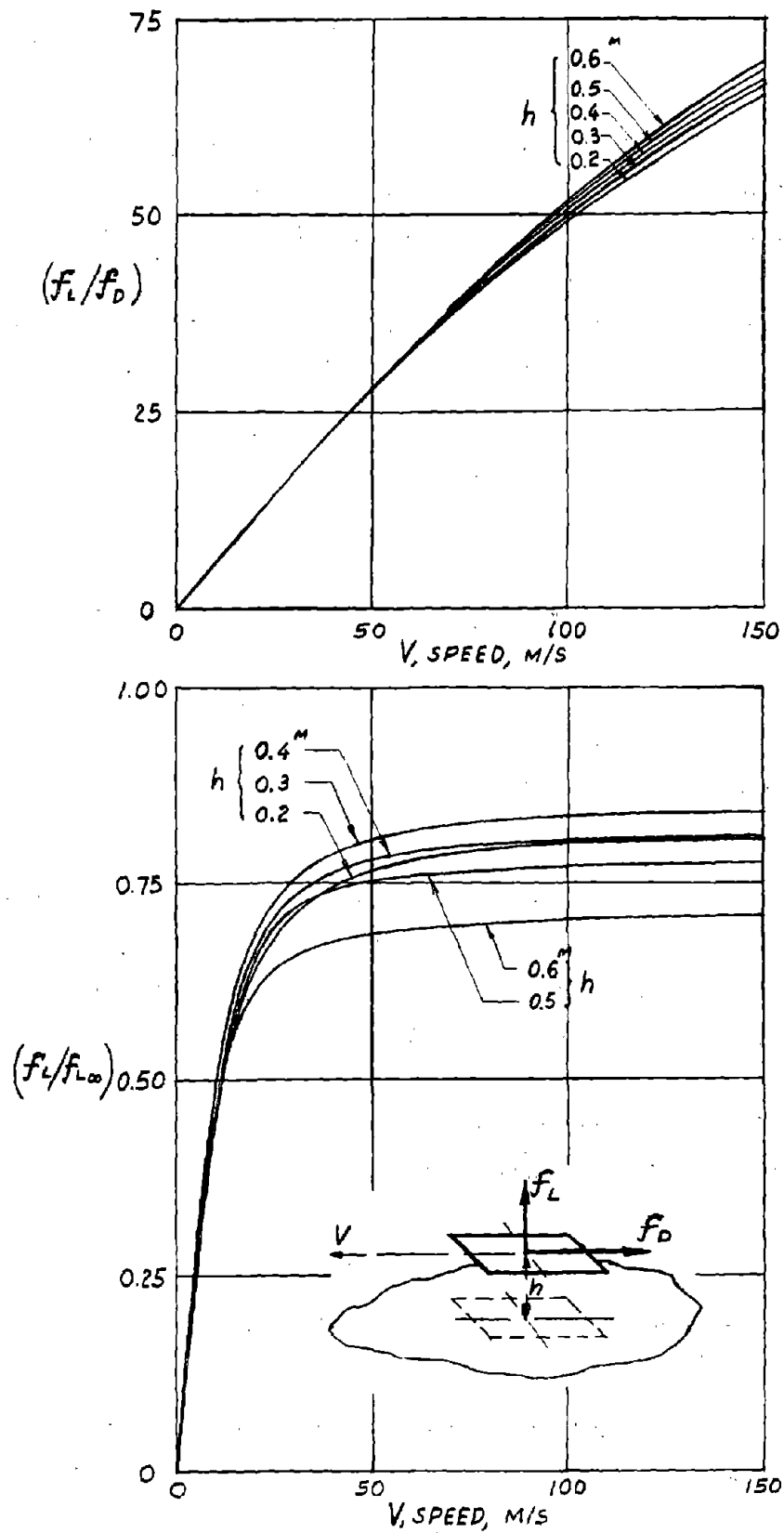


FIGURE A-2. EFFECT OF SPEED ON LIFT AND LIFT-DRAG RATIO FOR A 0.5M BY 3.0M COIL OVER AN INFINITE 2.54CM 1100-H14 SHEET

$$f_{L,134}/f_{L\infty} = 0.8380$$

Force and moment coefficients for a 0.5 by 3.0 m rectangular coil at various positions relative to an L-shaped rectangular corner are presented in Figures A-3 through A-5, in terms of a coil with 1000 ampere turns. Thus, from Figure A-3, it follows that the lift coefficient for a single coil is $0.7187 \text{ N}/(\text{KNI})^2$ at the nominal coil position ($h = h' = 0.3 \text{ m}$). The total lift force at 134 m/s for the case of nominal coil positions and zero control current in the control coils is:

$$f_{L,134} = 4(0.8380)(0.7187)(\text{KNI})^2 = 2.4091 (\text{KNI})^2 = 444800 \text{ N}$$

hence

$$\text{KNI} = (444800/2.4091)^{1/2} = (184635)^{1/2} = 429.69$$

or each main coil is to have 4.3×10^5 ampere turns for this condition.

With the vehicle in its nominal position, lateral forces and rolling moments acting on individual coils balance each other due to symmetrical placement of coils about the longitudinal centerline of the vehicle.

Force and moment coefficients for interaction between a main coil and a control coil of identical centerline dimensions are shown in Figures A-6 through A-8, for a separation of 0.1 m between coil planes. Note that in Figures A-6, A-7, and A-8 a second coil is shown at two positions; $d = 0.1 \text{ m}$ and $d = -0.1$. These results are generalized in nature so that the net forces between two coils can be decomposed as described below. Physically, the $d = -0.1$ results for MAGLEV means the main coil is at a height of $h + 0.1$, and the control coil at a height of h .

When there is a current in the control coil, the net forces and moment on the coil set as seen by the vehicle may be decomposed into four parts as follows:

- (a) Effects of the images of the main coil on the main coil, expressed as force components and a moment referred to the longitudinal center line of the main coil.

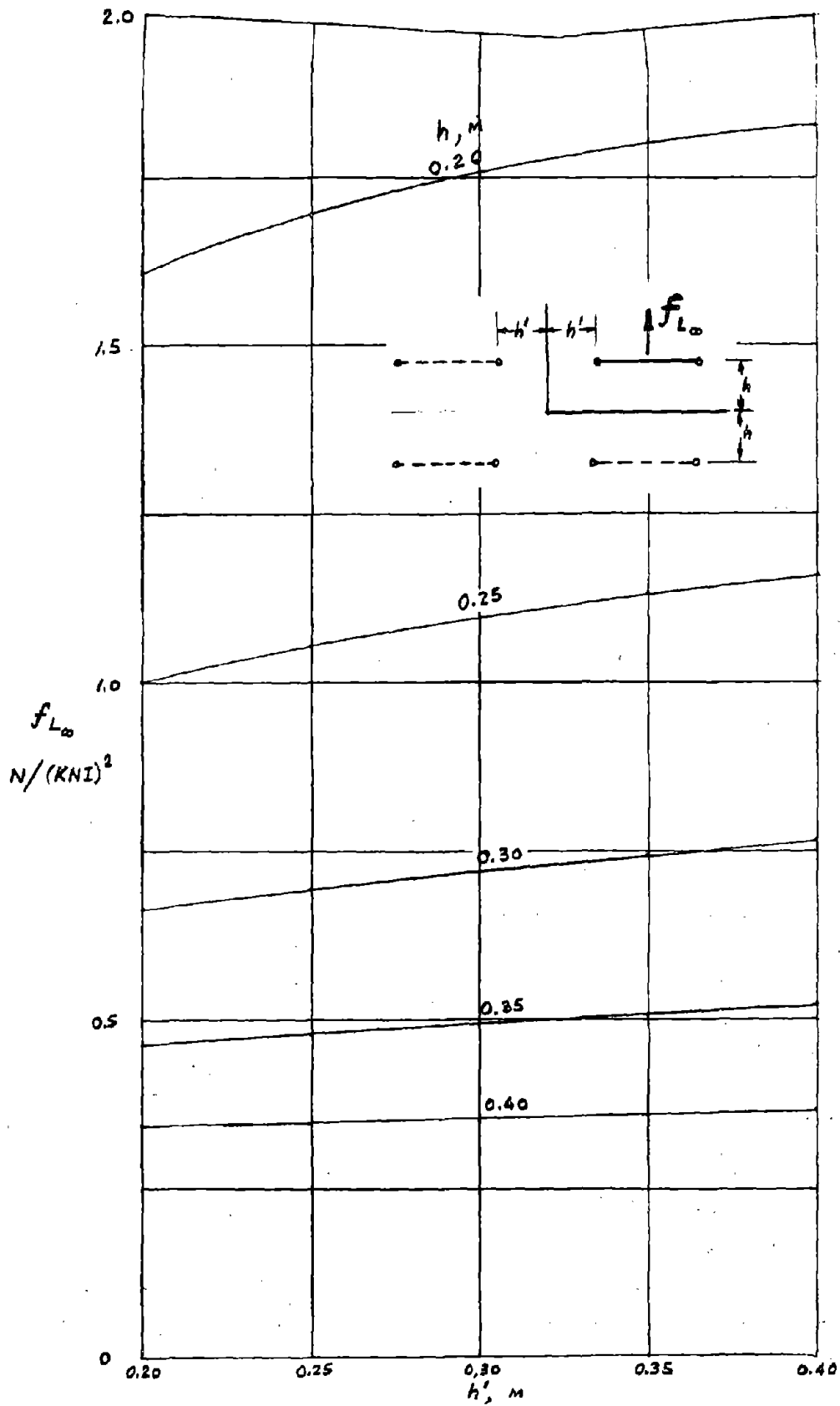


FIGURE A-3. LIFT COEFFICIENT AT INFINITE SPEED FOR 0.5 BY 3.0M COIL OVER L-CORNER.

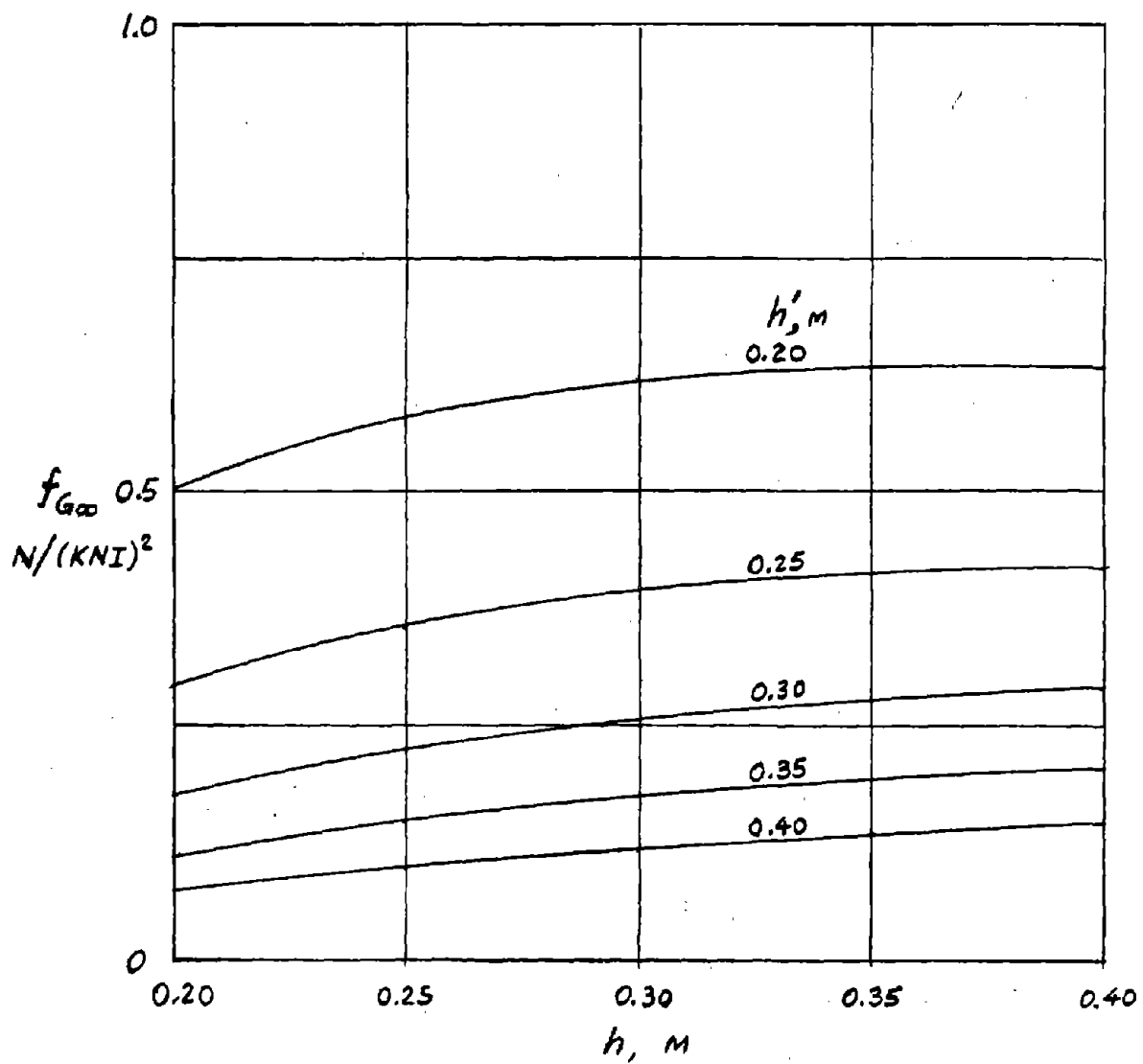
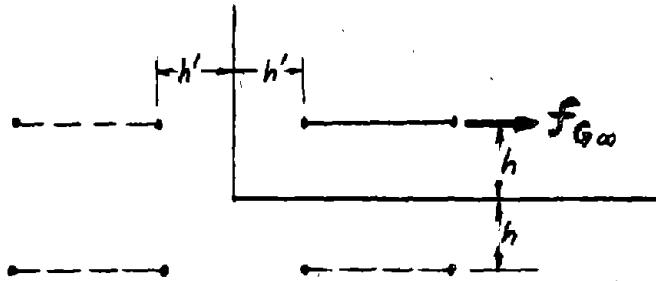


FIGURE A-4. LATERAL FORCE COEFFICIENT AT INFINITE SPEED FOR 0.5 BY 3.0M COIL OVER L-CORNER

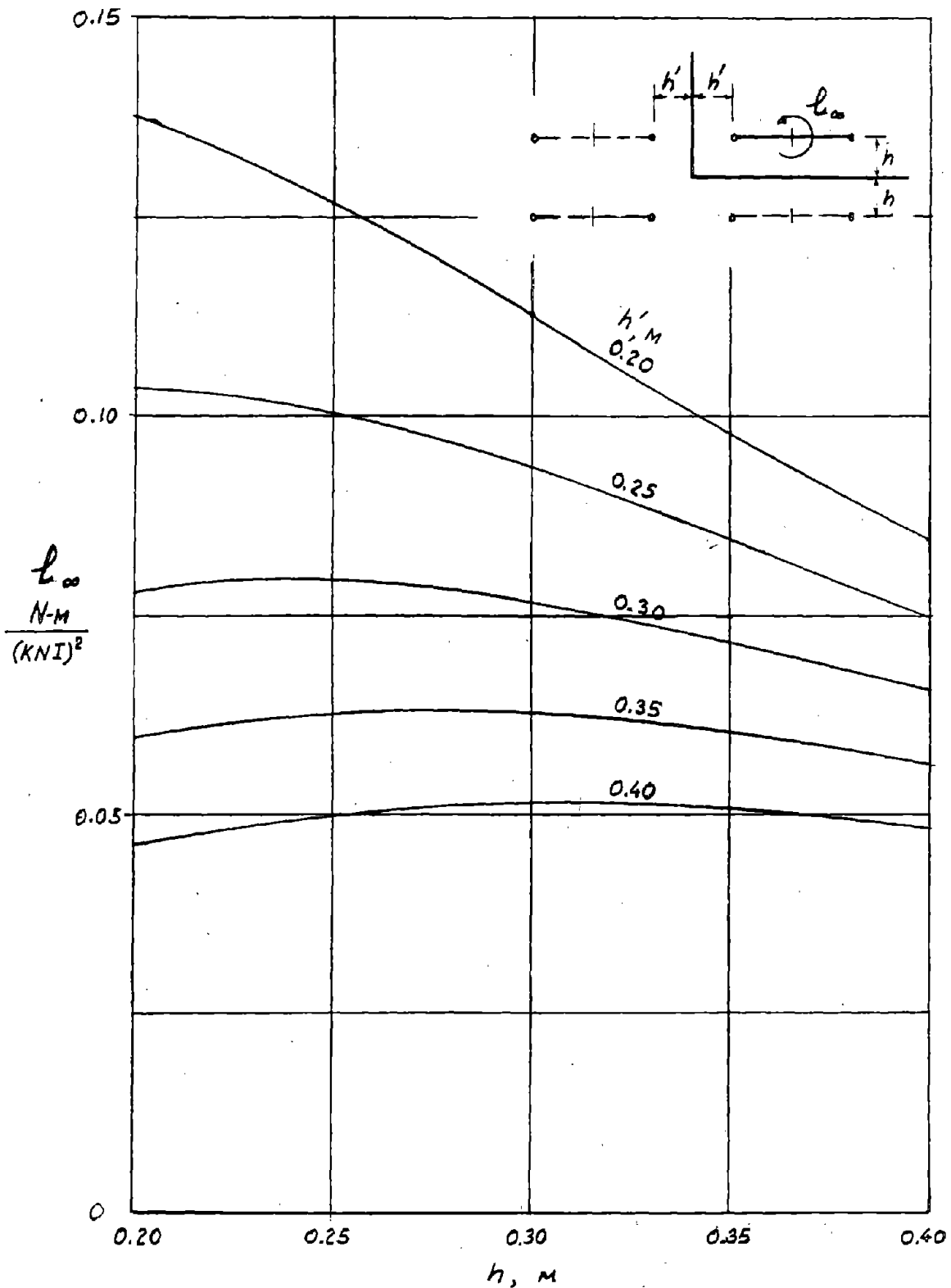


FIGURE A-5. MOMENT COEFFICIENT AT INFINITE SPEED FOR 0.5 BY 3.0M COIL OVER L-CORNER

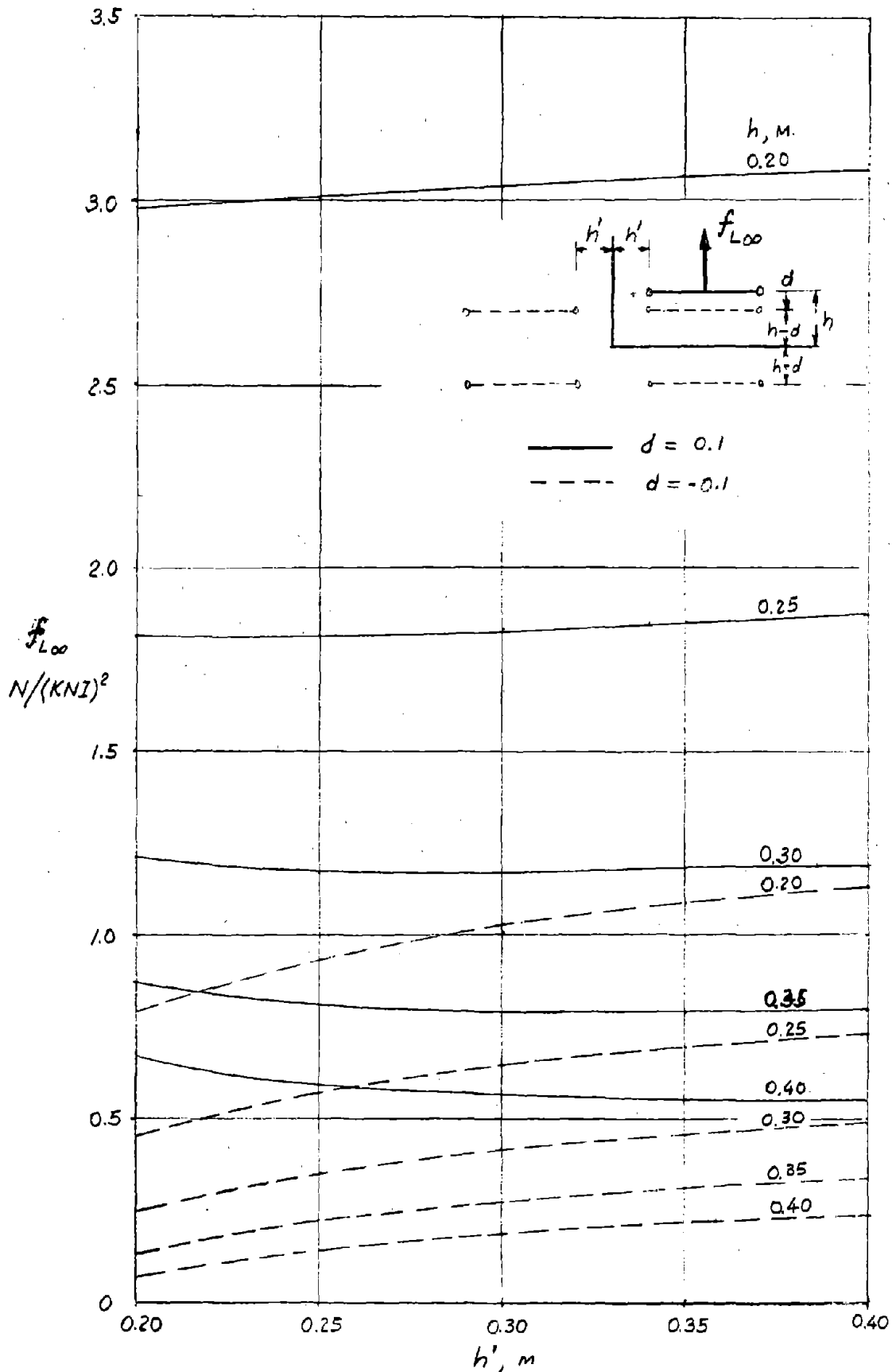


FIGURE A-6. LIFT COEFFICIENT AT INFINITE SPEED DUE TO CONTROL COIL; 0.5 BY 3.0M COILS OVER L-CORNER

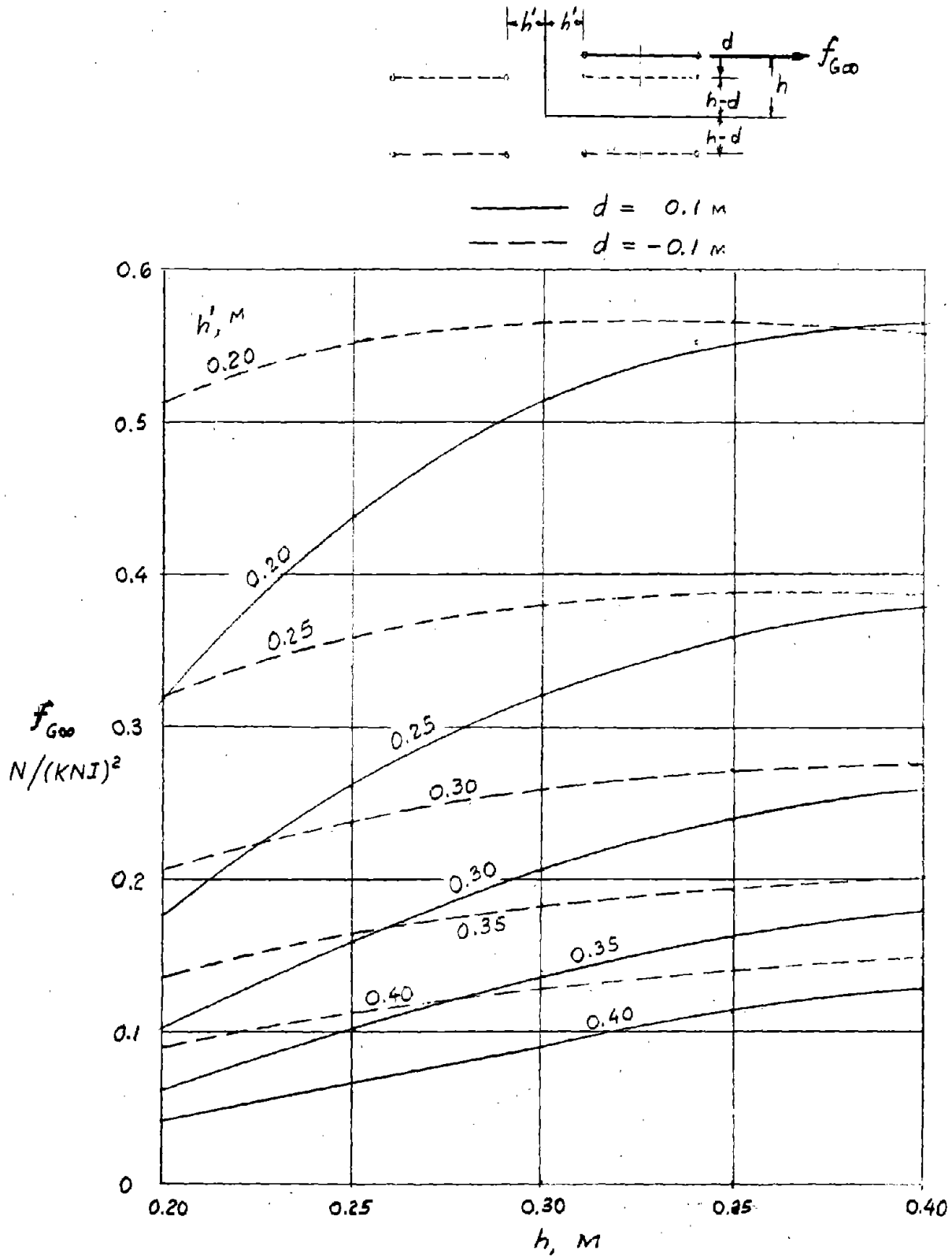
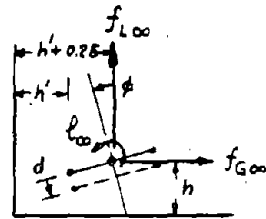
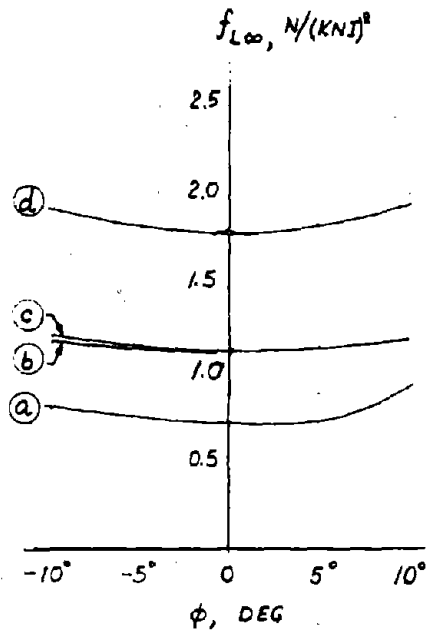


FIGURE A-7. LATERAL FORCE COEFFICIENTS AT INFINITE SPEED DUE TO CONTROL COIL; 0.5 BY 3.0M COILS OVER L-CORNER



	h	h'	d
(a)	0.3	0.3	0
(b)	0.3	0.3	0.1
(c)	0.2	0.3	-0.1
(d)	0.2	0.3	0

LETTER CODE CORRESPONDS
TO DISCUSSION IN PARA. 3

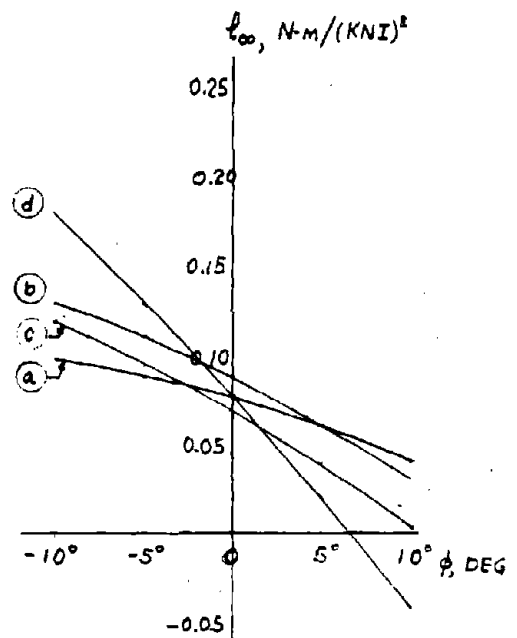
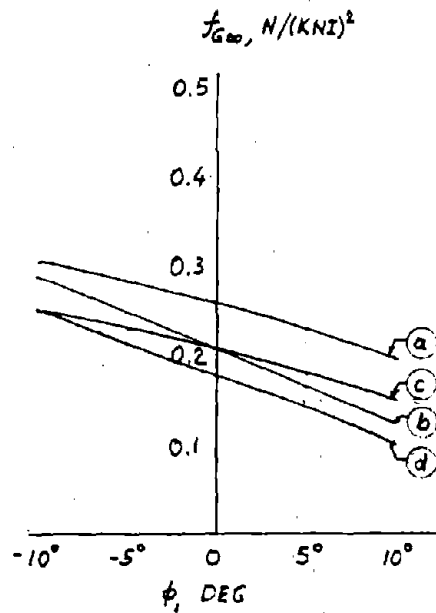


FIGURE A-8. FORCE AND MOMENT COEFFICIENTS AT INFINITE SPEED FOR 0.5 BY 3.0M COILS WITH 0.1M SEPARATION OVER AN L-CORNER

- (b) Effects of the images of the control coil on the main coil, expressed as force components and a moment referred to the longitudinal center line of the main coil.
- (c) Effects of the images of the main coil on the control coil, expressed as force components and a moment referred to the longitudinal center line of the control coil.
- (d) Effects of the images of the control coil on the control coil, expressed as force components and a moment referred to the longitudinal center line of the control coil.

To obtain the total forces and moment as seen by the vehicle, it is convenient to recombine the above components with appropriate weighting, namely, multiplication with the appropriate $I_1 I_2$ factors, and to make use of a common reference point. The geometrical center of the main coil provides a natural and convenient reference point, and the weighting factor can be expressed in terms of a control current parameter defined by

$$\alpha \equiv (KNI)_c / (KNI) = (KNI)_c / 429.69 \text{ (Example case)}$$

Contributions from (b) and (c) are thus linear in α and the contribution from (d) is quadratic in α . Since the effect of the magnitude of the current occurs only in the factor $(KNI)^2$, all force and moment coefficients can be normalized to correspond to the vehicle weight for the nominal coil position with zero control current. Data presented in Section 4.3.2 are based on these normalized force and moment coefficients.

All force coefficients for $\phi = 0$ have been obtained through formal differentiation of mutual inductance expressions, and those for $\phi \neq 0$ have been obtained by numerical differentiation. Additional differentiation with respect to spatial variables, both formal and numerical, leads to coefficients for Taylor expansions of all relevant force and moment coefficients about the nominal coil position as follows:

$$F_L = F_{L0} + F_{Lh} \cdot \Delta h + F_{Lh'} \cdot \Delta h' + F_{L\phi} \cdot \Delta \phi + F_{L\alpha} \cdot \alpha$$

and similar expressions for F_G and L . These expressions are directly applicable to linear analyses discussed in detail in this report. They are also

used in a subsequent appendix to generate a set of first order equations of motion to be used as a starting point for analyses of stability, transfer function, and ride quality of the revenue vehicle. Relevant data for this first order expansion are repeated below for reference. Using the local coordinate system defined in Figure A-1, the lift force (F_L), the lateral force (F_G) and the rolling moment (L) for each coil are given by:

$$F_L = 1.1120(05) - 8.9372(05) \Delta h + 8.2437(04) \Delta h' - 1.2899(04) \Delta \phi + 3.3981(05) \alpha$$

$$F_G = 3.9640(04) + 8.2437(04) \Delta h - 3.2430(05) \Delta h' - 4.7202(04) \Delta \phi + 6.3715(04) \alpha$$

$$L = 1.1768(04) - 1.2899(04) \Delta h - 4.7202(04) \Delta h' - 2.3642(04) \Delta \phi + 2.7473(04) \alpha$$

Pitching moment and yawing moment about the center of each coil have been neglected in the above treatment, primarily because amplitudes in pitch and yaw will be much smaller than amplitude in roll. This is due to the large longitudinal separation of the forward and the rear coils compared to the lateral separation between the left side and the right side coils. Therefore, the major contributions to pitching and yawing moments about the vehicle center of gravity consist of moments due to lift, lateral and fore-and-aft force components acting at the centers of four main coils. The neglected moment components about the coil centers may become important in detailed structural design studies of coil mounting assemblies, and should be evaluated at that time.

Other polynomial fits for all force and moment coefficients can be used to represent force behavior for the typical levitation coil configuration. Relevant data required for a point mass heave study are presented in Figure A-9, to describe the lift force characteristics of the configuration for various coil positions above the horizontal guideway surface at a cruise speed of 134 m/s.

In particular, nonlinearity of the control current parameter α in the force and moment characteristics can be obtained directly by considering a more extensive expansion of contributions of types (b), (c), and (d) to the

10^6

TYPICAL MAGLEV VEHICLE

0.5 M BY 3.0 M COIL

(4.2969×10^5 AT)

$h = h' = 0.3$ M

OVER 2.54 CM 1100-H14 GUIDEWAY

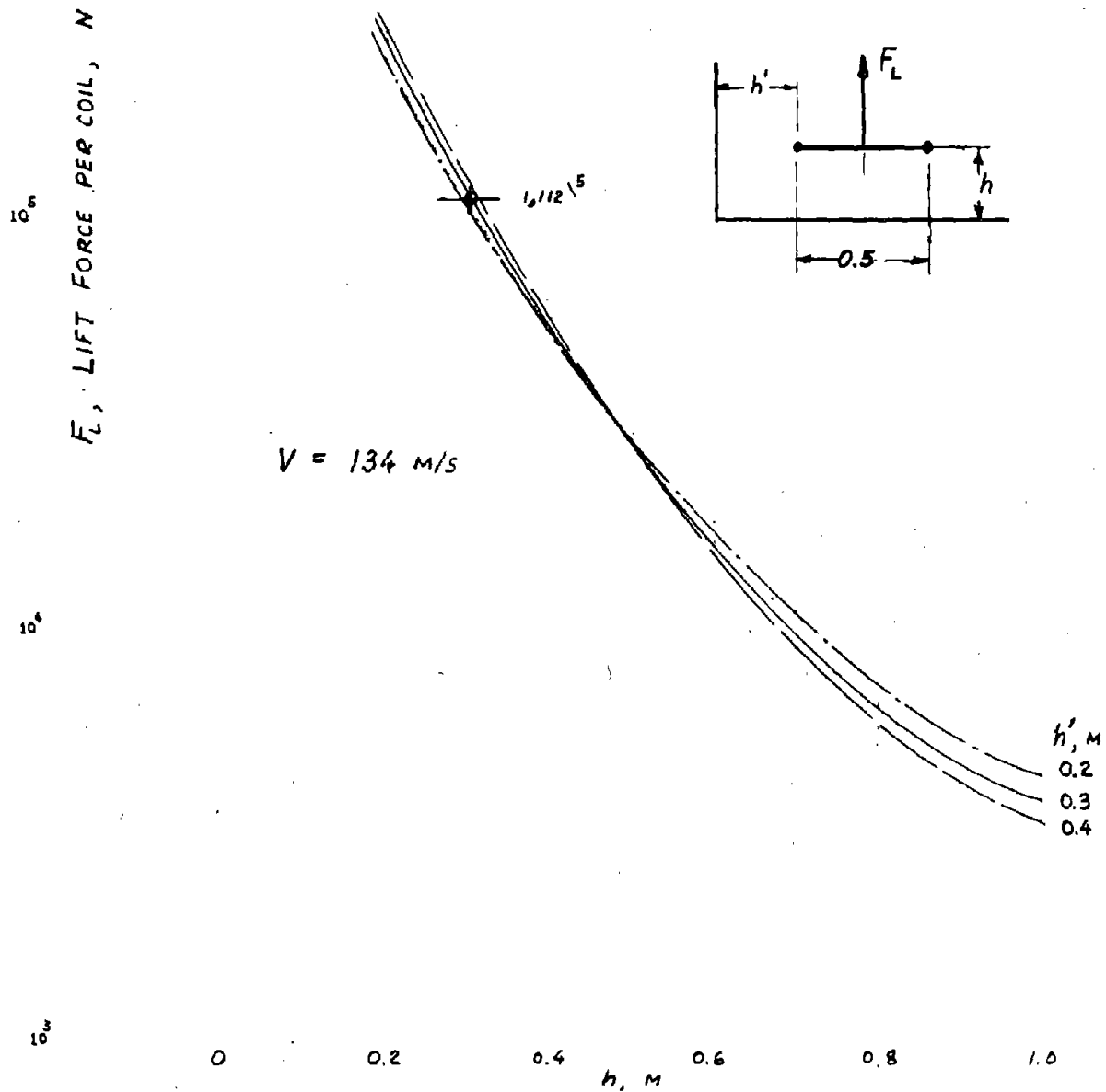


FIGURE A-9. LIFT FORCE PER COIL FOR MAGLEV AT 134 M/S

net forces. For a 0.5 by 3.0 m levitation coil at the nominal position of $h = h' = 0.3$ m, this more extensive expansion has the following form:

	Δh	$\Delta h'$	ϕ	α	X
$F_L = 1.1120(05)$	-8.9372(05)	+8.2437(04)	-1.2899(04)	+3.3981(05)	1
	-3.0328(06)	+2.4477(05)	+6.6260(03)	+2.7177(05)	α
	-2.6868(06)	+1.6119(05)	+2.9376(04)		α^2
$F_G = 3.9640(04)$	+8.2437(04)	-3.2430(05)	-4.7202(04)	+6.3715(04)	1
	+2.4477(05)	-5.4840(05)	-1.4250(05)	+2.7417(04)	α
	+1.6119(05)	-2.6359(05)	+9.2180(04)		α^2
$F = 1.1768(04)$	-1.2899(04)	-4.7202(04)	-2.3642(04)	+2.7473(04)	1
	+6.2601(03)	-1.4250(05)	-1.0240(05)	+1.4795(04)	α
	+2.9376(04)	+9.2180(04)	-1.0968(05)		α^2

REFERENCES

- A-1 Reitz, J. R., "Forces on Moving Magnets due to Eddy Currents," J. Applied Physics, Vol 41, p. 2067, 1970
- A-2 Reitz, J. R. and Davis, L. C., "Force on a Rectangular Coil Moving above a Conducting Slab," J. Applied Physics, Vol 43, p. 1547, 1972
- A-3 Borcherts, R. H. and Davis, L. C., "Force on a Coil Moving over a Conducting Surface Including Edge and Channel Effects," J. Applied Physics, Vol 43, p. 2418, 1972

APPENDIX B

MATHEMATICAL REPRESENTATION OF VEHICLE CHARACTERISTICS

By C. C. Wan and L. C. Sutherland

Equations of motion for a vehicle traveling at constant speed over an at-grade guideway are formulated in this appendix to provide a mathematical representation of vehicle characteristics. Effects of guideway irregularities in both vertical and horizontal directions are included in this formulation. The final form of the equations obtained for stability and ride quality studies pertains to the control concept discussed in Section 4.3.2 of this report.

B.1 VEHICLE COORDINATE SYSTEM

The MAGLEV revenue vehicle is equipped with four identical levitation coil and control coil assemblies mounted near the four corners of the vehicle and symmetrically disposed about the longitudinal centerline of the body. A right-handed coordinate system is employed for studies of vehicle dynamics. The origin of this system is located at the nominal vehicle center of gravity. The positive Z-axis points downward along the direction of gravity, the positive Y-axis points to the right, and the positive X-axis points forward in the direction of motion and is parallel to the longitudinal axis of the vehicle in its normal (undisplaced) position. The principal axes of the vehicle are assumed to be parallel to the inertial XYZ-system when the vehicle is in its normal position. Orientation of the vehicle in a displaced position is expressed by the usual Euler angles between the body axes and the inertial XYZ-frame.

A sketch of relevant geometrical characteristics is shown in Figure B-1. The following symbols are used: (Numerical values represent characteristics of the preliminary revenue vehicle. As stated in Appendix A, some of these values have been modified for the final baseline configuration.)

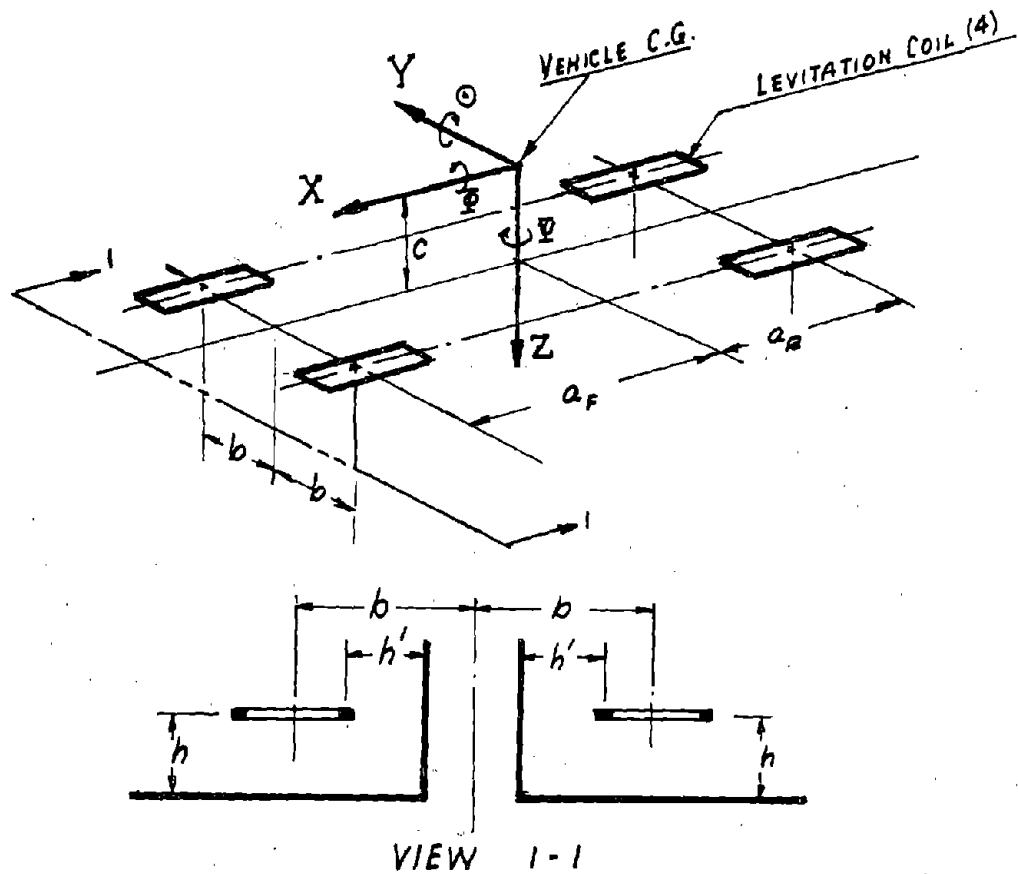


FIGURE B-1. LEVITATION COILS AND GUIDEWAY GEOMETRY

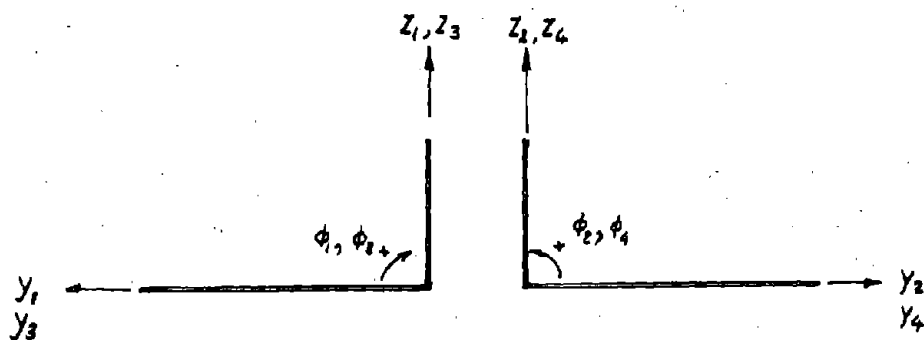


FIGURE B-2. LOCAL COORDINATE SYSTEM FOR COIL ASSEMBLIES

- a_F location of the center line of the forward coil assembly from the vehicle center of gravity (= 9.00 m)
- a_R location of the center line of the aft coil assembly from the vehicle center of gravity (= 7.65 m)
- b half track width, location of the center line of the coil assemblies from the vehicle longitudinal center line (= 0.965 m)
- c elevation of the plane of main levitation coils below the vehicle center of gravity (= 1.21 m)
- h nominal elevation of main levitation coils above the guideway (= 0.3 m)
- h' nominal separation between the vertical surface of the guideway and the near-side center line of coil winding (= 0.3 m)
- D Magnet "wheel" base = a_F + a_R (= 16.65 m)

B.2 LOCAL COORDINATE SYSTEM FOR LEVITATION COILS

Forces and moments expressions derived in Appendix A for individual levitation coil and control coil assemblies are referred to the center of the main levitation coil. This necessitates the selection of local coordinate systems, one for each coil assembly, as illustrated in Figure B-2. In order to simplify the analytical expressions, force components have been defined parallel to a set of coordinate system axes which remain normal to the horizontal and vertical surfaces of the guideway element, and the moment accounts only for the rolling component about the longitudinal centerline of the main levitation coil. (Pitch and yaw moments about the center of each coil are ignored because angular amplitudes in pitch and yaw are much smaller than roll amplitudes.) Guideway irregularities in the horizontal and vertical directions are compatible with the local coordinate system. With all displacements normal to the guideway surfaces treated as positive in a direction away from the surfaces, the use of these local coordinate systems leads to a compact representation of reactions as seen by the vehicle.

Only vertical and horizontal displacements of guideway surfaces are considered in the present study, primarily because field data on irregularities in guideway twist are very limited and this type of irregularity is expected to be relatively small. The four principal types of guideway irregularities are illustrated in Figure B-3. The numbering sequence of the four coil assemblies is also indicated in this figure.

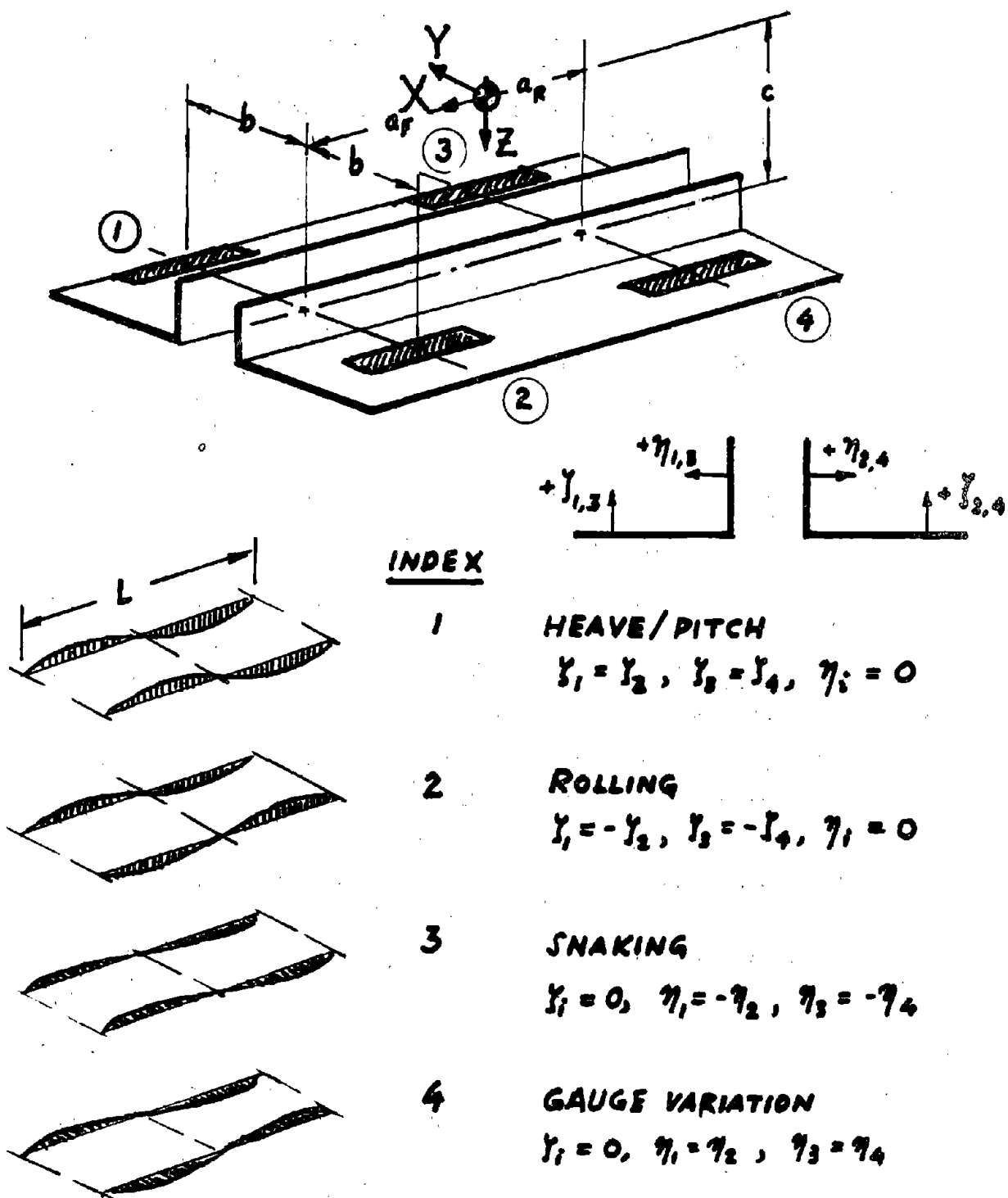


FIGURE B-3. TYPES OF GUIDEWAY IRREGULARITIES

B.3 EQUATIONS OF MOTION

Force equations are referred to the inertial XYZ-frame and moment equations are expressed in terms of the vehicle's body axes. At a constant forward speed the X-equation becomes a trivial identity defining the amount of thrust necessary to maintain the speed. The overturning moment due to thrust is an integral part of the equation for pitching. The resulting system of equations thus has five degrees of freedom, consisting of:

- Z downward displacement of vehicle cg (heave)
- Θ pitching rotation about the body pitch-axis
- Y lateral displacement of vehicle cg (sway)
- Φ rolling rotation about the body roll-axis
- Ψ yawing rotation about the body yaw-axis

These equations are displayed in matrix form in two separate groups in Tables B-1 and B-2. This separate display is possible because there is no coupling between the (Z, Θ) and the (Y, Φ , Ψ) groups when guideway irregularities are absent. Subscripts appearing in this summary display are defined in the following manner:

- (a) Subscripts in capital letters refer to the directions of the force components: L for upward lift force, G for lateral force.
- (b) Subscripts in lower case letters denote differentiation with respect to that variable; e.g., subscript h denotes a derivative with respect to h.
- (c) Numerical subscripts refer to individual coil assemblies; e.g., α_1 denotes the control current parameter for coil assembly 1.
- (d) External forces and moments from sources other than the coil assemblies are denoted by the subscript (ext). Thrust-induced pitching moment is included in this category.
- (e) Steady state forces and moments corresponding to nominal vehicle position are denoted by an additional subscript (0).

TABLE B-1. FORCE EQUATIONS FOR PITCH AND HEAVE

$$I_s \ddot{q}_s = A_s q_s + B_s \alpha + C_s \gamma + D_s \eta + L_s$$

$$K_i = \frac{1}{(f_L/f_b)_v} \quad q_s = \begin{bmatrix} Z \\ \Theta \end{bmatrix} \quad L_s = \begin{bmatrix} mg - 4F_{L0} + Z_{ext} \\ -4cK_i(F_{L0} + F_{G0}) + 2(a_F - a_R)F_{L0} + M_T + M_{ext} \end{bmatrix}$$

$$\alpha = \begin{bmatrix} \alpha_1 \\ \alpha_2 \\ \alpha_3 \\ \alpha_4 \end{bmatrix} \quad \gamma = \begin{bmatrix} \gamma_1 \\ \gamma_2 \\ \gamma_3 \\ \gamma_4 \end{bmatrix} \quad \eta = \begin{bmatrix} \eta_1 \\ \eta_2 \\ \eta_3 \\ \eta_4 \end{bmatrix}$$

$$I_s = \begin{bmatrix} m & 0 \\ 0 & B \end{bmatrix} \quad m = \text{VEHICLE WEIGHT (IN kg)} \\ B = \text{VEHICLE PITCHING INERTIA (IN kg.m}^2\text{)}$$

$$A_s = \begin{bmatrix} a_{zz} & a_{z\theta} \\ a_{\theta z} & a_{\theta\theta} \end{bmatrix}$$

$$X_h = K_i(F_{Lh} + F_{Gh})$$

$$a_{zz} = 4F_{Lh} \quad a_{z\theta} = -2(a_F - a_R)F_{Lh}$$

$$a_{\theta z} = -2(a_F - a_R)F_{Lh} + 4cX_h$$

$$a_{\theta\theta} = 2(a_F^2 + a_R^2)F_{Lh} - 2(a_F - a_R)[cX_h - K_i(F_{L0} + F_{G0})] + 4cF_{L0}$$

$$B_s = \begin{bmatrix} b_{zF} & b_{zR} & b_{z\alpha} & b_{z\beta} \\ b_{\theta F} & b_{\theta R} & b_{\theta\alpha} & b_{\theta\beta} \end{bmatrix}$$

$$b_z = -F_{L0}$$

$$b_{\theta F} = a_F F_{L0} - cK_i(F_{L0} + F_{G0})$$

$$b_{\theta R} = -a_R F_{L0} - cK_i(F_{L0} + F_{G0})$$

$$C_s = \begin{bmatrix} c_z & c_z & c_z & c_z \\ c_{\theta F} & c_{\theta F} & c_{\theta R} & c_{\theta R} \end{bmatrix}$$

$$c_z = F_{Lh}$$

$$c_{\theta F} = -a_F F_{Lh} + cK_i(F_{Lh} + F_{Gh})$$

$$c_{\theta R} = a_R F_{Lh} + cK_i(F_{Lh} + F_{Gh})$$

$$D_s = \begin{bmatrix} d_z & d_z & d_z & d_z \\ d_{\theta F} & d_{\theta F} & d_{\theta R} & d_{\theta R} \end{bmatrix}$$

$$d_z = F_{Lh}$$

$$d_{\theta F} = -a_F F_{Lh} + cK_i(F_{Lh} + F_{Gh})$$

$$d_{\theta R} = a_R F_{Lh} + cK_i(F_{Lh} + F_{Gh})$$

TABLE B-2. FORCE EQUATIONS FOR ROLL, SWAY, AND YAW MOTION

$$I_A \ddot{q}_A = A_A q_A + B_A \alpha + C_A \beta + D_A \eta + L_A$$

$$q_A = \begin{bmatrix} Y \\ \Phi \\ \Psi \end{bmatrix} \quad L_A = \begin{bmatrix} Y_{ext} \\ L_{ext} \\ N_{ext} \end{bmatrix}$$

$$I_A = \begin{bmatrix} m & 0 & 0 \\ 0 & A & 0 \\ 0 & 0 & C \end{bmatrix}$$

m = VEHICLE WEIGHT (IN kg)

A = VEHICLE ROLLING INERTIA (IN kg m²)

C = VEHICLE YAWING INERTIA (IN kg m²)

$$A_A = \begin{bmatrix} a_{yy} & a_{y\phi} & a_{y\psi} \\ a_{\phi y} & a_{\phi\phi} & a_{\phi\psi} \\ a_{\psi y} & a_{\psi\phi} & a_{\psi\psi} \end{bmatrix}$$

$$a_{yy} = 4 F_{Gh'} \quad a_{y\phi} = -4 (b F_{Gh'} + c F_{Ch'} + F_{G\phi}) = a_{\phi y}$$

$$a_{y\psi} = 2(a_F - a_R) F_{Gh'}$$

$$a_{\phi\phi} = 4 [b(b F_{Lh} + c F_{Lh'} + F_{L\phi} + L_h - F_{G\phi}) + c(b F_{Ch} + c F_{Ch'} + F_{C\phi} + L_h' + F_{L\phi}) + L_\phi]$$

$$a_{\phi\psi} = -2(a_F - a_R) (b F_{Lh'} + c F_{Ch'} + L_h') - 4c K_i (F_{L\phi} + F_{G\phi})$$

$$a_{\psi y} = 2(a_F - a_R) F_{Gh'} + 4b K_i (F_{Lh'} + F_{Gh'})$$

$$a_{\psi\phi} = -2(a_F - a_R) (b F_{Gh} + c F_{Ch'} + F_{C\phi} + F_{L\phi}) - 4b K_i [b F_{Lh} + c F_{Lh'} + F_{L\phi} + b F_{Ch} + c F_{Ch'} + F_{C\phi}]$$

$$a_{\psi\psi} = 2(a_F^2 + a_R^2) F_{Gh'} + 2(a_F - a_R) K_i [b(F_{Lh} + F_{Ch}) + F_{L\phi} + F_{G\phi}] - 4b F_{G\phi}$$

$$B_A = \begin{bmatrix} b_y & -b_y & b_\phi & -b_\phi \\ b_\phi & -b_\phi & b_{\psi F} & -b_{\psi R} \\ b_{\psi F} & -b_{\psi R} & b_{\psi R} & -b_{\psi R} \end{bmatrix}$$

$$b_y = F_{G\alpha} \quad b_\phi = -(b F_{L\alpha} + c F_{G\alpha} + L_\alpha)$$

$$b_{\psi F} = b K_i (F_{L\alpha} + F_{G\alpha}) + a_F F_{G\alpha} \quad b_{\psi R} = b K_i (F_{L\alpha} + F_{G\alpha}) - a_R F_{G\alpha}$$

$$C_A = \begin{bmatrix} c_y & -c_y & c_\phi & -c_\phi \\ c_\phi & -c_\phi & c_{\psi F} & -c_{\psi R} \\ c_{\psi F} & -c_{\psi R} & c_{\psi R} & -c_{\psi R} \end{bmatrix}$$

$$c_y = -F_{Gh} \quad c_\phi = b F_{Lh} + c F_{Gh} + L_h$$

$$c_{\psi F} = -b K_i (F_{Lh} + F_{Ch}) - a_F F_{Gh} \quad c_{\psi R} = -b K_i (F_{Lh} + F_{Ch}) + a_R F_{Gh}$$

$$D_A = \begin{bmatrix} d_y & -d_y & d_\phi & -d_\phi \\ d_\phi & -d_\phi & d_{\psi F} & -d_{\psi R} \\ d_{\psi F} & -d_{\psi R} & d_{\psi R} & -d_{\psi R} \end{bmatrix}$$

$$d_y = -F_{Ch'} \quad d_\phi = b F_{Lh'} + c F_{Ch'} + L_h'$$

$$d_{\psi F} = -b K_i (F_{Lh'} + F_{Ch'}) - a_F F_{Ch'} \quad d_{\psi R} = -b K_i (F_{Lh'} + F_{Ch'}) + a_R F_{Ch'}$$

Guideway irregularities, or deviations from nominal at-grade position, are denoted by ζ and η . Individual coil assembly displacements are related to the state of motion at the vehicle center of gravity through the usual rigid body transformation. Thus, the strokes of the i-th coil assembly in the vertical and lateral directions for the local coordinate system are given by:

$$\Delta h_i = -Z - Y_i \phi + X_i \theta - \zeta_i$$

$$\Delta h'_i = [Y - Z_i \phi + X_i \psi] \cdot (-1)^{i-1} - \eta_i$$

$$\phi_i = \phi (-1)^i$$

where X_i , Y_i and Z_i are the position coordinates of the center of the i-th levitation coil in the inertial XYZ frame. Values of these coordinates for the four coil assemblies are listed below for reference.

Coil No. (i)	X_i	Y_i	Z_i
1	a_F	b	c
2	a_F	-b	c
3	$-a_R$	b	c
4	$-a_R$	-b	c

Force and moments acting on the vehicle at the center of the i-th coil assembly, when referred to the inertial XYZ frame, become

$$(F_Z)_i = -(F_L)_i = -(F_{L0} + F_{Lh} \Delta h_i + F_{Lh'} \Delta h'_i + F_{L\phi} \phi_i + F_{L\alpha} \alpha_i)$$

$$(F_Y)_i = (-1)^{i-1} (F_G)_i = (F_{G0} + F_{Gh} \Delta h_i + F_{Gh'} \Delta h'_i + F_{G\phi} \phi_i + F_{G\alpha} \alpha_i) (-1)^{i-1}$$

$$(F_X)_i = -K_1 [(F_L)_i + (F_G)_i] ; (K_1 = 1/(F_L/F_D) \text{ at speed } V)$$

$$(L)_i = (-1)^i (L)_i = (L_0 + L_h \Delta h_i + L_{h'} \Delta h'_i + L_{\phi} \phi_i + L_{\alpha} \alpha_i) (-1)^i$$

The three force equations follow from summing all relevant force components along the three axes of the inertial XYZ-frame. The displaced position of the vehicle must be used, however, in summing all relevant moments about the vehicle

center of gravity. (The moment components are defined about the three principal body axes.) This summing process is expressed in matrix form as:

$$\begin{bmatrix} L \\ M \\ N \end{bmatrix} = \sum_1^4 \left\{ \begin{bmatrix} 0 & -Z_i & Y_i \\ Z_i & 0 & -X_i \\ -Y_i & X_i & 0 \end{bmatrix} \begin{bmatrix} 1 & \psi & -\theta \\ -\psi & 1 & \phi \\ \theta & -\phi & 1 \end{bmatrix} \begin{bmatrix} (F_X)_i \\ (F_Y)_i \\ (F_Z)_i \end{bmatrix} \right. \\ \left. + \begin{bmatrix} 1 & \psi & -\theta \\ -\psi & 1 & \phi \\ \theta & -\phi & 1 \end{bmatrix} \begin{bmatrix} (L)_i \\ (M)_i \\ (N)_i \end{bmatrix} \right\} + \begin{bmatrix} L_{\text{ext}} \\ M_{\text{ext}} \\ N_{\text{ext}} \end{bmatrix}$$

$(M)_i$ and $(N)_i$ are zeroes for the present study, having been neglected in the formulation of the magnetic force model as discussed previously.

The X-equation becomes trivial for constant speed operation as indicated above. The remaining five equations completely describe the dynamic characteristics of the vehicle for small displacements. The specification of a particular control law defining the functional relationship between control currents and the vehicle state of motion is needed to complete the mathematical description of the vehicle stability and control characteristics.

B.4 INCORPORATION OF CONTROL FUNCTION

The baseline control function envisioned for the revenue vehicle incorporates means for both relative damping (gap sensors) and absolute damping (accelerometers at coil assemblies). Signal filtering is employed to achieve certain desirable features at both low and high frequencies. In essence, weighting of relative signals is increased at low frequencies to improve track following, while weighting of absolute signals is increased at high frequencies to enhance ride quality. Pseudo-state variables are generated from these filtered signals from all four coil assemblies. This is accomplished by using an inverse transformation according to the geometric disposition of the coil assemblies relative to vehicle center of gravity. These pseudo-state variables are further modified by individual "modal" gain constants to ensure stability with adequate damping properties. A block diagram showing the major elements in this control

concept is presented in Figure B-4. Pertinent intermediate steps leading to the final equations of motion for both stability and ride quality studies are shown in Table B-3.

Techniques that may be used for studies of longitudinal (heave/pitch) and lateral (sway-roll-yaw) stability are described in Appendix C. Ride quality analyses make use of a modal superposition technique which treats the four types of guideway irregularities either singly or in combination with each other. This is described in Appendix D.

B.5 ONE AND TWO DEGREE-OF-FREEDOM DYNAMIC MODELS

It was observed during the derivation of the equations of motion that the heave/pitch modes decoupled from the sway/roll/yaw modes. Furthermore, by examining the terms that produce the coupling between the pitch and heave modes and between the sway/roll and yaw modes it is seen that only drag and longitudinal c.g. offsets are involved. Since these effects are small it is possible, to a close approximation, to study heave, pitch and yaw individually with a single-degree-of-freedom model, and to study the coupled sway/roll modes with a two-degree-of-freedom model.

Considering the heave mode first, from the pitch/heave equations given previously in this appendix, with the coupling terms set to zero,

$$\ddot{m}Z = a_{zz} + (b_z \ b_z \ b_z \ b_z) \begin{bmatrix} \alpha_1 \\ \alpha_2 \\ \alpha_3 \\ \alpha_4 \end{bmatrix} + (c_z \ c_z \ c_z \ c_z) \begin{bmatrix} \zeta_1 \\ \zeta_2 \\ \zeta_3 \\ \zeta_4 \end{bmatrix}$$

where a_{zz} , b_z and c_z are as defined previously. The α_i are the control currents and the ζ_i are the guideway deviations at the four corners. For the heave mode, the four corners move together, resulting in

$$\zeta_i = Z_g$$

where Z_g represents the deviation of the guideway from nominal at-grade position. The control currents are determined by multiplying out the symmetric

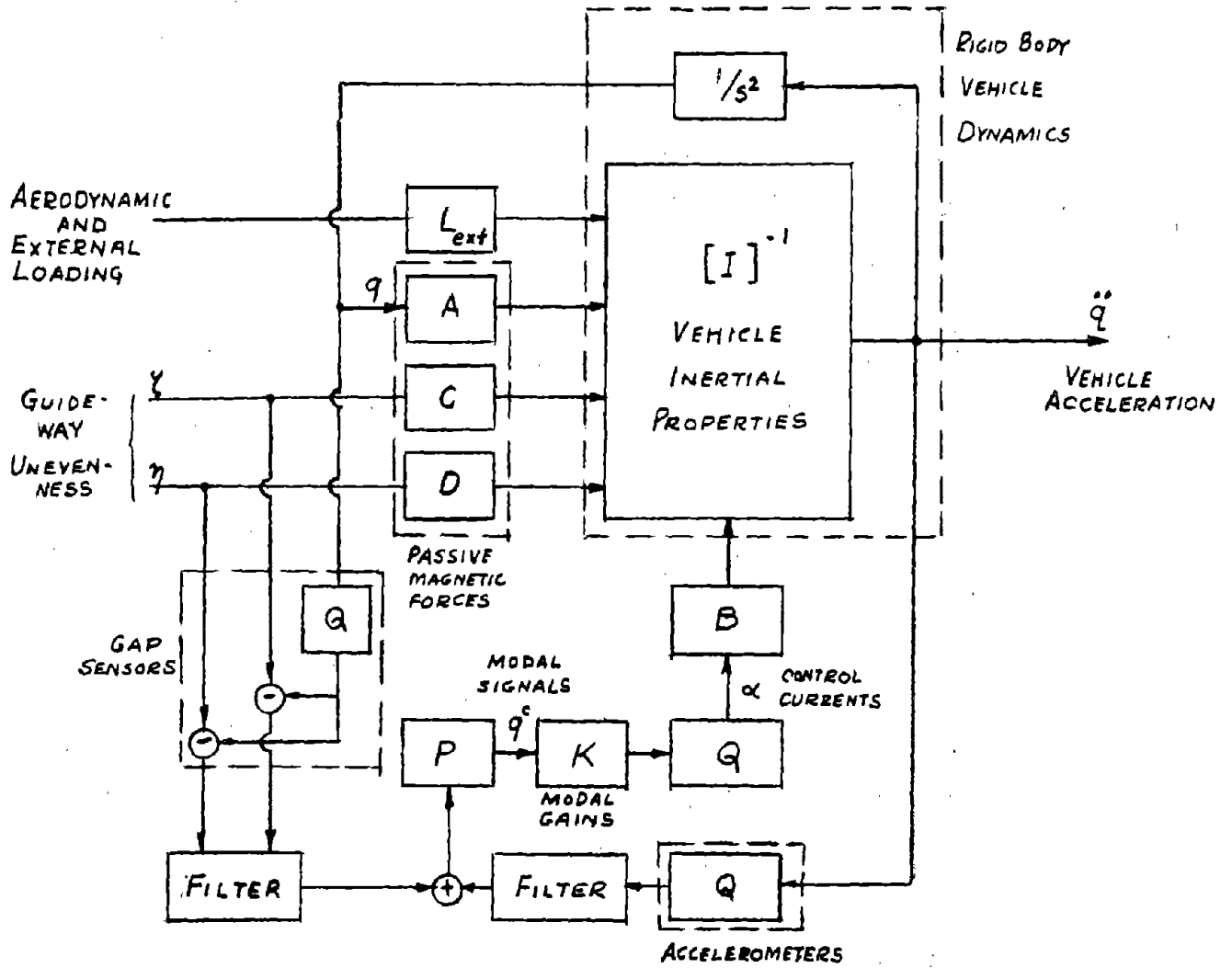


FIGURE B-4. BLOCK DIAGRAM FOR MAGLEV CONTROL DYNAMICS AND RIDE QUALITY CHARACTERISTICS

TABLE B-3. DETAILS OF THE EQUATIONS OF MOTION

COIL ASSEMBLY DISPLACEMENTS

$$z = \begin{bmatrix} z_1 \\ z_2 \\ z_3 \\ z_4 \end{bmatrix} \quad y = \begin{bmatrix} y_1 \\ y_2 \\ y_3 \\ y_4 \end{bmatrix} \quad q_s = \begin{bmatrix} Z \\ \Theta \end{bmatrix} \quad q_A = \begin{bmatrix} Y \\ \Phi \\ \Psi \end{bmatrix}$$

$$\begin{bmatrix} z \\ y \end{bmatrix} = \begin{bmatrix} Q_{SS} & Q_{SA} \\ 0 & Q_{AA} \end{bmatrix} \begin{bmatrix} q_s \\ q_A \end{bmatrix}$$

$$Q_{SS} = \begin{bmatrix} -1 & a_F \\ -1 & a_F \\ -1 & -a_R \\ -1 & -a_R \end{bmatrix} \quad Q_{SA} = \begin{bmatrix} 0 & -b & 0 \\ 0 & b & 0 \\ 0 & -b & 0 \\ 0 & b & 0 \end{bmatrix} \quad Q_{AA} = \begin{bmatrix} 1 & -c & a_F \\ -1 & c & -a_F \\ 1 & -c & -a_R \\ -1 & c & a_R \end{bmatrix}$$

$$\begin{bmatrix} P_{SS} & 0 \\ P_{AS} & P_{AA} \end{bmatrix} = \begin{bmatrix} Q_{SS} & Q_{SA} \\ 0 & Q_{AA} \end{bmatrix}^{-1}$$

$$P_{SS} = \begin{bmatrix} -\frac{a_R}{2D} & -\frac{a_R}{2D} & -\frac{a_F}{2D} & -\frac{a_F}{2D} \\ \frac{1}{2D} & \frac{1}{2D} & -\frac{1}{2D} & -\frac{1}{2D} \end{bmatrix} \quad (D = a_F + a_R)$$

$$P_{AS} = \begin{bmatrix} -\frac{c}{4b} & \frac{c}{4b} & -\frac{c}{4b} & \frac{c}{4b} \\ -\frac{1}{4b} & \frac{1}{4b} & -\frac{1}{4b} & \frac{1}{4b} \\ 0 & 0 & 0 & 0 \end{bmatrix}$$

$$P_{AA} = \begin{bmatrix} \frac{a_R}{2D} & -\frac{a_R}{2D} & \frac{a_F}{2D} & -\frac{a_F}{2D} \\ 0 & 0 & 0 & 0 \\ \frac{1}{2D} & -\frac{1}{2D} & -\frac{1}{2D} & \frac{1}{2D} \end{bmatrix}$$

$$P_{AS} Q_{SA} = \begin{bmatrix} 0 & c & 0 \\ 0 & 1 & 0 \\ 0 & 0 & 0 \end{bmatrix}$$

$$P_{AA} Q_{AA} = \begin{bmatrix} 1 & -c & 0 \\ 0 & 0 & 0 \\ 0 & 0 & 1 \end{bmatrix}$$

TABLE B-3. DETAILS OF THE EQUATIONS OF MOTION (Continued)

GAPS

$$h = \begin{bmatrix} \Delta h_1 \\ \Delta h_2 \\ \Delta h_3 \\ \Delta h_4 \end{bmatrix} \quad H = \begin{bmatrix} \Delta h'_1 \\ \Delta h'_2 \\ \Delta h'_3 \\ \Delta h'_4 \end{bmatrix} \quad \xi = \begin{bmatrix} \xi_1 \\ \xi_2 \\ \xi_3 \\ \xi_4 \end{bmatrix} \quad \eta = \begin{bmatrix} \eta_1 \\ \eta_2 \\ \eta_3 \\ \eta_4 \end{bmatrix}$$

$$\begin{bmatrix} h \\ h' \end{bmatrix} = \begin{bmatrix} z \\ \gamma \end{bmatrix} - \begin{bmatrix} \xi \\ \eta \end{bmatrix}$$

FILTERED SIGNALS $\begin{bmatrix} p \\ p' \end{bmatrix}$

$$p = \begin{bmatrix} p_1 \\ p_2 \\ p_3 \\ p_4 \end{bmatrix} \quad p' = \begin{bmatrix} p'_1 \\ p'_2 \\ p'_3 \\ p'_4 \end{bmatrix}$$

$$H_s = (K_z \ddot{z} + K_z \frac{\tau_z}{1 + \tau_z s}) \cdot I_4 \quad H_A = (K_y \ddot{y} + K_y \frac{\tau_y}{1 + \tau_y s}) \cdot I_4 \quad I_4 = \begin{bmatrix} 1 & 0 & 0 & 0 \\ 0 & 1 & 0 & 0 \\ 0 & 0 & 1 & 0 \\ 0 & 0 & 0 & 1 \end{bmatrix}$$

$$H_h = (K_h \ddot{h} + K_h \frac{s}{1 + \tau_h s}) \cdot I_4 \quad H_{h'} = (K_{h'} \ddot{h}' + K_{h'} \frac{s}{1 + \tau_{h'} s}) \cdot I_4$$

$$\begin{bmatrix} p \\ p' \end{bmatrix} = \begin{bmatrix} H_s & 0 \\ 0 & H_A \end{bmatrix} \begin{bmatrix} \ddot{z} \\ \ddot{y} \end{bmatrix} + \begin{bmatrix} H_h & 0 \\ 0 & H_{h'} \end{bmatrix} \begin{bmatrix} h \\ h' \end{bmatrix}$$

$$= \begin{bmatrix} -s^2 H_s + H_h & 0 \\ 0 & -s^2 H_A + H_{h'} \end{bmatrix} \begin{bmatrix} Q_{0s} & Q_{0A} \\ 0 & Q_{AA} \end{bmatrix} \begin{bmatrix} q_s \\ q_A \end{bmatrix} - \begin{bmatrix} H_h & 0 \\ 0 & H_{h'} \end{bmatrix} \begin{bmatrix} \xi \\ \eta \end{bmatrix}$$

$$K_{0s} = -s^2 H_s + H_h$$

$$\bar{K}_{0A} = -s^2 H_A + H_{h'}$$

TABLE B-3. DETAILS OF THE EQUATIONS OF MOTION (Continued)

MODAL SIGNALS

q^c

$$q^c = \begin{bmatrix} q_s^c \\ q_A^c \end{bmatrix} = \begin{bmatrix} P_{SS} & 0 \\ P_{AS} & P_{AA} \end{bmatrix} \begin{bmatrix} p \\ p' \end{bmatrix}$$

$$= \begin{bmatrix} K_{OS} & 0 \\ 0 & K_{OA} \end{bmatrix} \begin{bmatrix} q_s \\ q_A \end{bmatrix} - \begin{bmatrix} P_{SS} H_h & 0 \\ P_{AS} H_h & P_{AA} H_h' \end{bmatrix} \begin{bmatrix} \xi \\ \eta \end{bmatrix} \quad \left(K_{OA} = \bar{K}_{OA} + [K_{OS} - \bar{K}_{OA}] P_{AS} Q_{SA} \right)$$

MODAL GAINS

K_S, K_A

$$K_S = \begin{bmatrix} K_Z & 0 \\ 0 & K_\theta \end{bmatrix}$$

$$K_A = \begin{bmatrix} K_Y & 0 & 0 \\ 0 & K_\phi & 0 \\ 0 & 0 & K_\psi \end{bmatrix}$$

CONTROL CURRENT PARAMETER COMMANDS

α

$$\alpha = \begin{bmatrix} \alpha_1 \\ \alpha_2 \\ \alpha_3 \\ \alpha_4 \end{bmatrix} = - \begin{bmatrix} Q_{SS} & Q_{AA} \end{bmatrix} \begin{bmatrix} K_S & 0 \\ 0 & K_A \end{bmatrix} \begin{bmatrix} q_s^c \\ q_A^c \end{bmatrix}$$

$$= - [Q_{SS} K_S K_{OS}] q_s - [Q_{AA} K_A K_{OA}] q_A + [Q_{SS} K_S P_{SS} + Q_{AA} K_A P_{AS}] [H_h] \xi + [Q_{AA} K_A P_{AA}] [H_h'] \eta$$

EQUATIONS OF MOTION WITH CONTROL FUNCTION

$$[s^2 I_S - A_S + B_S Q_{SS} K_S K_{OS}] q_s = [B_S Q_{SS} K_S P_{SS} H_h + C_S] \xi + [D_S] \eta + [L_S]$$

$$[s^2 I_A - A_A + B_A Q_{AA} K_A K_{OA}] q_A = [B_A Q_{AA} K_A P_{AS} H_h + C_A] \xi + [B_A Q_{AA} K_A P_{AA} H_h' + D_A] \eta + [L_A]$$

control current matrices, resulting in the following expression (using Laplace Transform notation*):

$$\alpha_i = K_z (H_h + H_z S^2)Z + K_z H_h Z_g$$

where K_z is the heave mode gain,

$$H_h = K_h + \frac{K_h S}{1 + \tau_h S}$$

$$H_z = \frac{K_z \tau_z}{1 + \tau_z S} + K_{z\ddot{z}}$$

where K_h is position feedback gain, K_h is the relative rate gain, K_z is the absolute rate gain, $K_{z\ddot{z}}$ is the acceleration feedback gain, τ_h and τ_z are the relative and absolute signal filter time constants, and S denotes the Laplace operator. The resulting basic heave equation (in Laplace Transform notation) is

$$mS^2Z = a_{zz}Z + 4b_z K_z (H_h + H_z S^2)Z + 4(b_z K_z H_h + 4c_z)Z_g$$

By multiplying out the filter terms the heave equation of motion (in differential notation) is given by

$$a_0 \ddot{Z} = -a_1 \dot{Z} - a_2 \ddot{Z} - a_3 \dot{Z} - a_4 Z + b_0 \ddot{Z}_g + b_1 \dot{Z}_g + b_2 Z_g$$

where

$$a_0 = m\tau_z \tau_h - 4b_z K_z K_{z\ddot{z}} \tau_z \tau_h$$

$$a_1 = m(\tau_z + \tau_h) - 4b_z K_z [K_{z\ddot{z}}(\tau_z + \tau_h) + K_z \tau_z \tau_h]$$

$$a_2 = m - a_{zz} \tau_z \tau_h - 4b_z K_z [K_h \tau_z \tau_h + (K_h + K_z) \tau_z + K_{z\ddot{z}}]$$

$$a_3 = -a_{zz}(\tau_z + \tau_h) - 4b_z K_z [K_h(\tau_z + \tau_h) + K_h]$$

$$a_4 = -a_{zz} - 4b_z K_z K_h$$

$$b_0 = 4\tau_z [\tau_h c_z + b_z K_z (K_h \tau_h + K_h)]$$

*For convenience, the symbol for a quantity and its Laplace Transform will be used interchangeably in the following discussion.

$$b_1 = 4[c_z(\tau_z + \tau_h) + b_z K_z(\tau_h K_h + K_h + \tau_z K_h)]$$

$$b_2 = 4[c_z + b_z K_z K_h]$$

The equation can also be written in polynomial form,

$$\frac{z}{z_g} = \frac{b_0 s^2 + b_1 s + b_2}{a_0 s^4 + a_1 s^3 + a_2 s^2 + a_3 s + a_4}$$

which can be used for frequency response and PSD analysis

Equations for pitch and yaw can also be derived using the same technique.

For pitch

$$B\ddot{\theta} = a_{\theta\theta}\theta + (b_{\theta_F} b_{\theta_F} b_{\theta_R} b_{\theta_R}) \begin{bmatrix} \alpha_1 \\ \alpha_2 \\ \alpha_3 \\ \alpha_4 \end{bmatrix} + (c_{\theta_F} c_{\theta_F} c_{\theta_R} c_{\theta_R}) \begin{bmatrix} \zeta_1 \\ \zeta_2 \\ \zeta_3 \\ \zeta_4 \end{bmatrix}$$

where, assuming that for the decoupled pitch motion

$$\zeta_1 = \zeta_2 = a_{Fg}\theta, \zeta_3 = \zeta_4 = -a_{Rg}\theta$$

Again solving for the α_i and substituting, the basic pitch equation becomes

$$BS^2\theta = a_{\theta\theta}\theta - 2(b_{\theta_F} a_{Fg} - b_{\theta_R} a_{Rg})K_{\theta}(H_h + H_z S^2)\theta \\ + 2[(b_{\theta_F} a_{Fg} - b_{\theta_R} a_{Rg})K_{\theta}H_h + (c_{\theta_F} a_{Fg} - c_{\theta_R} a_{Rg})]\theta_g$$

The resulting differential equation is given by

$$a_0 \theta'''' = -a_1 \theta''' - a_2 \theta'' - a_3 \theta' - a_4 \theta + b_0 \theta_g'' + b_1 \theta_g' + b_2 \theta_g$$

where now

$$a_0 = B\tau_z \tau_h + 2(b_{\theta_F} a_{Fg} - b_{\theta_R} a_{Rg})K_{\theta}K_z \tau_z \tau_h$$

$$a_1 = B(\tau_z + \tau_h) + 2(b_{\theta_F} a_{Fg} - b_{\theta_R} a_{Rg})K_{\theta}[K_z(\tau_z + \tau_h) + K_z \tau_z \tau_h]$$

$$a_2 = B - a_{\theta\theta} \tau_z \tau_h + 2K_{\theta}(b_{\theta_F} a_{Fg} - b_{\theta_R} a_{Rg})[K_h \tau_z \tau_h + (K_h + K_z)\tau_z + K_z]$$

$$a_3 = -a_{\theta\theta}(\tau_z + \tau_h) + 2K_{\theta}(b_{\theta_F} a_F - b_{\theta_R} a_R)[K_h(\tau_z + \tau_h) + K_h]$$

$$a_4 = -a_{\theta\theta} + 2K_{\theta}(b_{\theta_F} a_F - b_{\theta_R} a_R)K_h$$

$$b_0 = \tau_z[2(c_{\theta_F} a_F - c_{\theta_R} a_R)\tau_h + 2(b_{\theta_F} a_F - b_{\theta_R} a_R)K_{\theta}(K_h\tau_h + K_h)]$$

$$b_1 = 2(c_{\theta_F} a_F - c_{\theta_R} a_R)(\tau_z + \tau_h) + 2(b_{\theta_F} a_F - b_{\theta_R} a_R)(\tau_h K_h + K_h + \tau_z K_h)$$

$$b_2 = 2(c_{\theta_F} a_F - c_{\theta_R} a_R) + 2(b_{\theta_F} a_F - b_{\theta_R} a_R)K_z K_h$$

In polynomial form

$$\frac{\theta}{g} = \frac{b_0 s^2 + b_1 s + b_2}{a_0 s^4 + a_1 s^3 + a_2 s^2 + a_3 s + a_4}$$

By analogy, the yaw equation can also be written, i.e.,

$$a_0 \ddot{\psi} = a_1 \ddot{\psi} - a_2 \dot{\psi} - a_3 \psi + b_0 \ddot{\psi}_g + b_1 \dot{\psi}_g + b_2 \psi_g$$

where

$$a_0 = C\tau_y \tau_h' + 2(b_{\psi_F} a_F - b_{\psi_R} a_R)K_{\psi} K_{\psi} \tau_y \tau_h'$$

$$a_1 = C(\tau_y + \tau_h) + 2(b_{\psi_F} a_F - b_{\psi_R} a_R)K_{\psi}[K_{\psi}(\tau_y + \tau_h) + K_{\psi} \tau_y \tau_h']$$

$$a_2 = C - a_{\psi\psi} \tau_y \tau_h' + 2(b_{\psi_F} a_F - b_{\psi_R} a_R)K_{\psi}[K_h \tau_y \tau_h' + (K_h' + K_y) \tau_y + K_y]$$

$$a_3 = -a_{\psi\psi}(\tau_y + \tau_h) + 2(b_{\psi_F} a_F - b_{\psi_R} a_R)K_{\psi}[K_h(\tau_y + \tau_h) + K_h]$$

$$a_4 = a_{\psi\psi} + 2(b_{\psi_F} a_F - b_{\psi_R} a_R)K_{\psi} K_h$$

$$b_0 = \tau_y[2(d_{\psi_F} a_F - d_{\psi_R} a_R)\tau_h' + 2(b_{\psi_F} a_F - b_{\psi_R} a_R)K_{\psi}(K_h \tau_h' + K_h)]$$

$$b_1 = 2(d_{\psi_F} a_F - d_{\psi_R} a_R)(\tau_y + \tau_h) + 2(b_{\psi_F} a_F - b_{\psi_R} a_R)K_{\psi}(\tau_h K_h + K_h + \tau_y K_h)$$

$$b_2 = 2(d_{\psi_F} a_F - d_{\psi_R} a_R) + 2(b_{\psi_F} a_F - b_{\psi_R} a_R)K_{\psi} K_h'$$

In polynomial form

$$\frac{\psi}{\psi_g} = \frac{b_0 s^2 + b_1 s + b_2}{a_0 s^4 + a_1 s^3 + a_2 s^2 + a_3 s + a_4}$$

The derivation of the 2 DOF sway/roll equations is similar to the derivation of the 1 DOF equations. The major difference is the inclusion of guideway roll. Starting again with the 5 DOF equations given previously and considering only roll/sway,

$$\begin{bmatrix} m & 0 \\ 0 & A \end{bmatrix} \begin{bmatrix} \ddot{y} \\ \ddot{\phi} \end{bmatrix} = \begin{bmatrix} a_{yy} & a_{y\phi} \\ a_{\phi y} & a_{\phi\phi} \end{bmatrix} \begin{bmatrix} y \\ \phi \end{bmatrix} + \begin{bmatrix} b_y & b_y & b_y & b_y \\ b_\phi & b_\phi & b_\phi & b_\phi \end{bmatrix} \begin{bmatrix} \zeta_1 \\ -\zeta_2 \\ \zeta_3 \\ -\zeta_4 \end{bmatrix} \\ + \begin{bmatrix} c_y & c_y & c_y & c_y \\ c_\phi & c_\phi & c_\phi & c_\phi \end{bmatrix} \begin{bmatrix} \zeta_1 \\ -\zeta_2 \\ \zeta_3 \\ -\zeta_4 \end{bmatrix} + \begin{bmatrix} d_y & d_y & d_y & d_y \\ d_\phi & d_\phi & d_\phi & d_\phi \end{bmatrix} \begin{bmatrix} \eta_1 \\ -\eta_2 \\ \eta_3 \\ -\eta_4 \end{bmatrix} \\ + \begin{bmatrix} e_y & e_y & e_y & e_y \\ e_\phi & e_\phi & e_\phi & e_\phi \end{bmatrix} \begin{bmatrix} \phi_1 \\ -\phi_2 \\ \phi_3 \\ -\phi_4 \end{bmatrix} + \begin{bmatrix} Y_{\text{ext}} \\ L_{\text{ext}} \end{bmatrix}$$

where the guideway motions are

$$\begin{bmatrix} \zeta_1 \\ -\zeta_2 \\ \zeta_3 \\ -\zeta_4 \end{bmatrix} = \begin{bmatrix} -b\phi_g \\ -b\phi_g \\ -b\phi_g \\ -b\phi_g \end{bmatrix}$$

$$\begin{bmatrix} \eta_1 \\ -\eta_2 \\ \eta_3 \\ -\eta_4 \end{bmatrix} = \begin{bmatrix} y_g - C\phi_g \\ y_g - C\phi_g \\ y_g - C\phi_g \\ y_g - C\phi_g \end{bmatrix}$$

$$\begin{bmatrix} \phi_1 \\ -\phi_2 \\ \phi_3 \\ -\phi_4 \end{bmatrix} = \begin{bmatrix} \phi_g \\ \phi_g \\ \phi_g \\ \phi_g \end{bmatrix}$$

and the control currents are

$$\begin{bmatrix} \alpha_1 \\ -\alpha_2 \\ \alpha_3 \\ -\alpha_4 \end{bmatrix} = \begin{bmatrix} -K_y(H_h' - H_y S^2)y \\ " \\ " \\ " \end{bmatrix}$$

$$+ \begin{bmatrix} [c(K_\phi - K_y)(H_h + H_z S^2) + cK_y(H_h' + K_y S^2) + K_y H_y g]\phi \\ " \\ " \\ " \end{bmatrix}$$

$$\begin{bmatrix} K_y H_y g \\ " \\ " \\ " \end{bmatrix} + \begin{bmatrix} c[(K_y - K_\phi)H_h - K_y H_h']\phi_g \\ " \\ " \\ " \end{bmatrix}$$

Substituting in for the guideway motions and the control currents gives the basic sway/roll equations

$$\begin{bmatrix} m & 0 \\ 0 & A \end{bmatrix} \begin{bmatrix} \ddot{y} \\ \ddot{\phi} \end{bmatrix} = \begin{bmatrix} a_{yy} & a_{y\phi} \\ a_{\phi y} & a_{\phi\phi} \end{bmatrix} \begin{bmatrix} y \\ \phi \end{bmatrix} \\
 + \begin{bmatrix} -4b_y K_y (H_h' + H_y S^2) & 4b_y [c(K_\phi - K_y)(H_h + H_z S^2) + cK_y (H_h + H_y S^2) + K_y H_y g] \\ -4b_\phi K_y (H_h' + H_y S^2) & 4b_\phi [c(K_\phi - K_y)(H_h + H_z S^2) + cK_y (H_h + H_y S^2) + K_y H_y g] \end{bmatrix} \begin{bmatrix} y \\ \phi \end{bmatrix} \\
 + \begin{bmatrix} 4b_y K_y H_h' + 4d_y & 4b_y c[(K_y - K_\phi)H_h - K_y H_h'] - 4bc_y - 4cd_y + 4e_y \\ 4b_\phi K_y H_h' + 4d_\phi & 4b_\phi c[(K_y - K_\phi)H_h - K_y H_h'] - 4bc_\phi - 4cd_\phi + 4e_\phi \end{bmatrix} \begin{bmatrix} y_g \\ \phi_g \end{bmatrix}$$

where the signal filters are

$$H_h = K_h + \frac{K_h S}{1 + \tau S} \quad , \quad H_h' = K_h' + \frac{K_h' S}{1 + \tau S} \\
 H_z = K_z + \frac{K_z \tau}{1 + \tau S} \quad , \quad H_y = K_y + \frac{K_y \tau}{1 + \tau S}$$

Multiplying out the filter terms results in the following set of differential equations for the roll/sway motion:

$$\begin{aligned}
 a_{011} \ddot{y} + a_{111} \dot{y} + a_{211} y + a_{311} y + a_{012} \ddot{\phi} + a_{112} \dot{\phi} + a_{212} \phi + a_{312} \phi &= \\
 = b_{011} \dot{y}_g + b_{111} y_g + b_{012} \dot{\phi}_g + b_{112} \phi_g & \\
 a_{021} \ddot{y} + a_{121} \dot{y} + a_{221} y + a_{321} y + a_{022} \ddot{\phi} + a_{122} \dot{\phi} + a_{222} \phi + a_{322} \phi &= \\
 = b_{021} \dot{y}_g + b_{121} y_g + b_{022} \dot{\phi}_g + b_{122} \phi_g &
 \end{aligned}$$

where $\tau = \tau_z = \tau_h = \tau_y = \tau_h'$, and

$$a_{o_{11}} = m\tau + 4b_y K_y K_y \tau$$

$$a_{1_{11}} = m + 4b_y K_y (K_y \tau + K_y)$$

$$a_{2_{11}} = -a_{yy} \tau + 4b_y K_y (K_h \tau + K_h)$$

$$a_{3_{11}} = -a_{yy} + 4b_y K_y K_h'$$

$$a_{o_{12}} = -4b_y c \tau [(K_\emptyset - K_y) K_z + K_y K_y]$$

$$a_{1_{12}} = -4b_y c [(K_\emptyset - K_y) (K_z \tau + K_z) + K_y (K_y \tau + K_y)]$$

$$a_{2_{12}} = -a_{y\emptyset} \tau - 4b_y c [(K_\emptyset - K_y) (K_h \tau + K_h) + K_y (K_h \tau + K_h)]$$

$$-4b_y K_y g K_y \tau$$

$$a_{3_{12}} = -a_{y\emptyset} - 4b_y c [(K_\emptyset - K_y) K_h + K_y K_h'] - 4b_y K_y g (K_y \tau + K_y)$$

$$a_{o_{21}} = 4b_\emptyset K_y K_y \tau$$

$$a_{1_{21}} = 4b_\emptyset K_y (K_y \tau + K_y)$$

$$a_{2_{21}} = -a_{\emptyset y} \tau + 4b_\emptyset K_y (K_h \tau + K_h)$$

$$a_{3_{21}} = -a_{\emptyset y} + 4b_\emptyset K_y K_h'$$

$$a_{o_{22}} = A\tau - 4b_\emptyset c \tau [(K_\emptyset - K_y) K_z + K_y K_y]$$

$$a_{1_{22}} = A - 4b_\emptyset c [(K_\emptyset - K_y) (K_z \tau + K_z) + K_y (K_y \tau + K_y)]$$

$$a_{2_{22}} = -a_{\emptyset\emptyset} \tau - 4b_\emptyset c [(K_\emptyset - K_y) (K_h \tau + K_h) + K_y (K_h \tau + K_h)]$$

$$-4b_\emptyset K_y g K_y \tau$$

$$a_{322} = -a_{\emptyset\emptyset} - 4b_{\emptyset}c[(K_{\emptyset} - K_y)K_h + K_y K_{h'}] - 4b_{\emptyset}K_y g(K_{\emptyset} + K_y)$$

$$b_{o11} = 4b_y K_y (K_h \tau + K_{h'}) + 4d_y \tau$$

$$b_{l11} = 4b_y K_y K_{h'} + 4d_y$$

$$b_{o12} = -4b_y c[(K_{\emptyset} - K_y)(K_h \tau + K_{h'}) - K_y (K_{h'} \tau + K_{h'})]$$

$$-4bc_y \tau - 4cd_y \tau + 4e_y \tau$$

$$b_{l12} = -4b_y c[(K_{\emptyset} - K_y)K_h - K_y K_{h'}] - 4bc_y - 4cd_y + 4e_y$$

$$b_{o21} = 4b_{\emptyset}K_y (K_h \tau + K_{h'}) + 4d_{\emptyset} \tau$$

$$b_{l21} = 4b_{\emptyset}K_y K_{h'} + 4d_{\emptyset}$$

$$b_{o22} = -4b_{\emptyset}c[(K_{\emptyset} - K_y)(K_h \tau + K_{h'}) - K_y (K_{h'} \tau + K_{h'})]$$

$$-4bc_{\emptyset} \tau - 4cd_{\emptyset} \tau + 4e_{\emptyset} \tau$$

$$b_{l22} = -4b_{\emptyset}c[(K_{\emptyset} - K_y)K_h - K_y K_{h'}] - 4bc_{\emptyset} - 4cd_{\emptyset} + 4e_{\emptyset}$$

APPENDIX C

STABILITY ANALYSIS AND GAIN SELECTION

By C. C. Wan

The final form of the equations of motion for the MAGLEV vehicle (including control functions) revealed the fact that vehicle stability may be treated in two separate parts (Appendix B). Due to the symmetrical placement of the levitation coil assemblies on the vehicle, the vertical degrees of freedom (heave and pitch) and the lateral degrees of freedom (sidesway, roll, and yaw) are not dynamically coupled. Furthermore, the vehicle dynamics part of the equations for these two sets has the same mathematical form. A method of stability analysis of these two sets is described in this Appendix. Some sample results of variations in control gains are also presented to illustrate the process of gain selection.

C.1. DELINEATION OF CONTROL PARAMETERS

The baseline control concept for the vehicle includes both relative damping by means of gap sensors, and absolute damping by means of accelerometers attached to the coil assemblies. Allowing for the fact that identical networks are to be used for signal filtering at each of the four coil assemblies, it becomes necessary to consider the following eight control gains and four time constants to provide the required functions in both vertical and lateral directions.

- (a) Gap sensor - vertical direction

$$K_h + K_h^* s / (1 + \tau_h s) \rightarrow K_h, K_h^*, \tau_h$$

- (b) Gap sensor - lateral direction

$$K_{h'} + K_{h'}^* s / (1 + \tau_{h'} s) \rightarrow K_{h'}, K_{h'}^*, \tau_{h'}$$

(c) Acceleration - vertical direction

$$K_z + K_z \tau_z / (1 + \tau_z s) \rightarrow K_z, K_z, \tau_z$$

(d) Acceleration - lateral direction

$$K_y + K_y \tau_y / (1 + \tau_y s) \rightarrow K_y, K_y, \tau_y$$

These 16 filtered signals (four signals from each of the four sensor locations) are then transformed into five modal signals which are further modified by five modal gain constants before resolution into four control current commands. The five modal gain constants are:

- (a) Heave gain, K_z
- (b) Pitch gain, K_θ
- (c) Sidesway gain, K_y
- (d) Roll gain, K_ϕ
- (e) Yaw gain, K_ψ

Appropriate values for these gain constants and time constants are required to ensure vehicle stability and to provide adequate ride quality for specified guideway irregularity standards.

The question of vehicle stability is to be resolved first. It may be observed that some of the gain constants can be determined from consideration of simplified analyses, such as those treated in Section 4.3.2 of this report. A general approach would be to examine the behavior of the roots of the characteristic equation formed by equating the determinant of the coefficients of the vehicle state variables to zero. A numerical process for locating these roots without explicit expansion of the determinant is described in the following paragraphs.

C.2 FORMULATION OF THE CHARACTERISTIC EQUATION

The left-hand side of the equations of motion for the (Z, θ) group and the (Y, ϕ, ψ) group have the same form, as shown below:

$$[s^2 I_s - A_s + R_s K_{Os}(s)] q_s = \dots \quad (R_s = B_s Q_{ss} K_s)$$

$$[s^2 I_A - A_A + R_A K_{OA}(s)] q_A = \dots \quad (R_A = B_A Q_{AA} K_A)$$

where

$$K_{0s}(s) = s^2 H_s + H_h = \left(s^2 \left(K_z + K_z \frac{\tau_z}{1 + \tau_z s} \right) + \left(K_h + K_h \frac{s}{1 + \tau_h s} \right) \right) \cdot I_4$$

$$\bar{K}_{0A}(s) = s^2 H_A + H_{h'} = \left(s^2 \left(K_y + K_y \frac{\tau_y}{1 + \tau_y s} \right) + \left(K_{h'} + K_{h'} \frac{s}{1 + \tau_{y'} s} \right) \right) \cdot I_4$$

$$K_{0A}(s) = \bar{K}_{0A}(s) + [\bar{K}_{0A} - K_{0s}] P_{As} Q_{sA}$$

The subscripts will be dropped, and a number of new variables will be identified as follows: the $K_0(s)$ matrix is diagonal with identical elements which are a rational function in s , expressible as a fraction of two polynomials in s as:

$$K_0(s) = \frac{k_4 s^4 + k_3 s^3 + k_2 s^2 + k_1 s + k_0}{d_2 s^2 + d_1 s + d_0}$$

Expressions for the k 's and the d 's are summarized in Table C-1 in terms of t 's which are identified with the appropriate gain constants.

The left-hand side of the equations of motion may be written as

$$\left[s^2 I - A + \frac{k_4 s^4 + k_3 s^3 + k_2 s^2 + k_1 s + k_0}{d_2 s^2 + d_1 s + d_0} R \right] q = 0$$

or

$$\left[\begin{array}{l} s^4 [d_2 I + k_4 R] + s^3 [d_1 I + k_3 R] + s^2 [d_0 I - d_2 A + k_2 R] \\ + s [-d_1 A + k_1 R] + [-d_0 A + k_0 R] \end{array} \right] \bar{q} = 0$$

where

$$\bar{q} = \frac{1}{d_2 s^2 + d_1 s + d_0} q$$

The maximum possible order of the characteristic equation is thus $4N$ where N is the number of state variables. $N = 2$ for the (Z, θ) group and

TABLE C-1. EXPANSION OF SIGNAL FILTER FUNCTIONS

	t_1	t_2	t_3	t_4	t_5	t_6	t_7
$K_{0s}(s)$	τ_h	τ_f	K_h	K_h	K_z	K_f	K_{z0}
$\bar{K}_{0s}(s)$	τ_h'	τ_f'	K_h'	K_h'	K_z'	K_f'	K_{z0}'

$$K_o(s) = t_3 + \frac{t_4 s}{(1+t_1 s)} + \left[t_5 + \frac{t_6 t_2}{(1+t_2 s)} \right] s^2, t_2 \neq 0$$

$$= t_3 + t_7 s + t_9 s^2, t_1 = t_2 = 0$$

	$t_1 \neq t_2 \neq 0$	$t_1 = t_2 \neq 0$	$t_1 = 0$	$t_1 = t_2 = 0$
d_0	1	1	1	1
d_1	$t_1 + t_2$	t_1	t_2	0
d_2	$t_1 t_2$	0	0	0
k_0	t_3	t_3	t_3	t_3
k_1	$t_2 t_3 + (t_1 t_3 + t_4)$	$t_1 t_3 + t_4$	$t_2 t_3 + t_4$	$t_1 + t_4$
k_2	$t_2 (t_1 t_3 + t_4) + (t_5 + t_2 t_6)$	$t_5 + t_2 t_6$	$t_2 t_4 + (t_5 + t_2 t_6)$	t_5
k_3	$t_1 (t_5 + t_2 t_6) + t_2 t_5$	$t_2 t_5$	$t_2 t_5$	0
k_4	$t_1 t_2 t_5$	0	0	0

$N = 3$ for the (Y, Φ, Ψ) group. The lowest possible order is $2N$ for the case where $t_1 = t_2 = 0$.

The case of $t_1 = t_2 = 0$ corresponds to no signal filtering. In this case system damping is introduced as t_7 . It is interesting to note that when $t_1 = t_2 \neq 0$ the function $k_0(s)$ can be reduced to a simple polynomial (unit denominator) if $t_4 = t_6$ (for example, $= t_7$)

$$\begin{aligned} K_0(s) &= t_3 + \frac{t_4 s}{1 + t_1 s} + \left[t_s + \frac{t_6 t_1}{1 + t_1 s} \right] s^2 \\ &= t_3 + \frac{(t_4 + t_1 t_6 s) s}{1 + t_1 s} + t_s s^2 = t_3 + t_7 s + t_s s^2 \end{aligned}$$

The search for control parameter "s" can thus be made, in this case, without any consideration of signal filtering. The value of t_7 found in this manner can also be used to provide a convenient starting value in the search for both t_4 and t_6 for cases where signal filtering is considered.

C.3 EXPANSION OF THE CHARACTERISTIC DETERMINANT

For no signal-filtering explicit expansion of the characteristic determinant can readily be performed. However, when signal filtering is included, explicit expansion becomes unwieldy. A process based on an exact fit of a polynomial of n-th order through $(n+1)$ data points is used instead.

The highest power of the characteristic equation is known in advance, as it depends on the number of state variables involved in the problem, and on whether the two time-constants are equal to each other. Let this be M_0 . Select a sequence of $\pm s_i$ ($i = 1$ to M) and 0 for s, with

$$\begin{aligned} M &= M_0/2 && \text{For } M_0 \text{ even} \\ &= (M_0 + 1)/2 && \text{For } M_0 \text{ odd} \end{aligned}$$

Let D_i^\pm and D_0 denote, respectively, the numerical values of the characteristic determinant when s takes the values $\pm s_i$ and 0. Since

$$D(s) = a_0 + a_1 s + a_2 s^2 + \dots + a_i s^i + \dots + a_{M_0} s^{M_0} + \frac{a_{M_0+1} s^{M_0+1}}{\dots}$$

(where the last term is included only when M_0 is odd). It follows that

$$\begin{bmatrix} s_i^{2M} & s_i^{2M-1} & \dots & s_i^2 & s_i & 1 \\ -s_i^{2M} & -s_i^{2M-1} & \dots & s_i^2 & -s_i & 1 \\ 0 & 0 & \dots & 0 & 0 & 1 \end{bmatrix} \begin{bmatrix} a_{2M} \\ a_{2M-1} \\ \vdots \\ a_1 \\ a_0 \end{bmatrix} = \begin{bmatrix} D_i^+ \\ D_i^- \\ D_0 \end{bmatrix}$$

This relation may be reduced, through addition and subtraction of appropriate equation pairs, to

$$\begin{bmatrix} s_i^{2M-2} & s_i^{2M-4} & \dots & s_i^2 & 1 \\ \dots & \dots & \dots & \dots & \dots \\ a_2 & a_1 \end{bmatrix} \begin{bmatrix} a_{2M} & a_{2M-1} \\ a_{2M-2} & a_{2M-3} \\ \dots & \dots \\ a_2 & a_1 \end{bmatrix} = \begin{bmatrix} \frac{D_i^+ + D_i^- - 2D_0}{2s_i^2}, \frac{D_i^+ - D_i^-}{2s_i} \end{bmatrix}$$

The matrix containing elements which are even powers of s is precisely that occurring in the least-square fit of polynomials. Thus, a unique solution for the coefficient a_i can be obtained from the above matrix equation.

For M_0 odd, the coefficient a_{2M} is identically zero, although round-off in digital computers tends to result in certain residual value. It is only necessary to ignore the value for a_{2M} when M_0 is odd.

To avoid overflow during digital computation, the sequence s_i can be chosen in the following manner. Let $s_i = \beta^{i-1}$, and make use of the condition that the product of the left-handed diagonal of the characteristic determinant cannot exceed certain value, say 10^K , then

$$\prod_{i=1}^M s_i^{2(i-1)} \leq 10^K$$

or

$$\prod_{i=1}^M \beta^{2(i-1)^2} \leq 10^K$$

Since

$$\sum_{i=1}^M n^2 = M(M+1)(2M+1)/6$$

$$(\log_{10} \beta) (M-1) (2M-1) M/3 \leq K$$

or

$$\beta \leq 10^{\lceil 3K/(M-1)(2M-1)M \rceil}$$

For practical computation, β can be assigned the value of 2 or the above expression, whichever is smaller. For $K = 10$ the following values are obtained.

M	2	3	4	5	6	7	8
β	2	2	2	1.5	1.25	1.14	1.09

C.4. GAIN SELECTION

Once the coefficients of the characteristic equation are determined, the roots can be obtained by any of the known methods. Selection of gain constants thus becomes a search process, wherein the objective is that all roots must have negative real parts to ensure stability. Since the control function specified by a set of gain constants is incorporated into the vehicle dynamics, the response of the vehicle to guideway-related driving functions must satisfy certain requirements. Therefore, it would seem preferable to have system damping approaching critical damping. Two examples are presented below to illustrate some features of the gain selection process.

C.5. RESULTS FOR HEAVE/PITCH MODE WITHOUT SIGNAL FILTERING

Results for an illustrative case of the revenue vehicle heave/pitch mode are presented in Figure C-1, showing the effects of the control parameter K_2 and modal gain K_θ . It has been determined from a single-degree-of-freedom heave model that $K_h = -2.155$. For the example shown in Figure C-1, there is

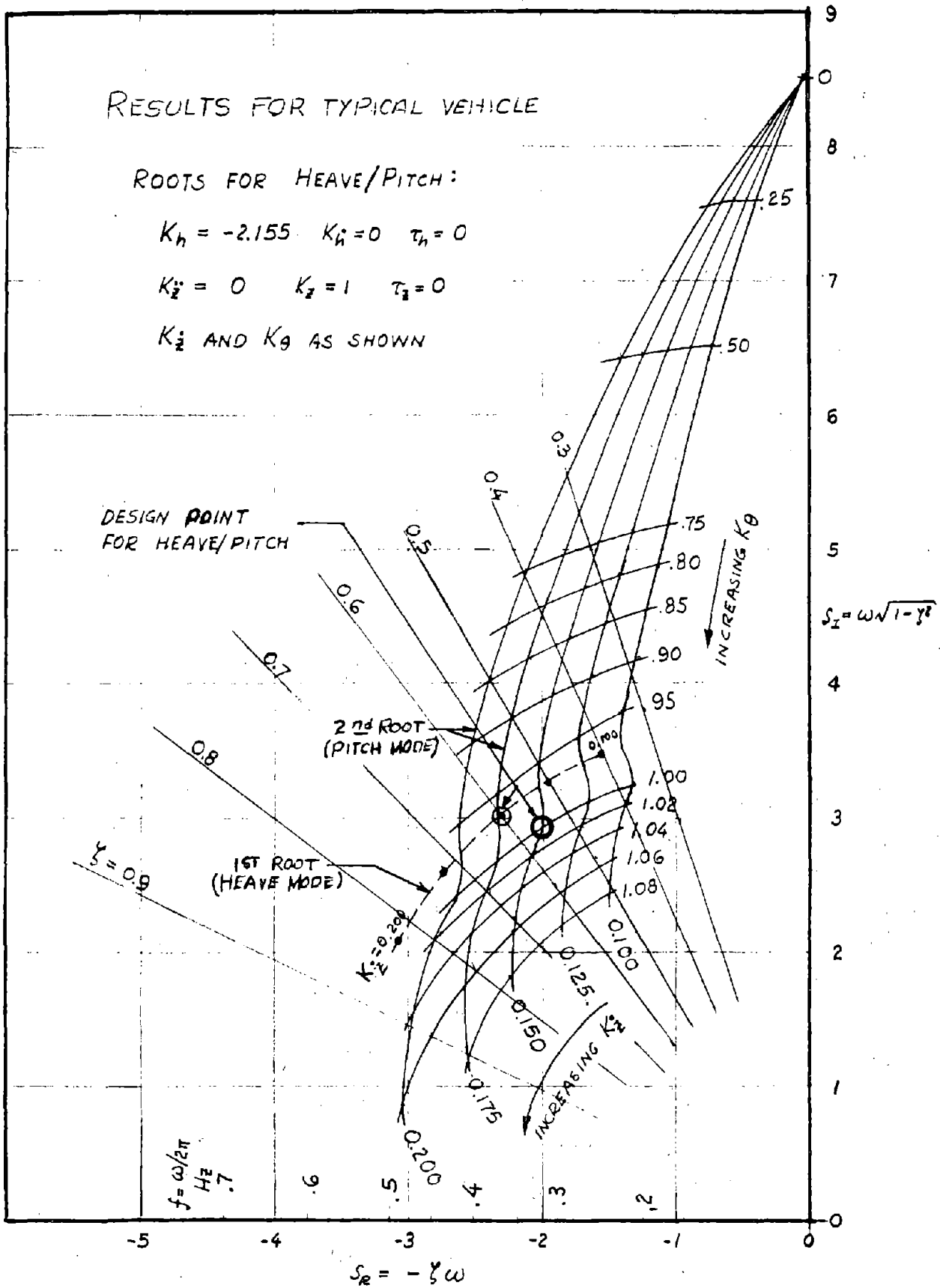


FIGURE C-1. EXAMPLE OF VERTICAL STABILITY

also zero acceleration feedback, i.e., $K_z = 0$. A value of 0.15 has been used for damping in heave (K_z), corresponding to a 0.6 damping ratio.

For the heave/pitch mode, one root is essentially a function of K_z , while the second root depends on both K_z and K_θ . The first root reflects the one-degree-of-freedom solution, which corresponds to an undamped frequency of 0.6 Hz and 0.6 damping ratio. Selection of a value of 1.0 for the modal gain in pitch (K_θ), gives rise to a second undamped frequency of 0.56 Hz with 0.55 damping ratio.

C.6. RESULTS FOR SIDESWAY/ROLL/YAW MODES WITH SIGNAL FILTERING

Three state variables are present in the lateral modes. It becomes necessary to seek gain constant combinations which will lead to a pair of double roots. The reason for this strategy stems from the fact that a change in gain produces opposite changes in system damping in two related modes. Results for one of a series of parameter studies for the sidesway/roll/yaw modes of the revenue vehicle are shown in Figure C-2. Values used for modal gains K_ϕ and K_ψ have been chosen from prior studies to be 1.25 and 3.5, respectively. K_h is taken to be zero to reduce response magnitudes, and K_z is taken to be -0.02 to improve system damping. A time constant of 0.637 is used for all channels.

A double root is found for $K_y \approx 0.518$ and $K_h = K_h' \approx 0.294$, corresponding to undamped frequencies of 0.60 Hz at 0.8 damping ratio and 1.02 Hz at 0.68 damping ratio.

$$K_h = 0 \quad K_y = -0.02 \quad K_\phi = 1.25$$

$$\tau_h = .637 \quad \tau_y = .637 \quad K_\psi = 3.5$$

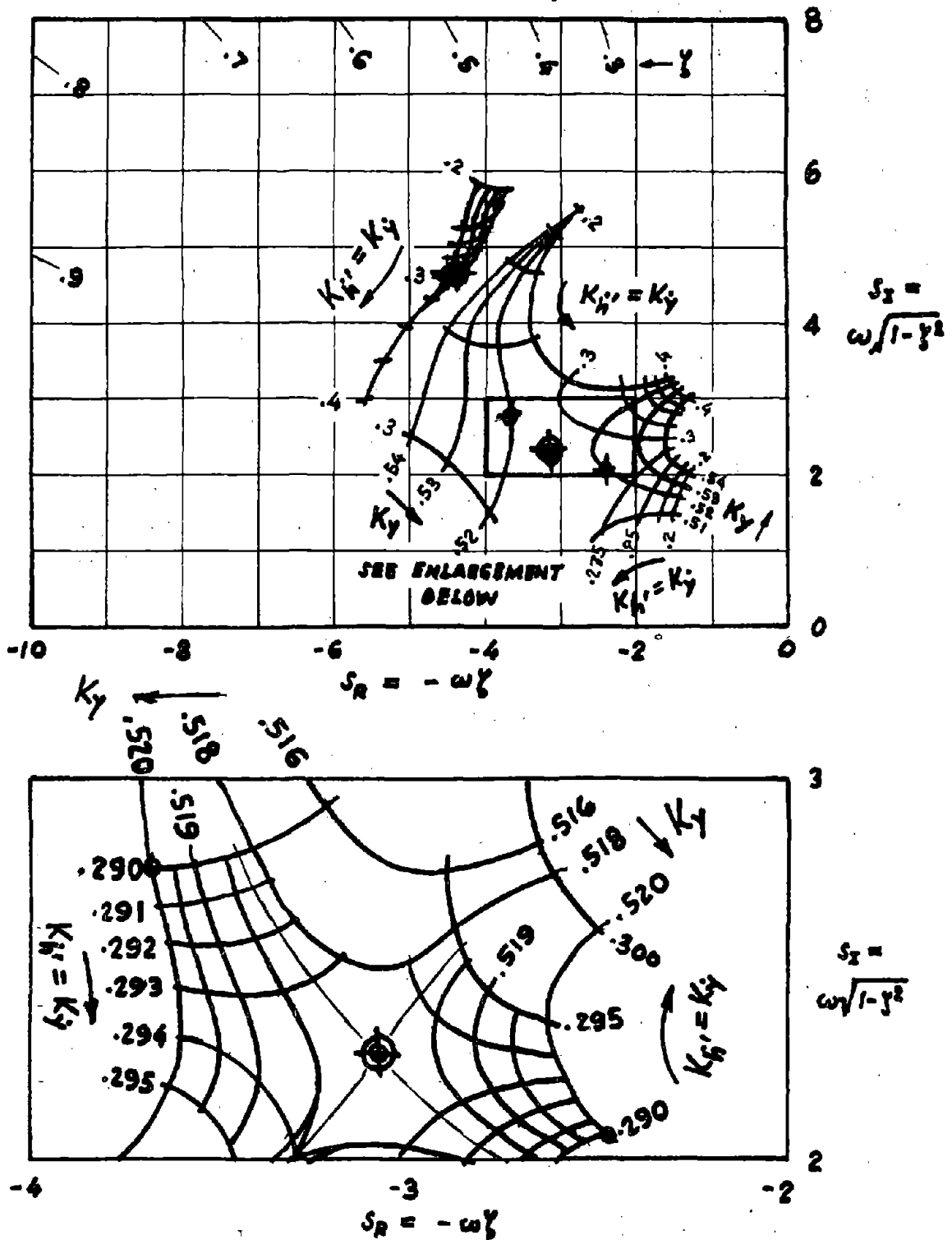


FIGURE C-2. EXAMPLE OF LATERAL MODE PARAMETRIC STUDY

APPENDIX D

FREQUENCY RESPONSE SOLUTION TECHNIQUES

By C. C. Wan

Calculation of vehicle response to guideway irregularities for ride quality assessment makes use of superposition of basic frequency responses for state variables as defined by the system of linearized equations of motion formulated in Appendix B. Techniques used to determine these frequency response functions and to construct ride quality power spectrum functions and assess control power requirements are summarized in this appendix.

D.1. FREQUENCY RESPONSE CALCULATIONS

Two types of terms are present in the right hand side of the equations formulated in Appendix B:

$$\begin{aligned}
 [s^2 I_S - A_S + B_S Q_{SS} K_S K_{OS}] q_S &= [B_S Q_{SS} K_S P_{SS} H_h + C_S] \zeta + [D_S] \eta + [L_S] \\
 [s^2 I_A - A_A + B_A Q_{AA} K_A K_{OA}] q_A &= [B_A Q_{AA} K_A P_{AA} H_h + C_A] \zeta + [B_A Q_{AA} K_A P_{AA} H_h + D_A] \eta \\
 &+ [L_A]
 \end{aligned}$$

The L matrices contain only constant terms which lead to the determination of the initial equilibrium position of the vehicle. The ζ and η matrices denote deviations of the guideway from nominal positions at the individual coil locations. For frequency response calculations, all these elements are periodic functions of time of the same frequency, and the use of complex amplitude coefficients accounts for any phase difference that may exist between the various elements. Due to the presence of the filter function in the K_{OA} , K_{OS} , H_h , and H_h matrices, frequency responses are most readily obtained at a given frequency by making the substitution $s = i\omega$, which leads to the solution of a system of simultaneous equations with complex coefficients.

D.2 DECOMPOSITION OF GUIDEWAY IRREGULARITIES

The ζ and η matrices contain eight amplitude coefficients which define the variation of guideway irregularities in two directions at each of the four

coil locations. These may be systematically resolved into symmetric and anti-symmetric components in order to facilitate further computations.

Consider a single L-shaped track with irregularities only in the vertical direction. For irregularities with a wavelength L , the profile of the guideway surface is characterized by

$$A \sin [(x-x_0)2\pi/L] = A \sin(\omega t - \phi_0) \quad \text{with } \omega = 2 V/L$$

where V is the forward speed of the vehicle and x_0 and ϕ_0 denote a phase measure of the particular component. It will be convenient to use the midpoint of the front and rear coil positions as a reference point for phase measurement, so that the four types of guideway irregularities, as illustrated in Figure D-1, can be combined to represent individual guideway profiles as follows:

$$\zeta_R = A_1 \sin(\omega t - \phi_0) + A_2 \sin(\omega t - \phi_z)$$

$$\zeta_L = A_1 \sin(\omega t - \phi_0) - A_2 \sin(\omega t - \phi_z)$$

$$\eta_R = A_3 \sin\omega t + A_4 \sin(\omega t - \phi_y)$$

$$\eta_L = -A_3 \sin\omega t + A_4 \sin(\omega t - \phi_y)$$

Guideway deviation under individual coils may be determined by adding an additional phase angle defined by

$$\beta = \pi(a_F + a_R)/L$$

Guideway deviation at any other points on the vehicle, at distance x from the vehicle center of gravity, may be determined by adding an additional phase angle defined by

$$\beta(x) = (2x - a_F + a_R)/L$$

D.3. UNIT SOLUTIONS

Unit solutions for frequency responses are readily obtained for the eight types of guideway irregularity configurations depicted in Figure D-1. For a vehicle with a finite "wheel base," each type of irregularity consists of an in-phase and out-of-phase component. Therefore, there are eight basic types of unit solutions. Amplitude coefficients and additional phase angles

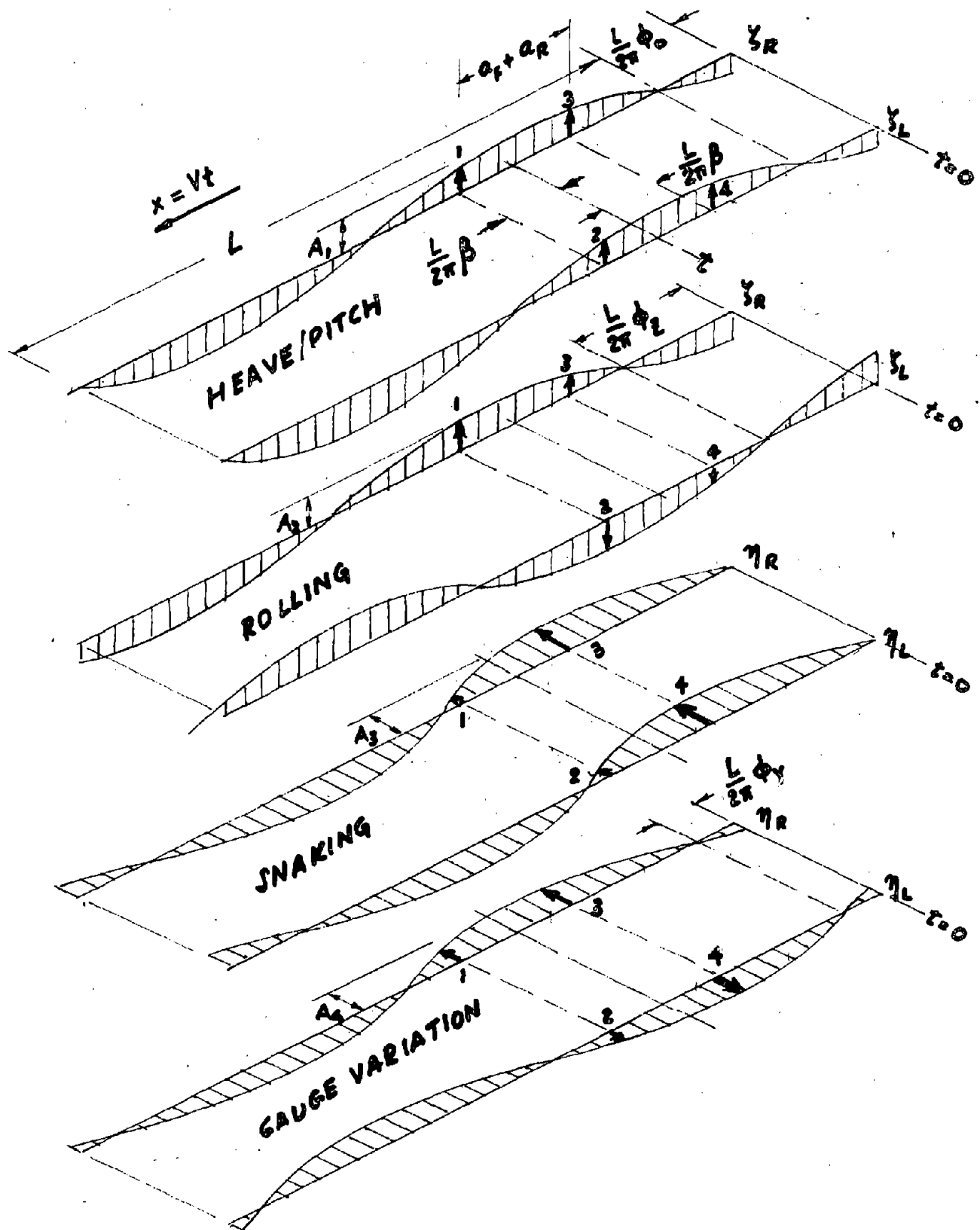


FIGURE D-1. DECOMPOSITION OF GUIDEWAY IRREGULARITIES

for each of these unit forcing functions (ζ and η) are listed in Table D-1. Frequency responses for the five vehicle state variables are thus determined as a (5,8) complex matrix for each value of frequency of interest.

D.4. CONTROL CURRENT COMMANDS AND POWER REQUIREMENT

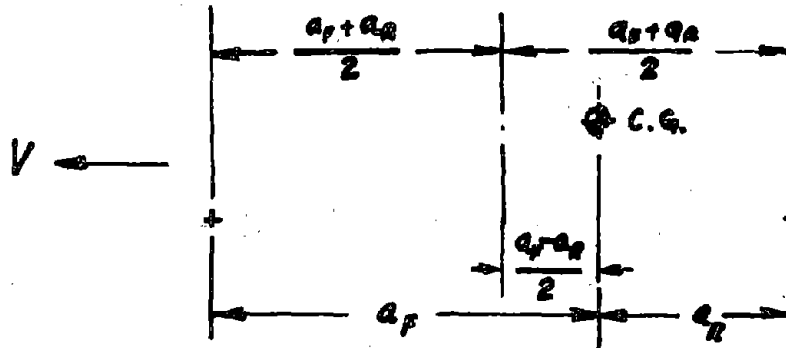
Control current commands for each coil result from a formal matrix multiplication process applied to the unit solution at each frequency. The control current commands are obtained as a weighted sum of the unit solution control current commands for each given irregularity specification.

Control power required (in addition to the I^2R loss in the control coil) is determined as the sum of work done by the control forces and moments on the associated displacements at each of the four coil assemblies. Computational procedures for both the current and power are summarized in Table D-2.

D.5. GENERATION OF RESPONSE AND RIDE QUALITY DATA

Frequency responses of vehicle displacements and accelerations at any arbitrary point on the vehicle are obtained by appropriate superposition of rigid body responses referred to the vehicle center of gravity. These are formed directly from the unit solutions as modulated by the amplitude of the specified guideway roughness power spectral density function. The power spectral density function describing the random characteristics of the guideway is applied directly to the square of related response quantities to generate the relevant response power spectral density variation.

TABLE D-1. UNIT INPUTS FOR GUIDEWAY IRREGULARITIES



$$\omega = 2\pi V/L$$

$$\beta = \omega(a_f + a_r)/2V$$

$$= \frac{\pi(a_f + a_r)}{L}$$

L = WAVELENGTH

RESPONSE TYPE	HEAVE / PITCH				SIDESWAY / ROLL / YAW			
TYPE IRREG.	A ₁		A ₄		A ₂		A ₃	
Y ₁	+1	+1	0	0	+1	+1	0	0
Y ₂	+1	+1	0	0	-1	-1	0	0
Y ₃	+1	-1	0	0	+1	-1	0	0
Y ₄	+1	-1	0	0	-1	+1	0	0
η ₁	0	0	+1	+1	0	0	+1	+1
η ₂	0	0	+1	+1	0	0	-1	-1
η ₃	0	0	+1	-1	0	0	+1	-1
η ₄	0	0	+1	-1	0	0	-1	+1
EFFECT OF "WHEEL BASE"	cβ	sβ	cβ	sβ	cβ	sβ	cβ	sβ
PHASE ANGLE RELATIVE TO TYPE 3 (A ₃)	-Φ ₀	-Φ ₀ +π/2	-Φ _γ	-Φ _γ +π/2	-Φ ₂	-Φ ₂ +π/2	0	+π/2

TABLE D-2. CONTROL CURRENT AND CONTROL POWER EQUATIONS

CONTROL CURRENT COMMANDS

$$\alpha = \begin{bmatrix} \alpha_1^R + \alpha_1^I \\ \alpha_2^R + \alpha_2^I \\ \alpha_3^R + \alpha_3^I \\ \alpha_4^R + \alpha_4^I \end{bmatrix} = - [Q_{SS} K_S K_{OS}] q_S - [Q_{AA} K_A K_{OA}] q_A + \\ + [Q_{SS} K_S P_{SS} + Q_{AA} K_A P_{AS}] [H_A] \gamma + [Q_{AA} K_A P_{AA}] [H_b] \gamma$$

MEAN CONTROL POWER (NOT INCLUDING I^2R LOSSES)

$$\langle P \rangle = \frac{\omega}{2} (P_{12} - P_{21}) \quad \text{WITH } P_{12} \text{ AND } P_{21} \text{ FROM}$$

$$\begin{bmatrix} P_{11} & P_{12} \\ P_{21} & P_{22} \end{bmatrix} = (F_{L\alpha}) A Q_{SS} q_S + (F_{L\alpha} + \frac{L\alpha}{b}) A Q_{SA} q_A + (F_{G\alpha}) A Q_A q_A$$

WHERE

$$[A] = \begin{bmatrix} \alpha_1^R & \alpha_2^R & \alpha_3^R & \alpha_4^R \\ \alpha_1^I & \alpha_2^I & \alpha_3^I & \alpha_4^I \end{bmatrix}$$

APPENDIX E

Q-FAN PROPULSION SYSTEM ACOUSTIC CHARACTERISTICS*

By B.S. Gatzert (Hamilton Standard)

E.1. FAN SOURCE NOISE

For the past several years Hamilton Standard has continued to develop both experimental and analytical tools for the design of quiet fans. To date four fans have been designed which incorporate the state-of-the-art noise reduction technology. Hamilton Standard uses a computer program that allows prediction of fan noise based on performance and configuration inputs. This method includes procedures for calculating rotor noise, stator noise, and jet noise. Emphasis has been placed on developing theoretically-based methods that do not rely on empirical corrections to establish correlation with test data.

The methodology used for the MAGLEV study has been shown to be accurate in correlation studies between measured and predicted fan noise levels. Figure E-1 shows this excellent agreement for the four fans tested. These results lend confidence to the predictions of unsuppressed MAGLEV fan noise.

Hamilton Standard is continuing its research in order to understand better the mechanisms of fan noise generation. Continued development will undoubtedly lead to reductions up to ~10 dB in source noise under cruise conditions. These reductions will be the result of understanding the basic noise generation mechanisms, incorporating systems to suppress the noise and/or designing the fan to avoid generation of noise. An example of a noise suppression system that may prove useful is boundary layer control. Such a system applied to the rotor could minimize the wake defect that creates fluctuating lift at the stator which produces the rotor-stator interaction noise.

*Some of the information presented in this appendix was given in the paper, "Quiet Air Propulsion for High Speed Ground Transportation", by F.B. Metzger at the International Conference on High Speed Ground Transportation, Arizona State University, January 7, 1975.

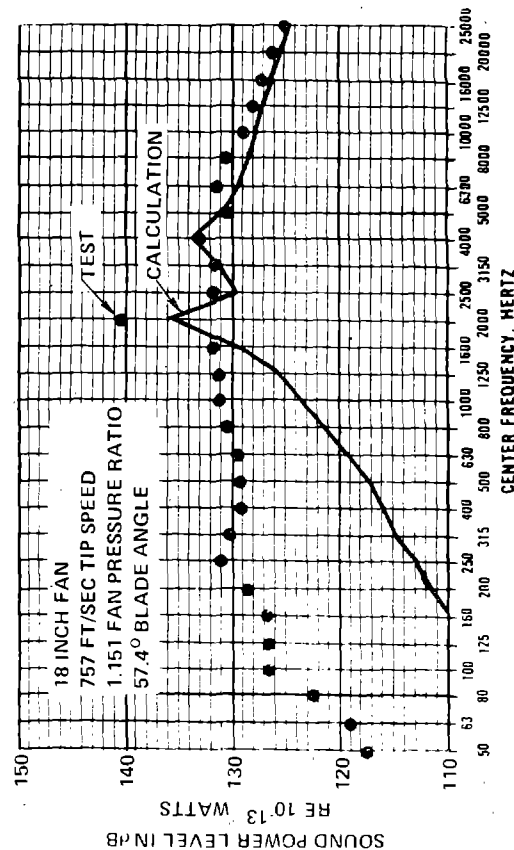
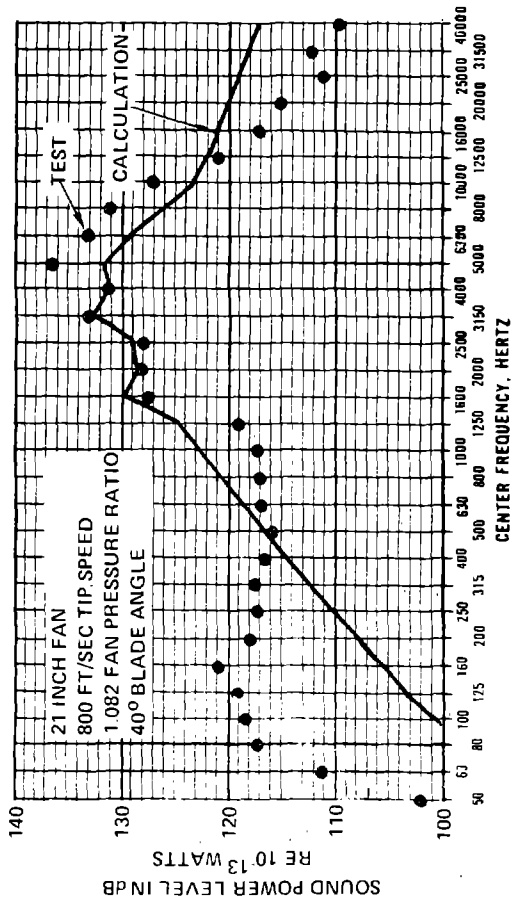
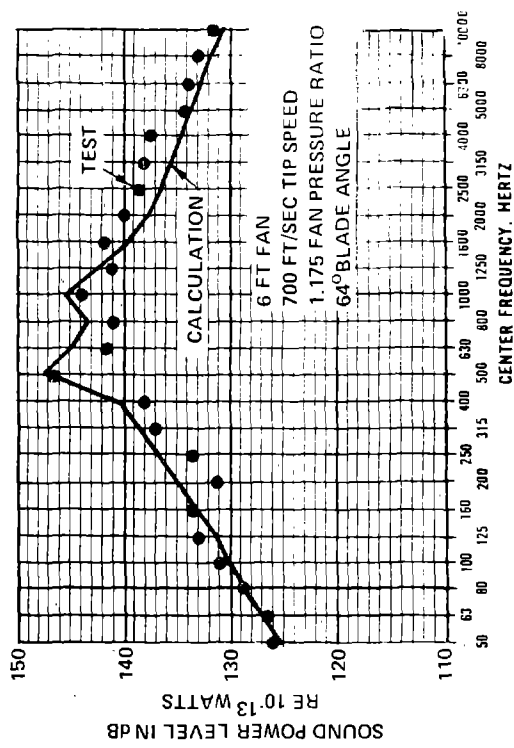
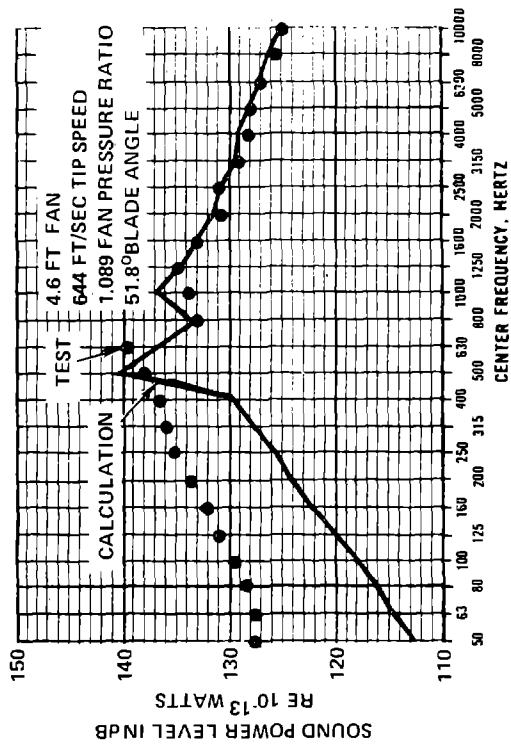


FIGURE E-1. COMPARISON OF TEST RESULTS WITH PREDICTIONS

U A

Hamilton
Standard

E.2 ENGINE SOURCE NOISE

Core engine noise has received little attention until very recent work sponsored by the United States Air Force Aero Propulsion Laboratory and the Federal Aviation Administration. This is due to the fact that the jet noise of early aircraft engines dominated the engine noise signature. The fan noise became the dominant engine noise in later low bypass ratio turbofans with inlet guide vanes. Only in the latest high bypass ratio turbofans used on widebodied transport aircraft has the core engine noise become noticeable.

The very high bypass ratio of the Q-FAN plus the acoustic treatment to suppress fan noise in the MAGLEV installation makes the understanding and control of the core engine noise extremely important in meeting the system noise objectives. In this study, Hamilton Standard used a generalization of existing turbo-shaft engine noise as a function of shaft horsepower. This generalization is shown in Figure E-2. This relatively good correlation lends creditability to the prediction of unsuppressed core engine noise.

Since current engines incorporate no source noise suppression technology, significant noise reductions can be expected in the future. The work by AiResearch under Air Force contract has resulted in a computer program for predicting the levels of current small turbo-shaft engines. The FAA-contracted work now underway at General Electric is more ambitious and includes a study of individual source noises such as combustor noise and turbine noise. Experiments have shown that increased spacing between rotor and stator can reduce turbine noise. The application of the knowledge obtained from the AiResearch and General Electric programs could result in further source noise reductions up to 10 dB, thus reducing the amount of external noise suppression required to achieve MAGLEV goals.

E.3 FAN NOISE SUPPRESSION

The computer program developed by Hamilton Standard for design of fan duct noise suppression is based on methodology first published by Boeing under NASA Langley contract. This work has been refined using data from tests at Pratt & Whitney Aircraft. The current computer program takes the rotor and stator noise spectra as input and separately considers the inlet duct, the duct between the rotor and stator, and the outlet duct. The direction of propagation of rotor and stator noise is recognized in the calculation

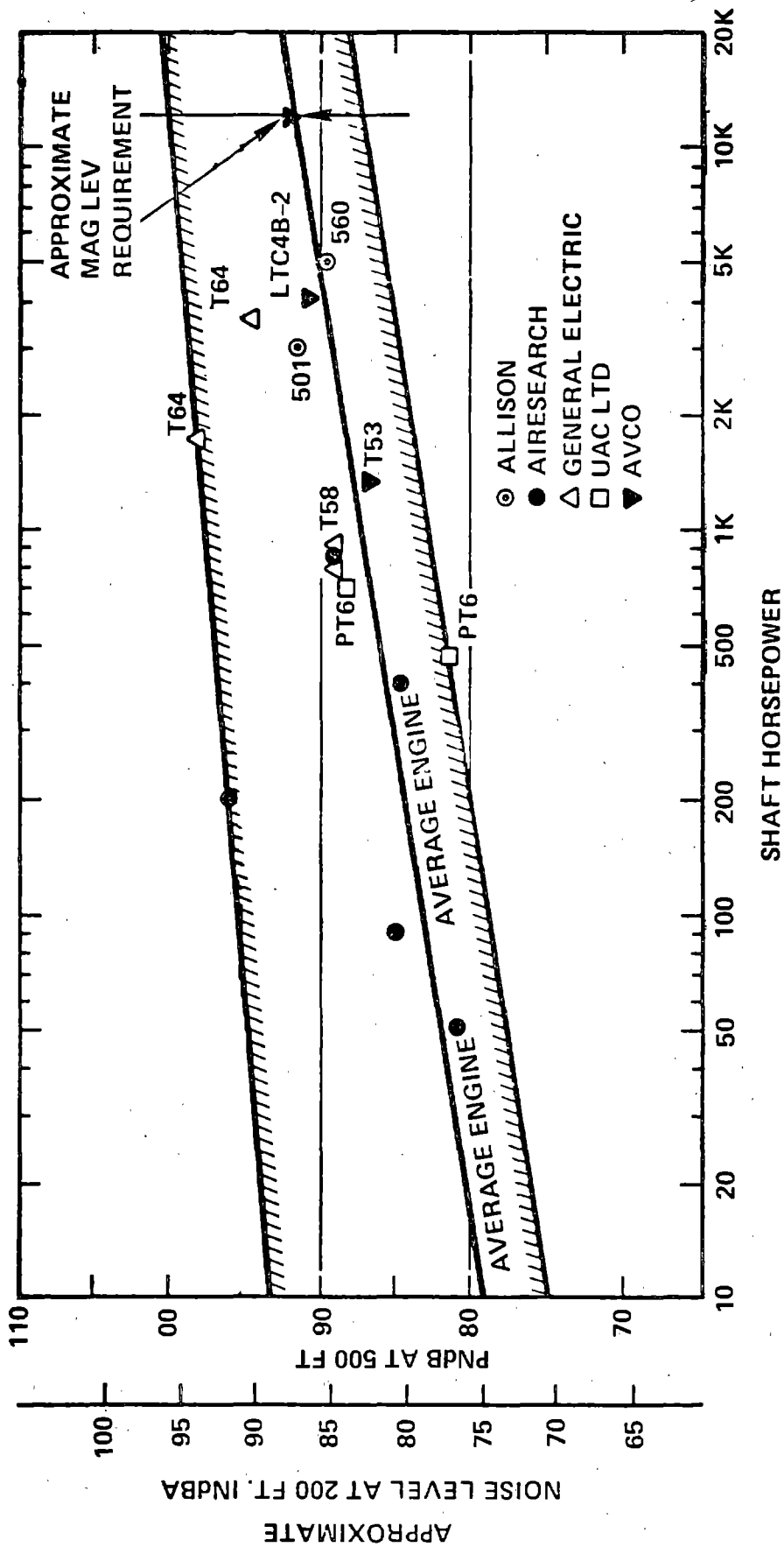


FIGURE E-2. TURBOSHAFT ENGINE NOISE LEVEL

procedure. Comparison of calculations with test results on a NASA 6 ft. diameter treated fan show excellent agreement (Figure E-3). A sectioned view of this NASA fan is shown in Figure E-4.

The treatments for the MAGLEV configuration were designed to reduce fan noise by 20 dB. It is judged that another 5 dB reduction could be achieved with continued technology efforts in acoustical treatments.

E.4 ENGINE NOISE SUPPRESSION

The same procedure as used for fan suppression design was employed for the treatment of the core engine on the MAGLEV. Experience in developing the inlet and exhaust suppression systems for the core engine used in the Lockheed L1011 Auxiliary Power Unit (APU) has shown that this technique is reliable. A comparison of measured and calibrated APU muffler attenuation is shown in Figure E-5.

In the future, progress is expected in development of engine duct treatments which are simpler and have lower performance losses without sacrificing the noise attenuation performance. The recent knowledge that core engine noise is a problem in high bypass ratio turbofans has prompted extensive work by all aircraft engine manufacturers to develop engine suppression systems. Since little work has been done in this area, substantial progress is expected, similar to the large gains that have been made in suppression of the fans of turbofan engines.

The MAGLEV gas turbine inlet noise can be easily attenuated, but exit noise attenuation is more difficult. The exit nozzle treatment reduces source noise by 13 dB. Continued engine treatment technology work could result in an additional 5 dB reduction.

E.5 SUMMARY

Figure E-6 indicates the potential for noise reduction of fan and gas turbine noise as estimated by Hamilton Standard. Two fans and two engines each at 86 dB(A) results in 92 dB(A) overall. This is the noise level estimated for full power with grade and headwind requirements. Two fans and two engines each at 80 dB(A) results in 86 dB(A) overall, the level estimated for

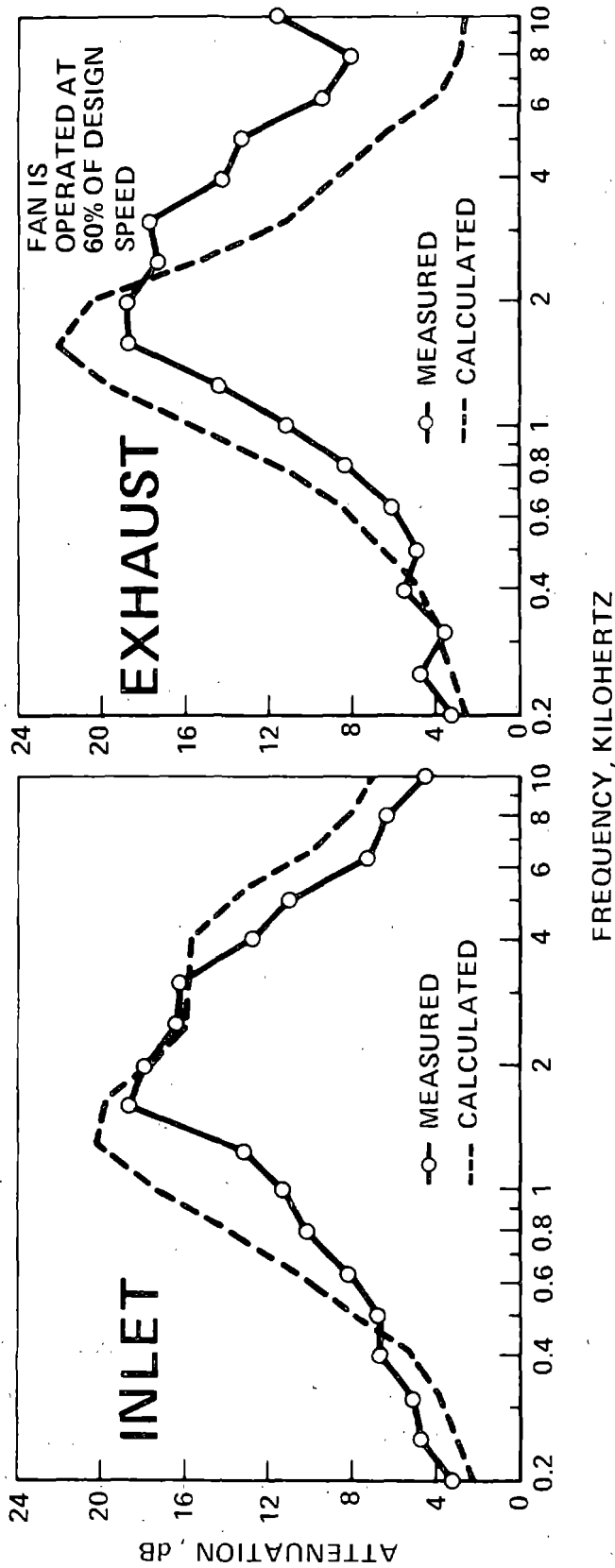


FIGURE E-3. COMPARISON OF QFI MEASURED ATTENUATION WITH ATTENUATION CALCULATED USING HAMILTON STANDARD METHOD

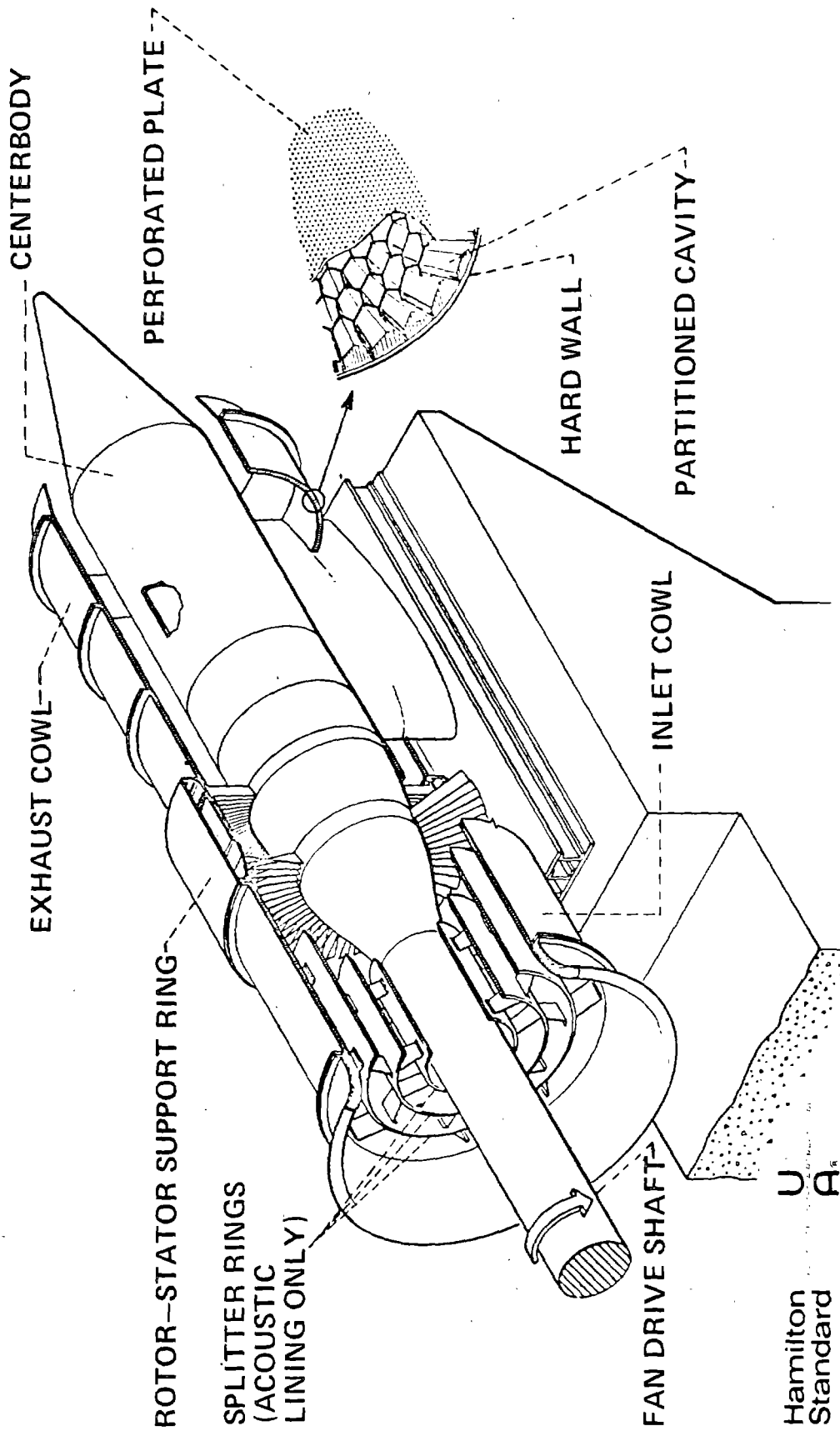


FIGURE E-4. CUTAWAY VIEW OF QF1 FAN AND SUPPRESSOR ASSEMBLY

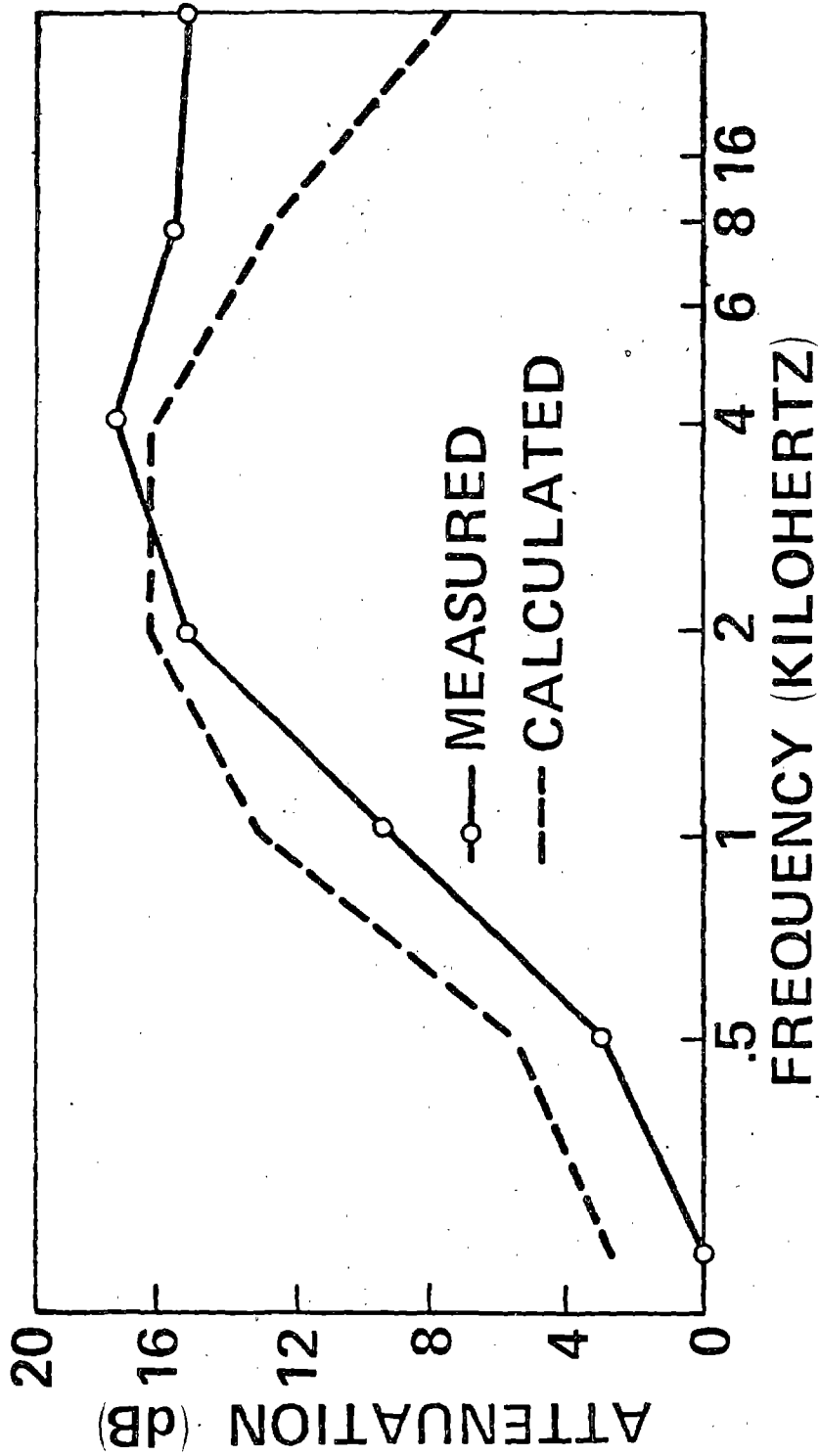


FIGURE E-5. COMPARISON OF APU MUFFLER MEASURED AND CALCULATED ATTENUATION USING HAMILTON STANDARD METHOD

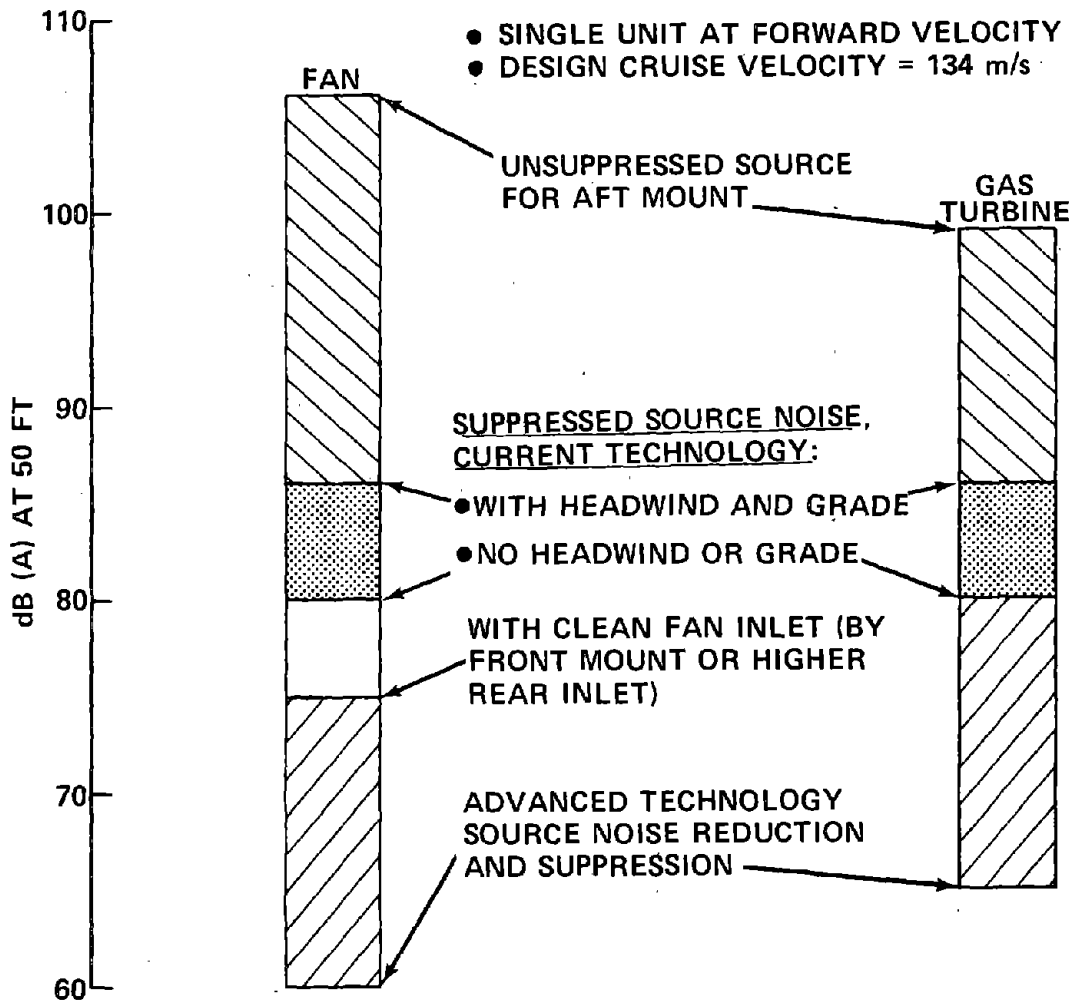


FIGURE E-6. MAGLEV PROPULSION NOISE PROJECTIONS

cruise operation without grade or headwind requirements. Further reductions in fan noise can be expected from application of advanced technology and a cleaner fan inlet. A cleaner fan inlet can be achieved by: (1) mounting the fan at the front of the vehicle, or (2) by raising the rear mount so that the boundary layer is not ingested. Engine noise reductions are also anticipated from the application of advanced technology.

Figure E-6 shows that the lowest noise for two fans will be 63 dB(A) and for two engines it will be 68 dB(A). The estimated overall noise level for advanced technology fans and engines is therefore 69 dB(A) at 50 feet.

Figure E-7 shows the MAGLEV Q-FAN noise level versus vehicle speed along with the DOT noise goal and Hamilton Standard's estimate of vehicle self-generated noise. Although this chart shows that the Q-FAN system is potentially quieter than the DOT goal, it is also quieter than the estimated vehicle self-generated noise level all the way down to about 70 m/s vehicle velocity. Note that these data are for a vehicle designed for 134 m/s. Should a lower design cruise speed be chosen for the Q-FAN system, noise levels will be lower than the projections shown in Figures E-6 and E-7. Obviously the Q-FAN design noise goals should be selected to be compatible with the vehicle design cruise velocity.

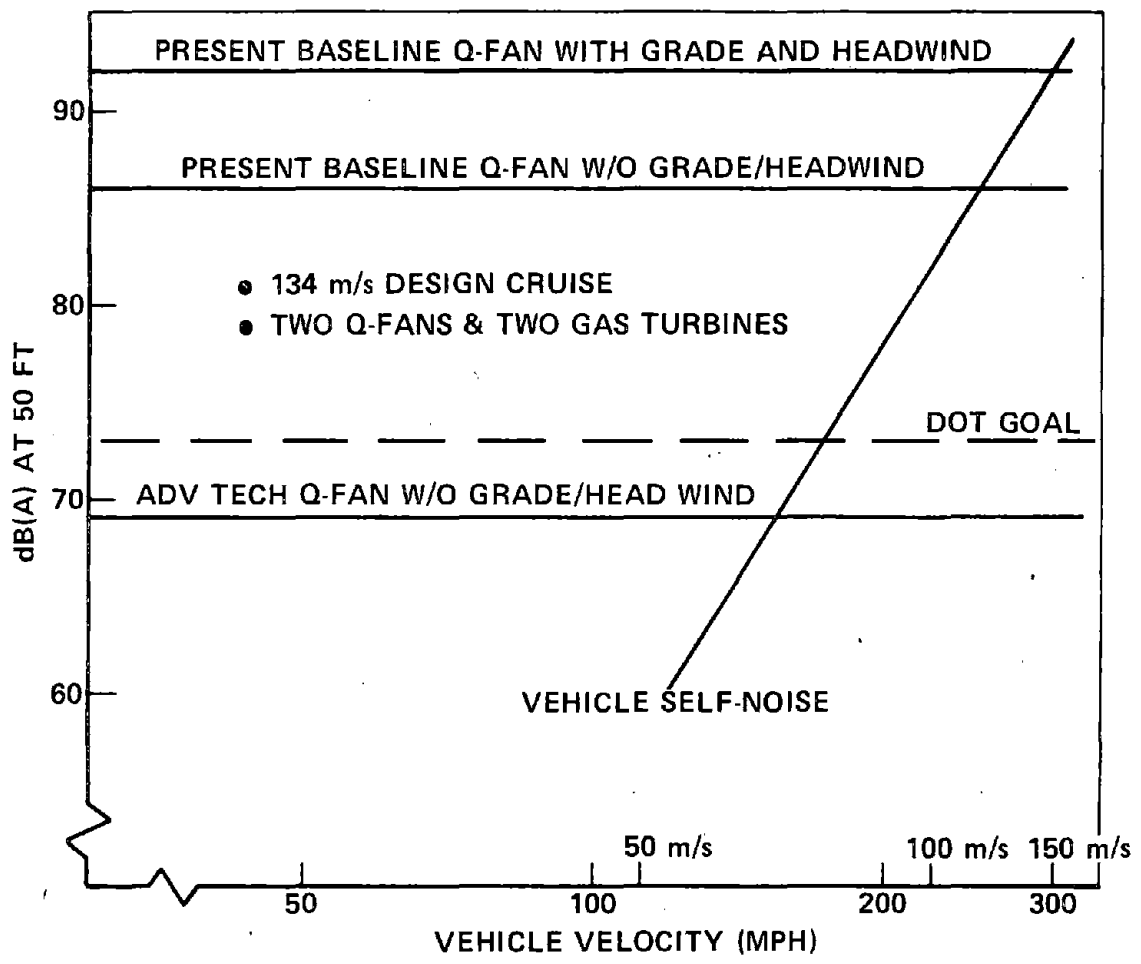


FIGURE E-7. Q-FAN SYSTEM NOISE LEVELS VS VEHICLE VELOCITY

APPENDIX F

FINAL REPORT

FOR

LINEAR SYNCHRONOUS MOTOR STUDIES

(In Support of Contract DOT-FR-40024 for
Federal Railroad Administration, Department
of Transportation, Washington, D. C. 20590)

ER 74-4420

December 1974

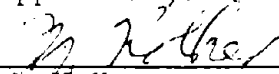
Prepared for

Aeronutronic Division
Philco-Ford Corporation
Newport Beach, California 92663

Prepared by:

C. H. Tang
W. J. Harrold

Approved by:


M. Kolker
Program Manager

RAYTHEON COMPANY
Equipment Development Laboratories
Advanced Development Laboratory
Wayland, Massachusetts 01778

ACKNOWLEDGMENT

The authors wish to acknowledge contributions to this study made by various members of the Advanced Development Laboratory. In particular, they wish to thank A. H. Greene and M. Kolker for discussions and reviews of the final report. O. Yuerhs' assistance on the use of the LINMOTR computer program is also acknowledged.



CONTENTS

SECTION		PAGE
1	INTRODUCTION	F-5
2	SUMMARY OF RESULTS	F-9
3	TMLV REQUIREMENTS	F-11
	3.1 TMLV Vehicle Specification	F-11
	3.2 Thrust and Power Requirements	F-11
4	LSM SYSTEM CONSIDERATIONS	F-13
	4.1 LSM System Configuration-Background Information	F-13
	4.2 LSM Advantages	F-13
	4.3 Comparison with Other Propulsion Systems	F-15
	4.3.1 Turbine-Propeller/Fan Systems	F-15
	4.3.2 LIM	F-15
	4.3.3 Turbine-LIM	F-16
	4.3.4 Electrified LIM	F-16
5	DESIGN ANALYSIS	F-17
	5.1 Mathematical Derivation and Computer Simulation	F-17
	5.1.1 Calculation of the Three-Phase Force on a Moving Vehicle Coil	F-17
	5.1.2 Calculation of the Forces Acting Between Current Carrying Coils	F-20
	5.1.3 Numerical Calculation of Forces and Torques	F-23
	5.2 Elemental LSM Unit and Force and Moment Matrix	F-26
	5.3 Computed Results	F-28
	5.4 Discussions	F-34
	5.4.1 Empirical Expressions of Forces and Moments	F-34
	5.4.2 Harmonic Contents of Forces and Moments	F-43
	5.4.3 Effects of Change Coil Dimensions	F-43



CONTENTS (Continued)

SECTION		PAGE
6	HYBRID LSM DESIGN	F-49
	6.1 Hybrid LSM Functions and Operational Principles	F-49
	6.2 Specific Hybrid LSM Design	F-50
	6.2.1 Estimate of Yaw Moment	F-51
	6.2.2 Estimate of Sway Control Force	F-51
	6.3 Evaluation of Specific Hybrid LSM Configuration	F-52
7	ON DETAILED LSM DESIGN PROBLEMS	F-58
	7.1 Selection of Coil Geometries of Vehicle Magnet/Guideway Winding	F-58
	7.2 Weight of the Superconducting Motor Magnets	F-59
	7.3 Estimated Weight of the Dewar System	F-60
	7.4 Guideway Winding Design	F-60
8	CONCLUSIONS AND RECOMMENDATIONS	F-62
	APPENDIX I Derivation of a Trigonometric Identity	F-64
	REFERENCES	F-66



1. INTRODUCTION

The objective of this work is to supply engineering studies of the force and moment models of a linear synchronous motor (LSM) system as applied to a high-speed, magnetically levitated passenger-carrying revenue vehicle. This work is in support of contract DOT-FR-40024, "Tracked Magnetically Levitated Vehicle Technology Program-Repulsion Scheme".

The specific study task is to perform an analysis of the axial, sway, and heave forces and the roll moment with respect to both the vehicle coil center for the elemental LSM unit and the c. g. of the vehicle for the hybrid LSM design. These forces and moments, which result from the currents in the guideway LSM propulsion windings interacting with propulsion magnets on board the vehicle, has been evaluated for vehicle control characteristics. The output of the study is a set of curves of the forces and roll moment as a function of various vehicle displacements.

An elemental LSM unit refers to an element of the multiple LSM windings, which may consist of both horizontal and vertical windings in a general configuration.

As will be seen, one important advantage of the LSM design is its ability to perform vehicle motion control, in addition to the main function of propulsion. Thus the range of the LSM application can vary from pure control to pure propulsion. A hybrid LSM refers to a LSM design where a limited control function is combined with the LSM propulsion design. The specific hybrid LSM studied for the TMLV application consists of two vertical LSM windings. This hybrid LSM design is configured for the sway and yaw control in addition to satisfying the TMLV propulsion requirement (Controls in other degree of freedom not considered here are achieved by control coils associated with the levitation magnets).

Figures 1a and 1b show respectively the transverse and the longitudinal cross sections of the specific hybrid LSM configuration. The configuration is furnished to the Raytheon Company by the Philco-Ford Corporation, based on the latter's design requirements of the inverted guideway.

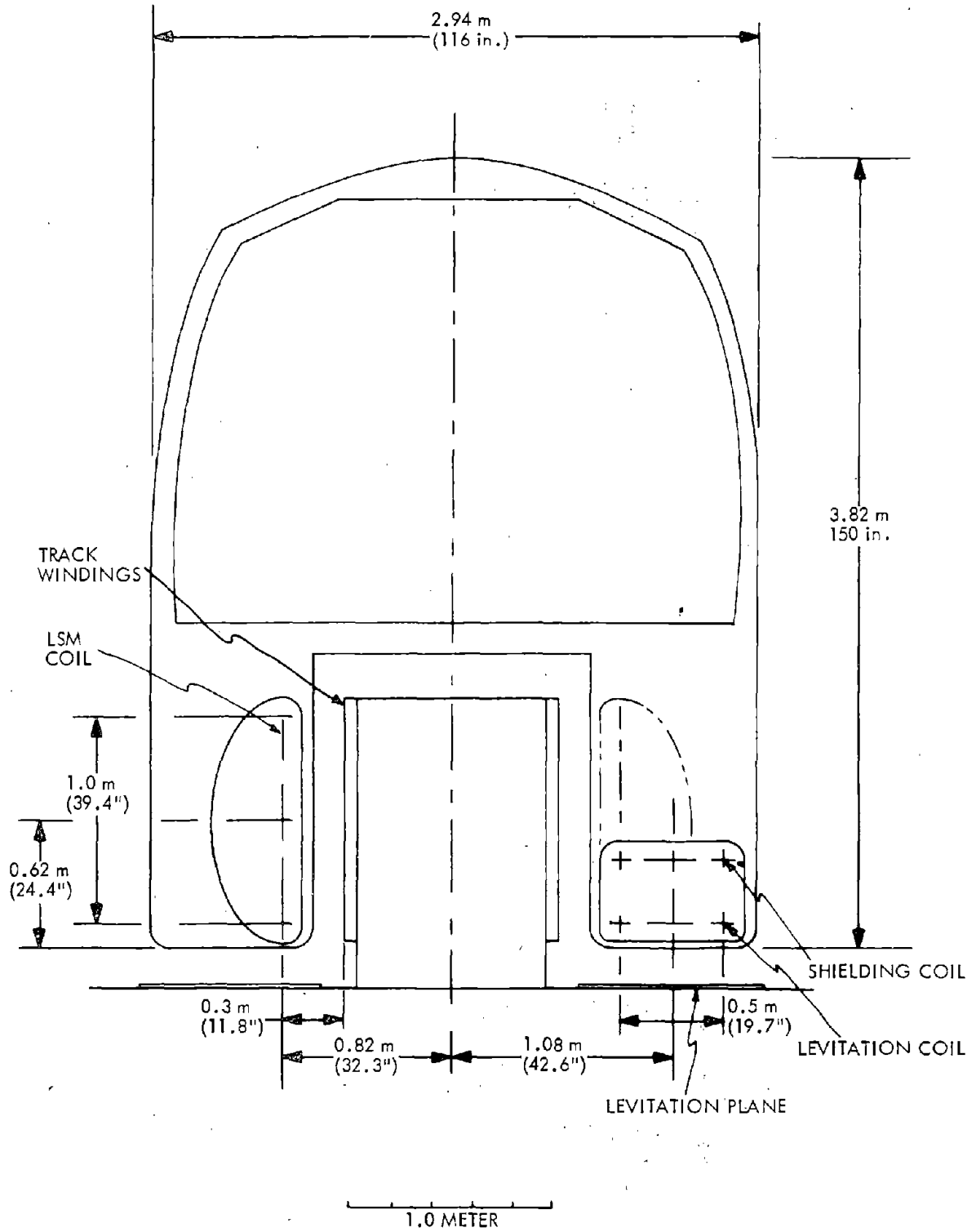


Figure 1a. Hybrid LSM - Transverse Cross Section

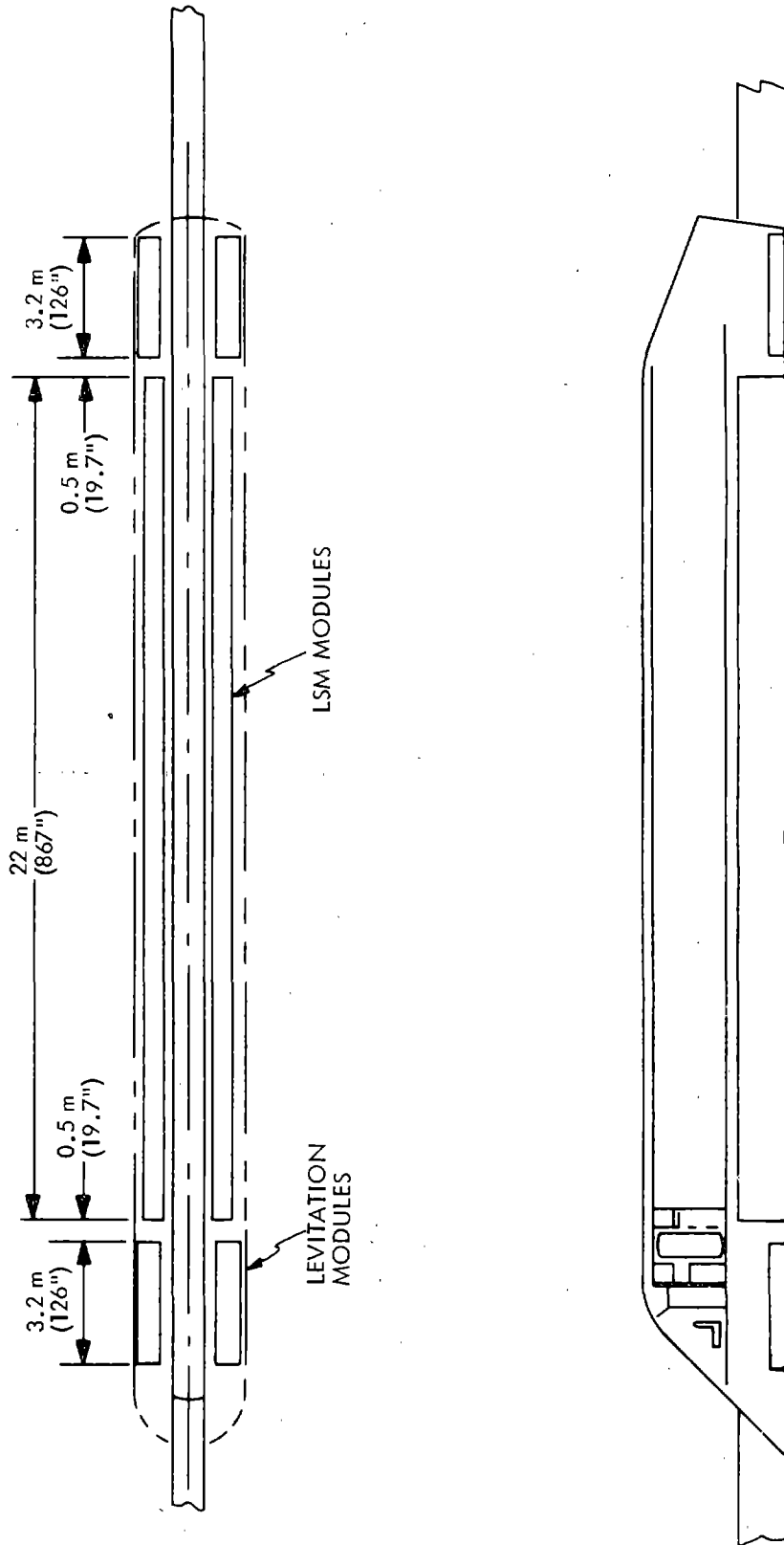
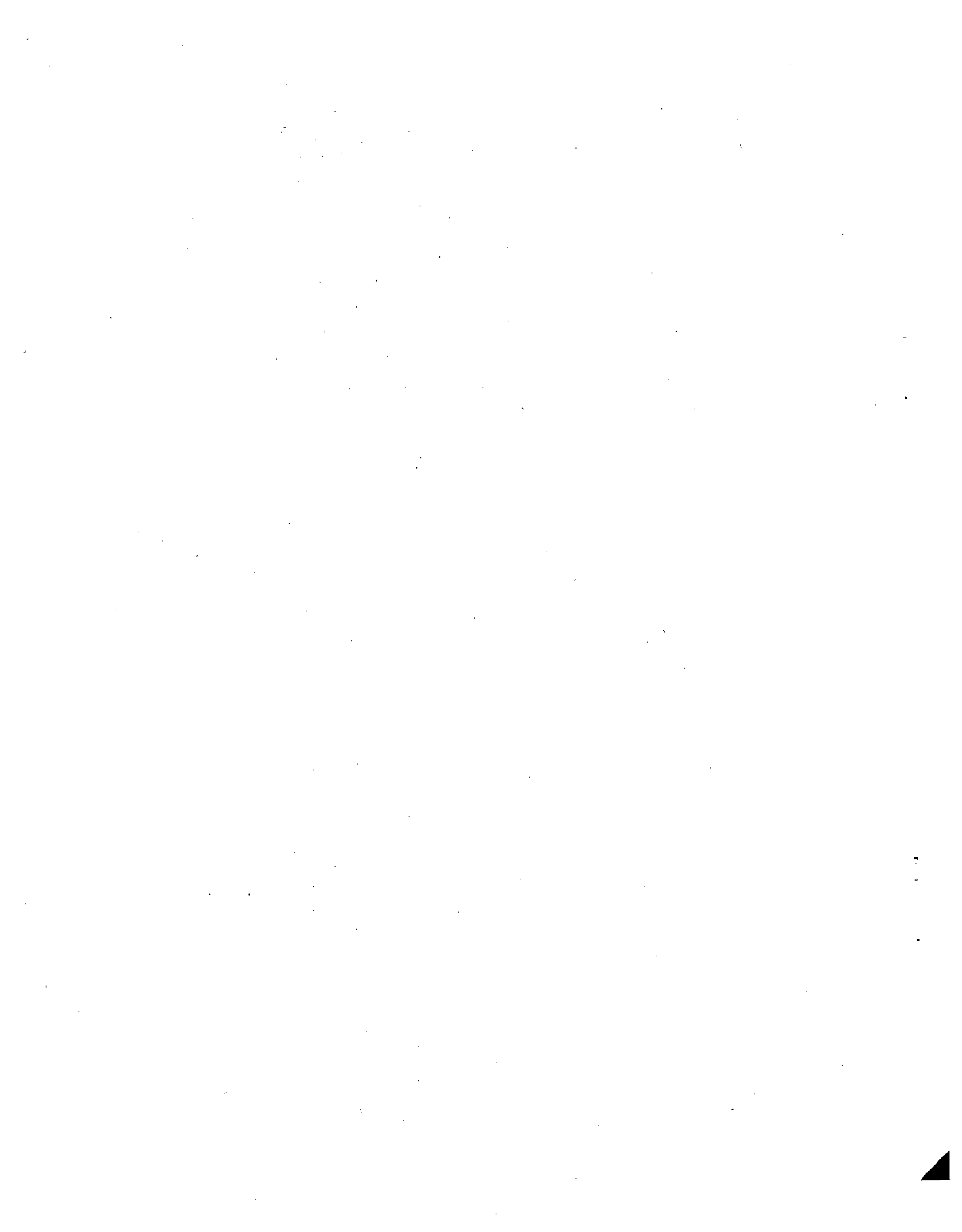


Figure 1b. Hybrid LSM - Longitudinal Configurations

The primary objective of this final report is to document results of the design study which has a special emphasis on the LSM force and moment model. In order to make the discussion of the LSM design in a more comprehensive manner, other elements of the LSM system are introduced and slightly elaborated. As such, they (particularly those contained in Sections 3 and 4) should not be considered as complete treatments. It should be recognized that there is much more work to be done with respect to them.

Another comment concerning the report content relates to the distinction between a LSM design concept and a LSM hardware system. It is felt, at this stage of the Maglev development, explicit analyses of various critical design concepts would have more impact on the ultimate system than brute force commitment on a set of hardware specifications. The latter can only come from well planned hardware development programs. A modest accomplishment achieved through the present study is the generation of a software tool for a more accurate LSM design. Further works are recommended.





2. SUMMARY OF RESULTS

Based on the propulsion system requirement of the baseline TMLV, the LSM system design problem was reviewed. It was shown that the power requirement of the TMLV is considerably less than those for the jet aircrafts. It also compares very favorably with the extrapolated data for the railcar (15 to 40 MW depending on the specific aerodynamic drag coefficients assumed).

It is pointed out that the LSM design concept allows an economic optimization of the long and short term thrust ratings. The active LSM guideway can be designed to accommodate the cruise (long term) and the acceleration (short term) with different sectionalized ratings. This can be done without penalizing the vehicle pay load. Other propulsion systems using passive guideways do not have this option.

Other advantages of the LSM propulsion system are also itemized together with a brief comparison of the LSM propulsion system with other propulsion systems.

The major emphasis of the present study effort is on an explicit design analysis of the LSM force and moment models. Mathematical bases for these evaluations are established. They are used to develop a set of versatile computer programs for generating various desired design data. These include:

- a. Force and moment computations for vehicle in normal position
- b. Force and moment computations for displaced vehicle
- c. Harmonic analysis of field, force and moment
- d. Evaluation of multiple LSM windings.

Using these computer programs, numerical results of the LSM force and moment are generated. From these results, a good understanding of the LSM force profile can be obtained. In addition, the computer programs are used for evaluating specific LSM designs.

From the analysis point of view, it is desirable to consider a general LSM system as composed of a number of elemental LSM units. Thus the explicit force and moment models on each elemental LSM can be used to obtain the total LSM system result. In the first order analysis, this can be done by straightforward coordinate transformations. The additional complication of mutual coupling effects can then be evaluated separately.

A hybrid LSM system configured for the sway and yaw control in addition to the propulsion main function is described. Specific design data estimated for the hybrid LSM are also discussed.

The report is concluded with a set of recommendations for further LSM design efforts.

3. TMLV REQUIREMENTS

3.1 TMLV VEHICLE SPECIFICATION

Major TMLV (Tracked Magnetically Levitated Vehicle) revenue vehicle design specifications (as established by the Philco-Ford Corporation for a 100 passenger vehicle) are:

- Vehicle weight = 45,400 Kg (100,000lb, 444.84 KN)
- Lift magnets = 2 (0.5^m x 1.5^m) coils at each corner
- Vehicle frontal area = 8.5 m²
- Guideway thickness = 2.54 cm (type 1100 - H14)
- Vehicle gap = 20 cm (control coil), 30 cm (lift coil)
- Vehicle coil current = 430 KAT/coil
- Lift-off speed = 30 m/s
- Thrust at Lift-off = 60 KN (0.05g), short term thrust rating
- Cruise speed = 134 m/s
- Thrust at cruise = 41 KN, long term thrust rating

3.2 THRUST AND POWER REQUIREMENTS

An analysis based on the given TMLV vehicle specifications is performed to derive the force and power requirements of the LSM system.

Assuming the following drag law

$$F_d = C_m v^{-1/2} + C_a v^2 \quad (1)$$

The required thrusts at the lift-off speed and the cruise speed imply

$$C_m = 2 \times 10^5$$

$$C_a = 1.3$$

Thus the vehicle drag can be empirically determined for all speeds. It can be shown that for this particular requirement, the magnetic drag equals the aerodynamic drag at 117 m/s (262 mph). Also, while both components of the lift-to-drag ratio change considerably as functions of the velocity, the resultant lift-to-drag ratio stays relatively constant (11 to 12).



From the drag law, the power requirement for propulsion is evaluated. The total power requirement at the cruising speed (5.5 MW) is approximately five times higher than that required at the lift-off-speed. But in order to reach the cruise speed the acceleration has to continue in an appropriate fashion. Thus the maximum required power depends on the scheduled acceleration.

If we assume the acceleration is to continue at 0.05g, then it will take 212 sec (corresponds to 17.6 km distance) to reach the cruise speed. Under the condition, the maximum required power is approximately 8.5 MW.

The maximum required power can be minimized by an optimum velocity schedule. It is desirable to allow initially a higher acceleration (but it should be less than 0.15g*, although a jet aircraft accelerates at 0.25-0.3g prior to takeoff) and then at a lower rate.

The above results compare very favorably with both the jet aircrafts and the extrapolated data for the railcar (15 to 40 MW depending on the specific aerodynamic drag coefficients).

*This assumption is based on requirements for the revenue system linear Synchronous Motor Studies established by the Philco-Ford Corporation, the maximum sustained or steady-state longitudinal acceleration shall not exceed 0.15g.

4. LSM SYSTEM CONSIDERATIONS

4.1 LSM SYSTEM CONFIGURATION-BACKGROUND INFORMATION

This brief discussion is to provide some background information on LSM design. Elements of a typical LSM system include:

a. Vehicle equipments

- Vehicle LSM magnets
- Accelerometers
- Magnetic field sensors
- Telemetry (or other devices for alternate approaches)

b. Guideway equipments

- Propulsion windings
- Power conditioner
- Power input system
- Control computer

References 1 through 7 give various basic design analyses of the LSM operation. Included in these references, one can find design information for the following considerations.

- Design of Vehicle LSM magnets
- Optimization of LSM winding geometry
- Effects of field harmonics
- Prediction of vertical force

Specific design information on the LSM cost model, the LSM electronic control and the design of cycloconverters can be found in references 8, 9 and 10 respectively.

4.2 LSM ADVANTAGES

As a propulsion system for tracked magnetically levitated vehicles, the LSM design stands out as a strong candidate for the ultimate Maglev system. This is due to a number of potential advantages of the LSM design over other options considered so far. Important advantages include:



- a. The large gap compatibility for a simpler suspension design and thus lower cost guideway fabrication.
- b. The multidimensional controllability for an improved vehicle ride quality.
- c. The synchronous feature for a shorter and more precise headway scheduling.
- d. The LSM guideway design concept allows an economic option for satisfying both the long and short term thrust ratings without penalizing the vehicle payload.
- e. High efficiency (better than 70%) and higher speed potential (higher than 300 mph)
- f. Quiet operation with minimal pollution

The item d is an important feature for the LSM guideway design, and it is not shared by other passive guideway designs. Because of the difference between the long term and the short term thrust ratings, the LSM guideway can be sectionalized to effect an economic transportation system design. Thus a major part of the guideway is designed for lower thrust ratings. Only up-hill and acceleration sections need a higher thrust rating. Thus this is done without penalizing the vehicle payload.

It is believed that the only real objection against the LSM design is the need of an active guideway which tends to indicate a high guideway cost.* However, there does not seem to exist any detailed cost data to support the objection as a real one.* Furthermore, it is clearly true that the active guideway is more compatible with higher traffic densities, while the passive guideway is more suited for lower traffic densities.* Although, the exact dividing line between the two situations is not yet known, it is reasonable to assume that various Maglev systems will be compared on the basis of high traffic densities.

*The comments of the Raytheon Co. noted above are not in consonance with the results of analyses carried out by Ford/Philco and reported in Volume 1 of this report. For example, there is no substantiation of the claim that an active guideway is more compatible with higher traffic densities than a passive guideway.



4.3 COMPARISON WITH OTHER PROPULSION SYSTEMS

The purpose of this discussion is to identify major design considerations and key trade-off factors associated with various propulsion options.

4.3.1 Turbine-Propeller/Fan Systems

Major design considerations for these systems are the reductions of the noise and the pollution effects. There is also a potential problem if operating these systems in an evacuated tunnel.* In addition, the weight of these systems is a key trade-off factor, particularly, according to estimates these systems would consume 2.6 tonnes of fuel per hour* (For a two hour trip, fuel alone amounts to 14% of the vehicle weight).¹¹

In addition, energy usage will be a very significant factor in all future transportation systems. The fan jet system requires the use of one particular fuel type.* In contrast, LSM, using electricity, offers the full spectrum of fuel methods for generating the electricity at its source. Also, assuming that the guideway electrical conductor current and voltage capacity are initially installed to handle whatever future system capacity is needed, power needs to feed the system can be increased as required by the most economic generation and distribution system available as the electrical power technology evolves in the decades to come. Thus, to improve energy usage efficiency in the overall Maglev operating system does not require retrofit or change in rolling stock, as is the case with an onboard propulsion system such as the fan jet*.

4.3.2 LIM

There are a number of reasons to believe that the design of LSM is much less a technical problem than that of LIM. Two reasons are emphasized here.

*Ford/Philco does not believe these comments to be valid. For example, there is no plan to operate in an evacuated tunnel; the weight of a ducted fan/gas turbine system is substantially less than an LSM propulsion system and the fuel weight including 15 percent reserve is only 9 percent of the vehicle gross weight. Also, a gas turbine can be operated on a wide variety of fuels, fossil or synthetic.

- a. Fringe field effect is less important in LSM (while it is critical in LIM)
- b. Prediction of field and force profile is more tractable in LSM (particular in comparison to those LIM systems where iron is used).

Assuming the above technical situation for LIM can be improved by further development, there are other problems that have to be contended with. For the linear induction motor to be efficient, the air gap between the vehicle and the reaction rail must be small. This condition is inconsistent with the vehicle suspension requirements which must allow considerable variations in vehicle guideway clearance in order to achieve a satisfactory ride quality. If the primary suspension is very stiff, then the linear induction motor can be directly mounted on the vehicle, but little ride quality is gained from the primary suspension and the secondary suspension must accommodate most of the required motion. If it is desired to use a soft primary suspension, then the LIM will have to be suspended separately in order to control the air gap size satisfactorily.

4.3.3 Turbine-LIM*

The vehicle can be propelled by a linear induction motor powered by gas turbine-alternator sets. While the turbine-propeller system is liable to be noisy and create exhaust, the turbine-LIM system just creates exhaust. In comparison with the electrified LIM system, the problem of power pick-up is eliminated. But major disadvantages of the turbine (such as engine weight and fuel weight) and the LIM systems (such as the narrow gap constraint) are still inherent in this combination.

4.3.4 Electrified LIM

In addition to the general incompatibility of the LIM system with large gap levitation, the major design problem associated with the electrified LIM system is the requirement of a reliable, high power pick-up system at high speed.

*This combination has not been considered on the TMLV Technology program.

5. DESIGN ANALYSIS

5.1 MATHEMATICAL DERIVATION AND COMPUTER SIMULATION

5.1.1 Calculation of the Three-Phase Force on a Moving Vehicle Coil

The force acting between single phase of the stator winding (excited with dc) and a single vehicle coil as the vehicle is translated along the stator can be decomposed into a Fourier series of space harmonics.

$$F_{dc}^1 = \sum_{n=1}^{\infty} f_n \cos n\kappa z \quad (2)$$

where $\kappa = \pi/\lambda_p$ and λ_p is the pole pitch of the stator winding. If a single phase of the winding is excited with alternating current, this expression becomes

$$F_{ac}^1 = \sum_{n=1}^{\infty} f_n \cos n\kappa z \cos \omega t \quad (3)$$

If the stator is excited with three-phase alternating current, three series similar to (3) are needed to describe the total force acting on the vehicle. The effect of the 120° and 240° spatial and temporal displacements of the three currents are dealt with in terms of phase shift. Thus, the three phase force acting on a single vehicle coil is given by

$$F^3 = \sum_{m=0}^2 \sum_{n=1}^{\infty} f_n \cos n \left(\kappa z - \frac{2m\pi}{3} \right) \cos \left(\omega t - \frac{2m\pi}{3} \right) \quad (4)$$

It is shown in Appendix I that this equation can be transformed by use of trigonometric identities into

$$F^3 = \frac{1}{2} \sum_{m=0}^2 \sum_{n=1}^{\infty} \left[\begin{aligned} &\cos (\omega t + n\kappa z) \cos (n+1) \frac{2m\pi}{3} + \\ &\cos (\omega t - n\kappa z) \cos (n-1) \frac{2m\pi}{3} + \\ &\sin (\omega t + n\kappa z) \sin (n+1) \frac{2m\pi}{3} + \\ &\sin (\omega t - n\kappa z) \sin (n-1) \frac{2m\pi}{3} \end{aligned} \right] \quad (5)$$



This equation can be further simplified through use of the trigonometric identity

$$\sum_{m=0}^2 e^{i \frac{2}{3} m \ell \pi} = \begin{cases} 3, & \ell = 0, 3, 6, \dots \\ 0, & \ell \neq 0, 3, 6, \dots \end{cases} \quad (6)$$

$$e^{i \frac{2}{3} m \ell \pi} = \cos \frac{2}{3} m \ell \pi + i \sin \frac{2}{3} m \ell \pi$$

it is clear that $\sum_{m=0}^2 \sin \frac{2}{3} m \ell \pi = 0$ for all ℓ

Therefore, equation (5) reduces to:

$$F^3 = \frac{1}{2} \sum_{n=1}^{\infty} f_n \left[\cos(\omega t + m \ell z) \sum_{m=0}^2 \cos(n+1) \frac{2m\pi}{3} + \cos(\omega t - m \ell z) \sum_{m=0}^2 \cos(n-1) \frac{2m\pi}{3} \right] \quad (7)$$

This can be further simplified by use of the trigonometric identity given in equation (6) and the fact that only odd number space harmonics are present because of the symmetry of the winding. The sums over the index m are tabulated here

n	n+1	$\sum_{m=0}^2 \cos(n+1) \frac{2m\pi}{3}$	n-1	$\sum_{m=0}^2 \cos(n-1) \frac{2m\pi}{3}$
1	2	0	0	3
3	4	0	2	0
5	6	3	4	0
7	8	0	6	3
9	10	0	8	0
11	12	3	10	0
13	14	0	12	3
15	17	0	14	0
17	18	3	16	0
19	20	0	18	3
21	22	0	20	0

From the information given in this table one can see that the three-phase force on a vehicle coil given in equation (7) reduces to:

$$F^3 = \frac{3}{2} \left[\begin{aligned} & f_1 \cos (\omega t - Kz) \\ & + f_5 \cos (\omega t + 5Kz) \\ & + f_7 \cos (\omega t - 7Kz) \\ & + f_{11} \cos (\omega t + 11Kz) \\ & + f_{13} \cos (\omega t - 13Kz) \\ & + f_{17} \cos (\omega t + 17Kz) \\ & + f_{19} \cos (\omega t - 19Kz) + \dots \end{aligned} \right] \quad (8)$$

One observes that the fundamental component travels with the velocity $v = \omega/K$. If the vehicle moves in synchronism with this wave, the only constant force is given by the first harmonic. All other components contribute only vibratory forces. In making the transformation

$$z = \omega t/K - s \quad (9)$$

where the slip s defines the displacement between the actual coil location and the crest of the traveling wave. One finds that

$$F^3 = \frac{3}{2} \left[\begin{aligned} & f_1 \cos (Ks) \\ & + f_5 \cos (6\omega t - 5Ks) \\ & + f_7 \cos (6\omega t - 7Ks) \\ & + f_{11} \cos (12\omega t - 11Ks) \\ & + f_{13} \cos (12\omega t - 13Ks) + \dots \end{aligned} \right] \quad (10)$$

The fifth and seventh space harmonic of the force, when transformed to the moving frame of reference, produce a sixth harmonic perturbation. Similarly, the eleventh and thirteenth harmonic are transformed to a twelfth harmonic perturbation.

The third, ninth and fifteenth space harmonics do not interact with a balanced three-phase stator winding.

It is clear from this analysis that the only constant forces acting on a vehicle, traveling in synchronism with the excitation of the three-phase stator winding, are associated with the fundamental component of force profile, and that they are proportional to the cosine of the slip s . Thus,

$$F_{dc} = \frac{3}{2} F_1 \cos \left(\frac{\pi s}{\lambda_p} \right) \quad (11)$$

It can similarly be shown that the vertical and lateral forces are proportional to the sine of the slip s .

$$F_{v,s} = \frac{3}{2} F_1^{v,s} \sin \left(\frac{\pi s}{\lambda_p} \right) \quad (12)$$

5.1.2 Calculation of the Forces Acting Between Current Carrying Coils

The total inductance of two coils connected in series is given by

$$L = L_1 + L_2 + 2M_{12} \quad (13)$$

If such a pair of coils is connected to a current generator one finds from consideration of several simple cases that the force acting between the coils tends to move them so as to increase the total inductance. If one of the coils is allowed to move under the influence of the force, a virtual displacement Δx of one of the coils produces three effects:

1. Virtual work $F \Delta x$ is performed on the restraining medium.
2. The increase in the total inductance of the system increases the energy stored in the magnetic field of the two coils by the amount

$$\Delta W = \frac{1}{2} I^2 \Delta L = I^2 \Delta M_{12} \quad (14)$$

3. The change in the flux linking the coils induces a voltage in the coils which results in an energy expenditure by the constant current source. The voltage across the load is given by

$$\begin{aligned} e &= \frac{d}{dt} (LI) \\ &= \frac{LdI}{dt} + I \frac{dL}{dt} \end{aligned} \tag{15}$$

But I is fixed, therefore

$$\begin{aligned} e &= I \frac{dL}{dt} \\ &= 2 I \frac{\partial M_{12}}{\partial t} \end{aligned} \tag{16}$$

The energy expended by the generator is therefore given by:

$$\begin{aligned} W_g &= \int_{-\infty}^{\infty} e I dt \\ &= \int_{-\infty}^{\infty} 2 I^2 \frac{\partial M_{12}}{\partial t} dt \\ W_g &= 2 I^2 \Delta M_{12} \end{aligned} \tag{17}$$

Now the energy expended by the generator is equal to the sum of the energy dissipated in the restraining medium and the energy stored in the field of the coils.

Thus

$$W_g = F\Delta x + I^2 \Delta M_{12}$$

or

$$2 I^2 \Delta M_{12} = F\Delta x + I^2 \Delta M_{12}$$

Thus, half of the energy delivered by the current generator is dissipated in moving against the restraining medium and the other half is stored in the magnetic field. The last equation is simplified to

$$F_x \Delta x = I^2 \Delta M_{12} \quad (18)$$

The change in the mutual inductance ΔM_{12} can be expanded into a Taylor series

$$\Delta M_{12} = \frac{\partial M_{12}}{\partial x} \Delta x + \frac{\partial^2 M_{12}}{\partial x^2} \frac{(\Delta x)^2}{2!} + \dots \quad (19)$$

For a virtual displacement, only the first term is significant. Therefore,

$$F_x = I^2 \frac{\partial M_{12}}{\partial x} \quad (20)$$

This is easily generalized to

$$\begin{aligned} \vec{F} &= I_1 I_2 \nabla M_{12} \\ \text{or} \quad \vec{F} &= I_1 I_2 \sum_{i=1}^3 \hat{u}_i \frac{\partial M_{12}}{\partial x_i} \end{aligned} \quad (21)$$

Calculation of the torque acting on a coil is derived in the same manner with the following relationships. The virtual work performed on the restraining media is given by

$$\Delta W = T \Delta \theta \quad (22)$$

The energy stored in the field of the increased inductance is given by

$$\Delta W = I^2 \Delta M_{12}$$

and the energy delivered by the current generator is

$$\Delta W = 2 I^2 \Delta M_{12}$$

The virtual change in inductance is expanded as

$$\Delta M_{12} = \frac{\partial M_{12}}{\partial \theta} \Delta \theta$$

Therefore

$$T_x = I_1^2 \frac{\partial M_{12}}{\partial \theta_x} \quad (23)$$

The torque is also easily generalized to

$$\vec{T} = I_1 I_2 \sum_{i=1}^3 \hat{a}_i \frac{\partial M_{12}}{\partial \theta_i} \quad (24)$$

5.1.3 Numerical Calculation of Forces and Torques

The program LINMOTR calculates the force and torque profiles of one or more vehicle coils as they are translated along a three-phase guideway (stator) winding in which one of the phases is excited with dc. It is shown in the section 5.1.1. how this information is used to determine the three-phase forces and torques acting on the vehicle.

To calculate the forces and torques from the relationships developed in the last section, a computer program LINMOTR was written.

The derivative of the mutual inductance is approximated by a difference calculation. Since the CDC 6700 computer on which their calculations are performed, uses 60 bit words and therefore, represents numbers to 14 decimal places in the normal single precision mode, no difficulty is encountered in taking small differences between large numbers.

If a unit of current is passed through one phase of the stator winding it will produce a magnetic field at the vehicle coil which can be characterized by the magnetic vector potential \vec{A} , which is defined by the relationship: $\vec{B} = \nabla \times \vec{A}$. If one integrates \vec{B} over the area of the coil to determine the total flux ϕ_{12} which links the vehicle coil, and applies Stokes' theorem one finds that:

$$\phi_{12} = \iint_s \vec{B} \cdot \vec{da} = \iint_s \nabla \times \vec{A} \cdot \vec{da} = \oint \vec{A} \cdot d\vec{l}. \quad (25)$$

Thus the mutual inductance between the two coils is given by:

$$M_{12} = \oint \vec{A} \cdot d\vec{\ell} \quad (26)$$

when the stator winding is excited by one ampere.

The computer program LINMOTR was written to perform this mutual inductance calculation. It was assumed that the coils can have any shape in three dimensions and are characterized by a multiplicity of straight line segments. The vector potential around a segment of wire is given by

$$\begin{aligned} \vec{A} &= \frac{\mu_0}{8\pi} \log_e \left\{ \frac{1 + \cos \theta_1}{1 - \cos \theta_1} \cdot \frac{1 - \cos \theta_2}{1 + \cos \theta_2} \right\} \mu_0 \theta_1, \theta_2 \neq 0, 180^\circ \\ &= \mu_0 / 4\pi \log_e (r_1 / r_2) \vec{u}_0, \theta_1 = \theta_2 = 0, 180^\circ \end{aligned} \quad (27)$$

where the parameters are defined in Figure 2.

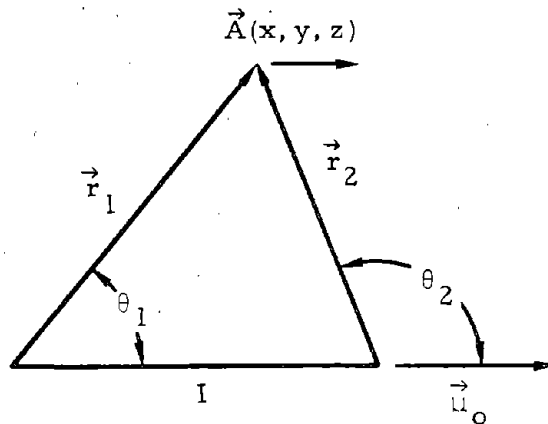


Figure 2. The vectors used in Equations (27) through (29)

This apparently complex relationship is easily evaluated by the following procedure. A convenient Cartesian coordinate system in which the coils can be defined is chosen. If the current carrying wire extends from (x_1, y_1, z_1) to (x_2, y_2, z_2) then the direction cosines of the wire are given by:

$$\alpha_o = \frac{x_2 - x_1}{L_o} \quad \beta_o = \frac{y_2 - y_1}{L_o} \quad \gamma_o = \frac{z_2 - z_1}{L_o}$$

$$L_o = \sqrt{(x_2 - x_1)^2 + (y_2 - y_1)^2 + (z_2 - z_1)^2}$$
(28)

The direction cosines α_n , β_n and γ_n of the vectors \vec{r}_1 and \vec{r}_2 are given by a similar relationship. From the definition of the scalar product one has:

$$\cos \theta_n = \hat{r}_n \cdot \hat{u}_o = \alpha_n \alpha_o + \beta_n \beta_o + \gamma_n \gamma_o$$
(29)

LINMOTR uses the relationships (27) through (29) to calculate the vector potential due to each segment of one phase of the stator winding. The line integral of the vector potential around the vehicle coil is computed numerically. The mutual inductance is calculated at twelve closely spaced coil positions at each of many equispaced intervals along the stator. The three components of force and the three components of torque acting on a vehicle coil are then calculated by numerical differentiation. The Fourier components of each force are then calculated by a numerical routine.

The computer program LINMOTR numerically calculates the mutual inductance between a linearly disposed array of guideway coils and one or more vehicle coils. Forces and torques are then determined by the relationships

$$\vec{F} = I_1 I_2 \sum_{i=1}^3 \hat{u}_i \frac{\delta M_{12}}{\delta X_i}$$

$$\vec{T} = I_1 I_2 \sum_{i=1}^3 \hat{u}_i \frac{\delta M_{12}}{\delta \theta_i}$$

where the derivatives are closely approximated by numerical differences.

The forces and torques are calculated at equally spaced intervals along the guideway for one half pole pitch. A numerical routine then calculates the Fourier components of each forces and torques.

If one calculates the forces and torques as functions of displacements and rotations from an initial vehicle position which is parallel to guideway, one finds that one need only calculate the forces and torques on one vehicle coil due to one phase of the guideway coil for:

- lateral displacement
- vertical displacement
- roll

The three phase forces and torques on the entire vehicle are then determined by multiplying the calculated forces and torques by $\frac{3}{2}N$ when N is the number of vehicle coils.

To calculate forces and torques as a function of pitch or yaw requires that forces and torques on each vehicle coil be calculated because of the non periodic relationship between the vehicle coils and the track coils. This procedure requires greater amounts of computer time.

5.2 ELEMENTAL LSM UNIT AND FORCE AND MOMENT MATRIX

The following specifications were used for generating the force and moment data

coil geometry	$1^m \times 1.1^m$
vehicle coil current	500,000 AT
guideway current	1,500 A

where the coil geometry is taken from the reference 3. Calculations of other coil sizes are discussed in Section 5.4.3.

Table 1 shows a matrix representation of forces and moments as functions of six independent displacements. As was mentioned, the evaluations of forces and moments due to the pitch and the yaw rotation of the coil are more involved than those due to other displacements. However, in the TMLV revenue system, forces and moments caused by these two rotational displacements of the coil are expected to be less important.

General properties of forces and moments are shown in the table. These symmetries are expressed with respect to the normal vehicle center position ($x = 0$, $y = 30$ cm).



Table 1. Force Moment Matrix

	side displacement	vertical displacement	longitudinal displacement	pitch displacement	yaw displacement	roll displacement
F_x (sideforce)	anti-symmetric	monotonic	anti-symmetric	anti-symmetric	anti-symmetric	anti-symmetric
F_y (vertical force)	symmetric	monotonic	anti-symmetric	symmetric	symmetric	symmetric
F_z (propulsion)	symmetric	monotonic	symmetric	symmetric	symmetric	symmetric
T_x (pitch)	symmetric	monotonic	symmetric	symmetric	symmetric	symmetric
T_y (yaw)	anti-symmetric	monotonic	symmetric	anti-symmetric	anti-symmetric	anti-symmetric
T_z (roll)	anti-symmetric	monotonic	anti-symmetric	anti-symmetric	anti-symmetric	anti-symmetric

5.3 COMPUTED RESULTS

The single phase forces and torques acting on the vehicle (see Figure 3) have been calculated as a function of displacement in the direction of motion (along the z axis). It must be kept in mind that the forces actually experienced by the vehicle as it moves in synchronism with the travelling wave are dependent on the slip* and lateral displacement. The three single phase forces F_x (side), F_y (lift) and F_z (propulsion) are shown as a function of slip s in Figure 4a for a vehicle which is laterally displaced by 10 cm. As shown in that figure the maximum vertical force F_y , exceeds the maximum propulsion force F_z but the forces experienced by the vehicle will normally be in the region where slip s is small. Three single phase torques acting on a single vehicle coil are shown as a function of slip s in Figure 4b.

When one adds three single phase forces as shown in Section 4.1, one finds that the fundamentals add to form a constant force which is 1.5 times the amplitude of the fundamentals. For a balanced three phase system the third harmonics cancel and the fifth harmonic which is traveling forward with the velocity $2f\lambda_p/5$ and the seventh harmonic which is traveling forward with the velocity $2f\lambda_p/7$ add to produce a sixth harmonic perturbation (λ_p is the pole pitch of the guideway coil).

The fundamental components of the single phase forces: F_x , F_y and F_z are shown as a function of lateral displacement in Figure 5. The fundamental components of the single phase torques: T_x which tends to produce pitch motion, T_y which tends to produce yaw motion and T_z which tends to produce roll are shown as a function of lateral displacement (x) in Figure 6.

As shown in these figures F_x , T_y and T_z are odd functions of lateral displacement, vanishing when the vehicle coils are centered over the guideway coils. On the other hand F_y (lift), F_z (propulsion) and T_x (pitch torque) are even functions of lateral displacement, which are maximum when the vehicle coils are centered over the guideway coils.

*Slip is defined here as the distance the center of a vehicle coil lag behind the point on the traveling wave at which the vertical force F_y vanishes.

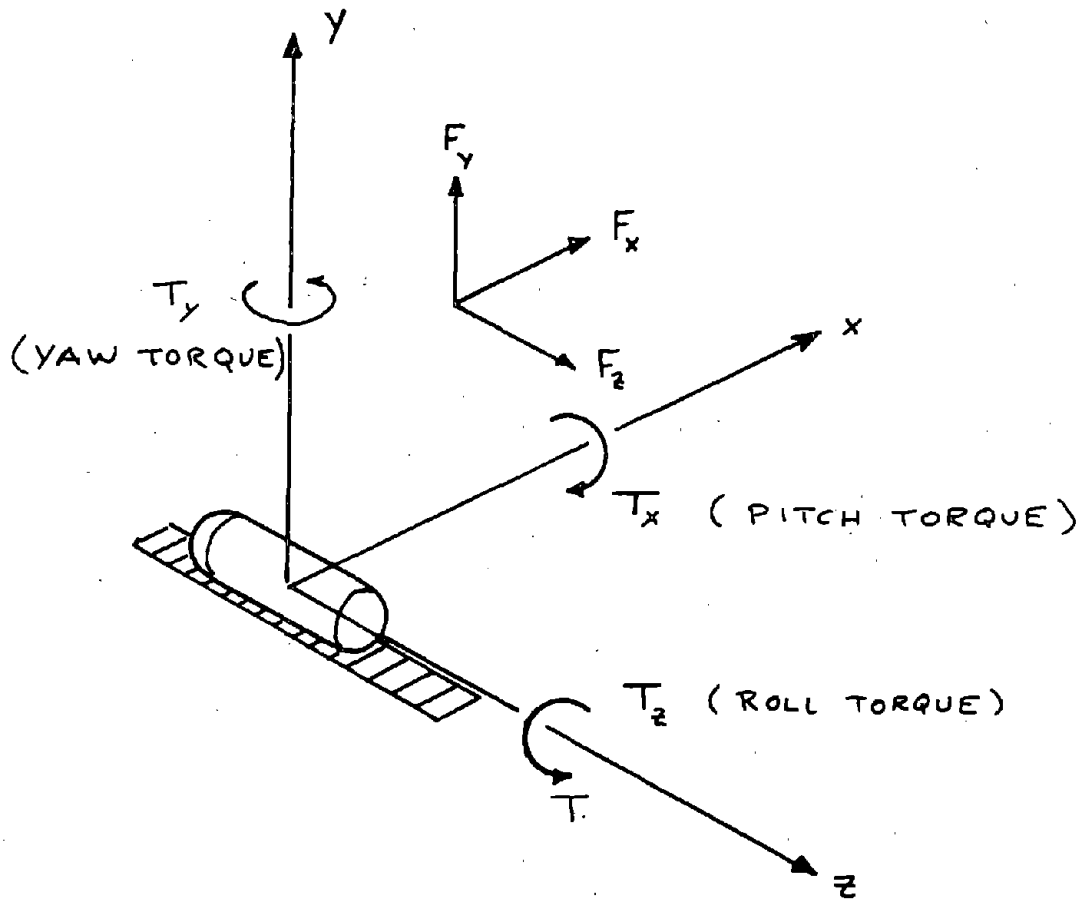


Figure 3. Coordinate System used to Specify Forces and Torques acting on the TMLV coils.

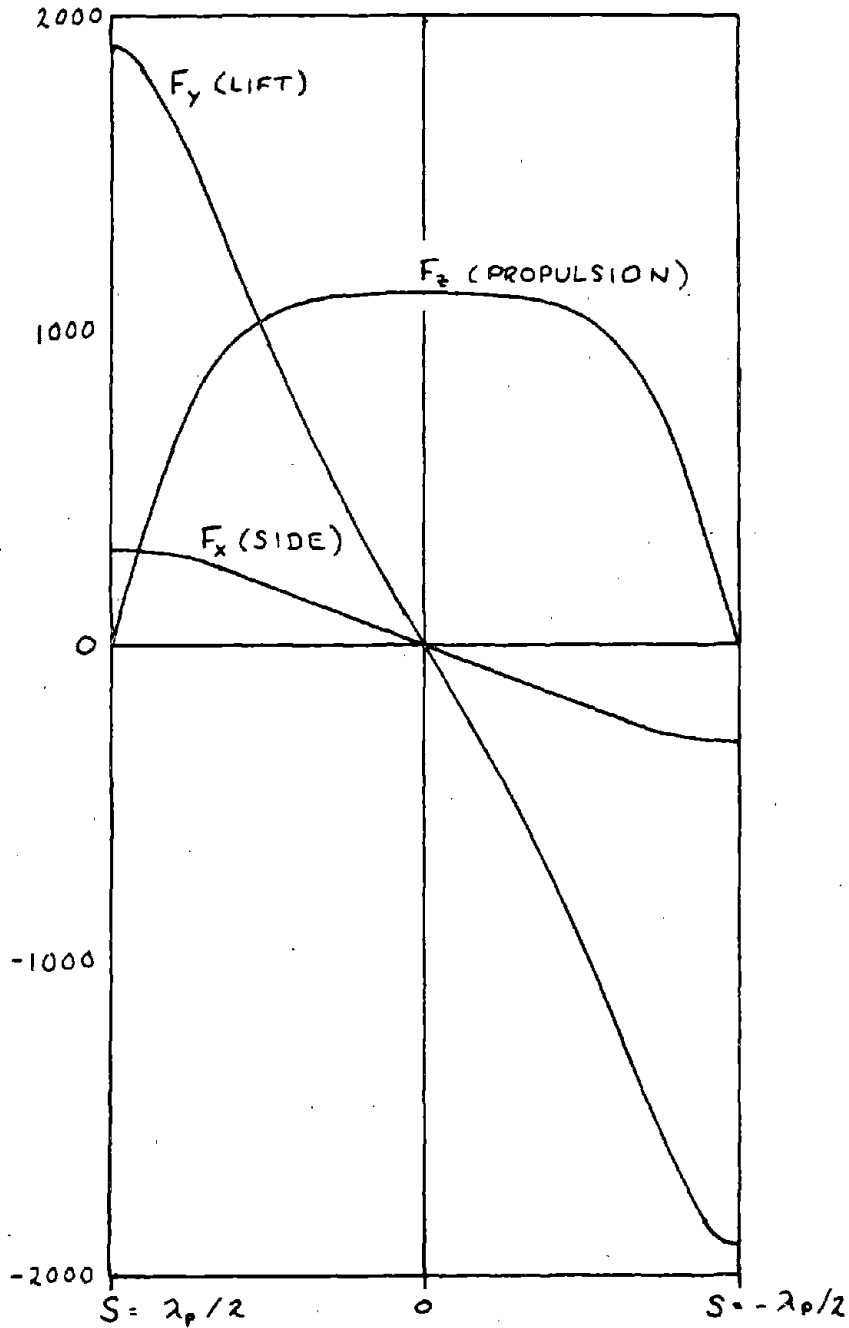


Figure 4a. Single phase forces (Newtons) acting on a single vehicle coil, which is laterally displaced 10 centimeters; as a function of slip. ($y = 30$ cm)

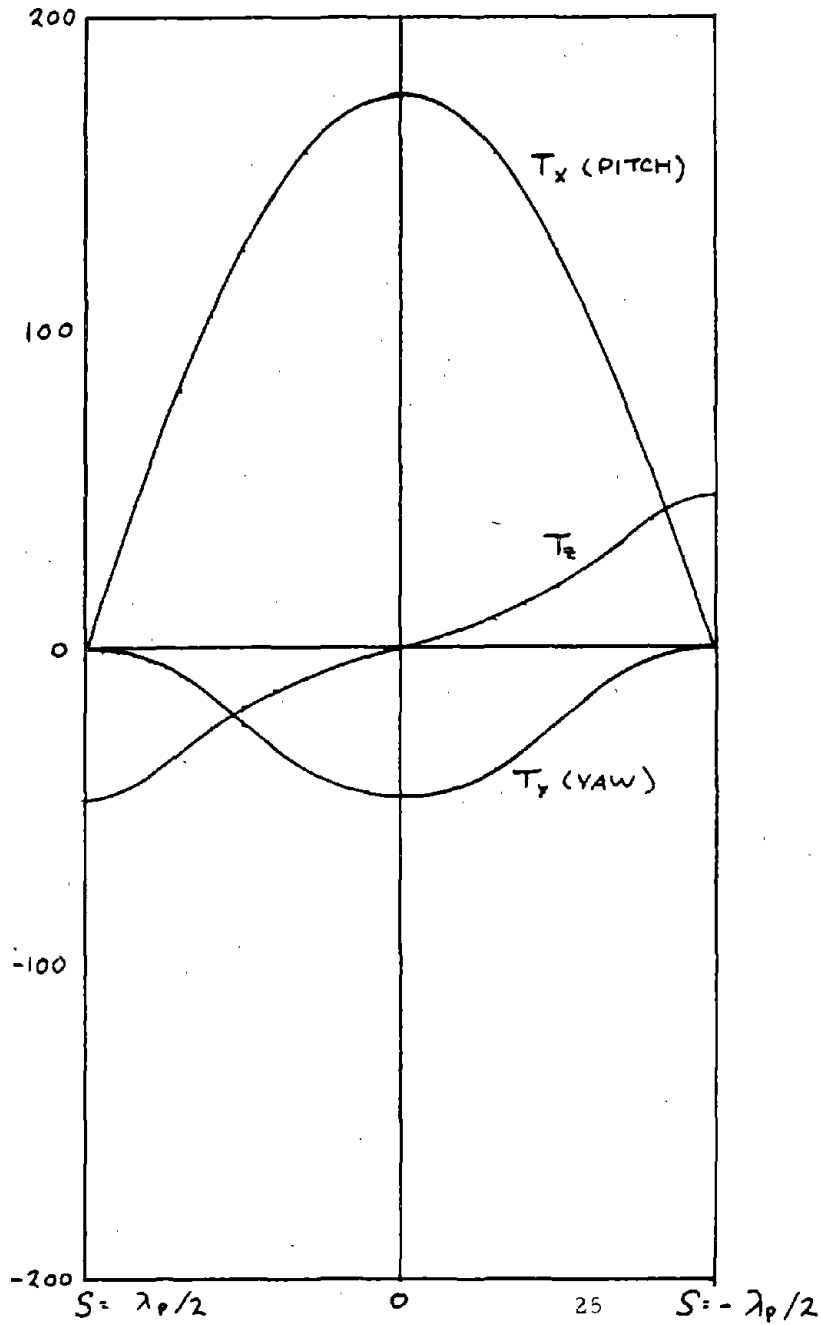


Figure 4b. Single phase torques in Newton-meters acting on a single vehicle coil which is laterally displaced 10 centimeters as a function of slip s ($y = 30$ cm).

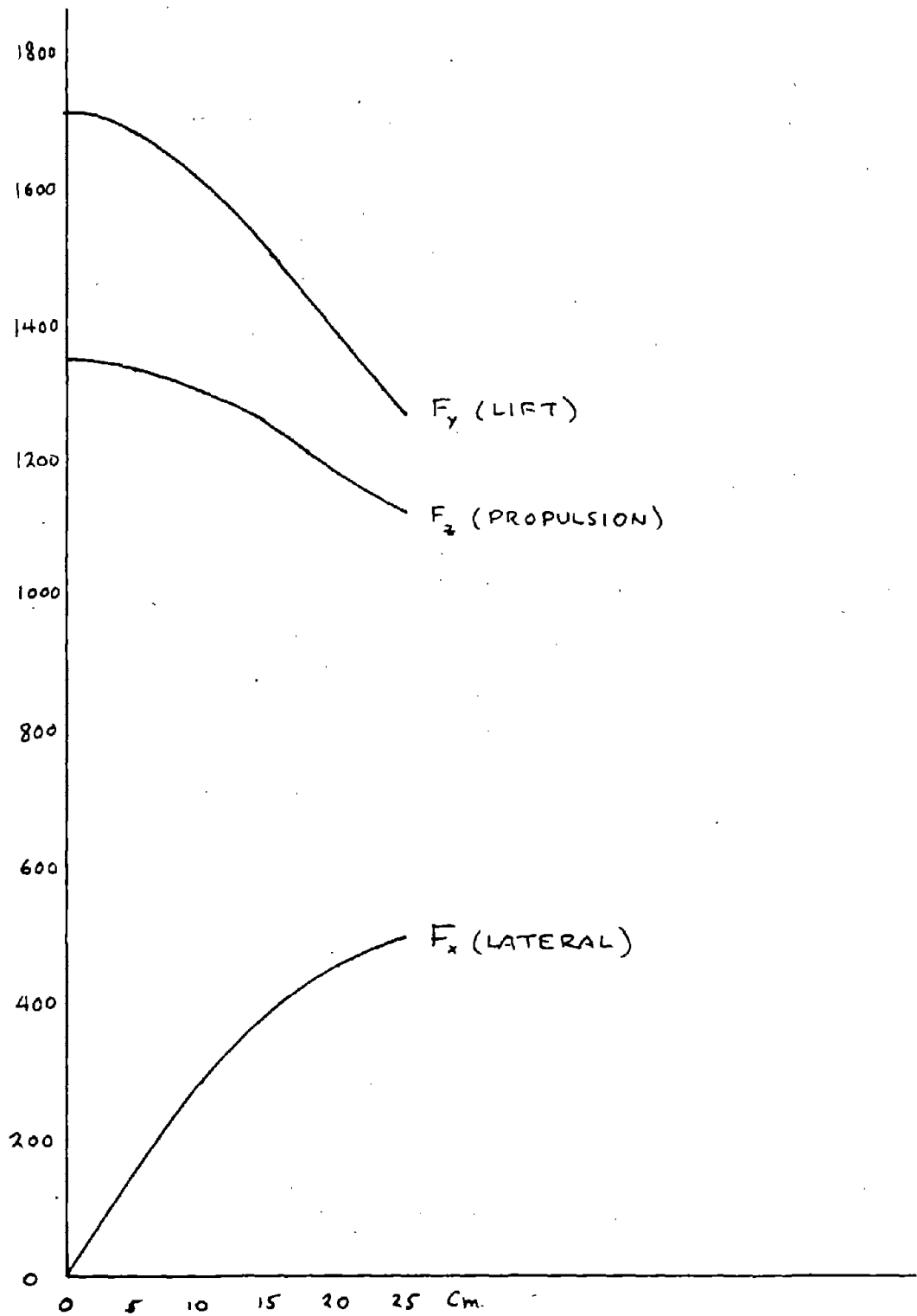


Figure 5. The amplitude of the fundamental component of the three single phase forces: F_x (lateral), F_y (lift) and F_z (propulsion) as a function of lateral displacement. ($h = y = 30$ cm)

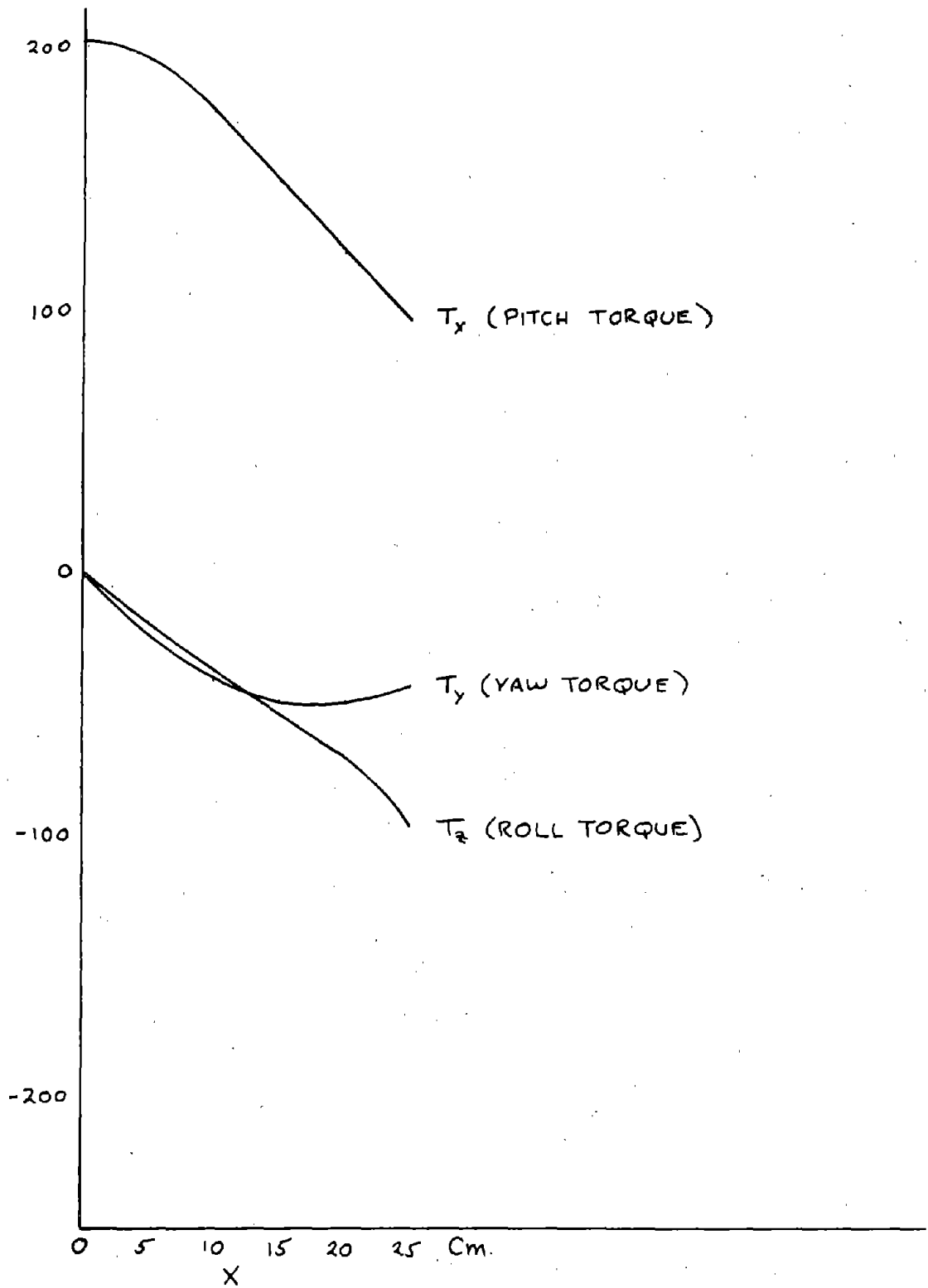


Figure 6. The amplitudes of the fundamental component of each of the three components of torque: T_x (pitch torque), T_y (yaw torque) and T_z (roll torque) as a function of lateral displacement. ($h = y = 30$ cm.)



The fundamental component of F_x , F_y and F_z are shown as functions of vertical displacement y and Figures 7, 8 and 9 for a lateral displacement x of 0, 10 and 20 cm. The functional dependence of these forces is approximately exponential. If the guideway were infinitely wide the functional dependence would be exactly exponential is discussed in Section 5.4.

It is noteworthy that the propulsion force shown in Figure 9 is much less dependent on lateral displacement than either of the other two forces. In fact, at an altitude of 30 cm the propulsion force lost by a lateral displacement of 20 cm can be recovered by a drop in altitude of 3.5 cm. The fundamental components of the torques acting on a single vehicle coil are shown in Figures 10, 11 and 12. The functional dependence of these torques is also approximately exponential with respect to vertical displacement, except for the pitch torque T_x at large lateral displacement (20 cm).

The three single phase forces F_x (side), F_y (lift) and F_z (propulsion) are shown as a function of the roll displacement in Figure 13a for a vehicle centered at $x = 0$ and $y = 30$ cm. Three single phase torques acting on a single vehicle coil similarly located are shown as a function of the roll angle in Figure 13b.

5.4 DISCUSSIONS

5.4.1 Empirical Expressions of Forces and Moments

It is of value to establish an analytical model for describing various force and moment responses as a function of vehicle displacement.

As a function of the gap displacement, forces and moments can be approximated very closely by an exponential function

$$(F, T) = (F_0, T_0) e^{-\gamma y}$$

which is expected from an understanding of field decay properties. The exponential decay characteristic is exactly true for an infinite structure. For finite vehicle magnets, the above expression can be replaced by

$$(F, T) = (F_1, T_1) e^{-\alpha y + \beta y^2}$$

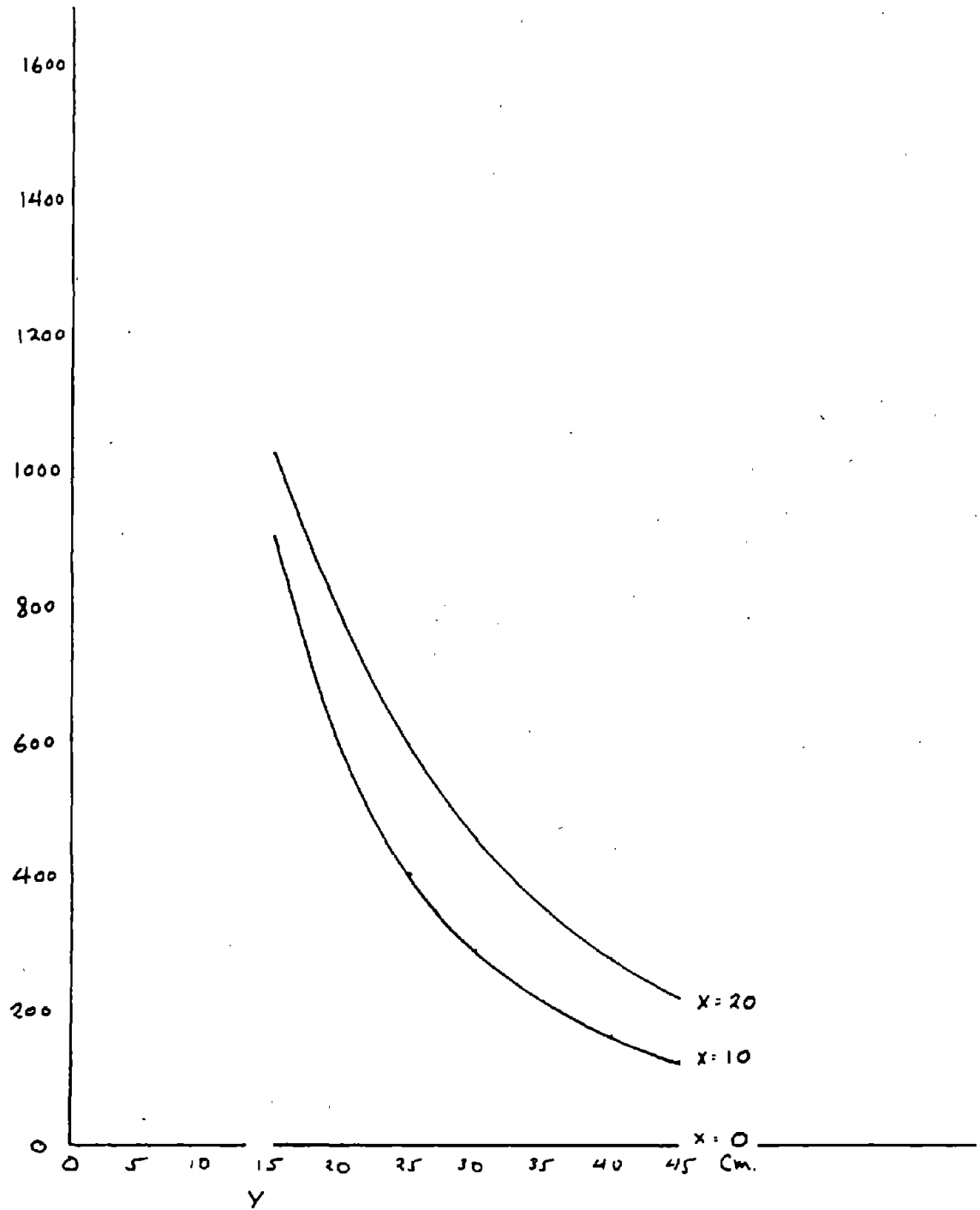


Figure 7. The amplitude in Newtons of the fundamental component of the single phase lateral force F_x acting on a single vehicle coil as a function of vertical displacement y for three lateral displacements $x = 0, 10, 20$ cm.

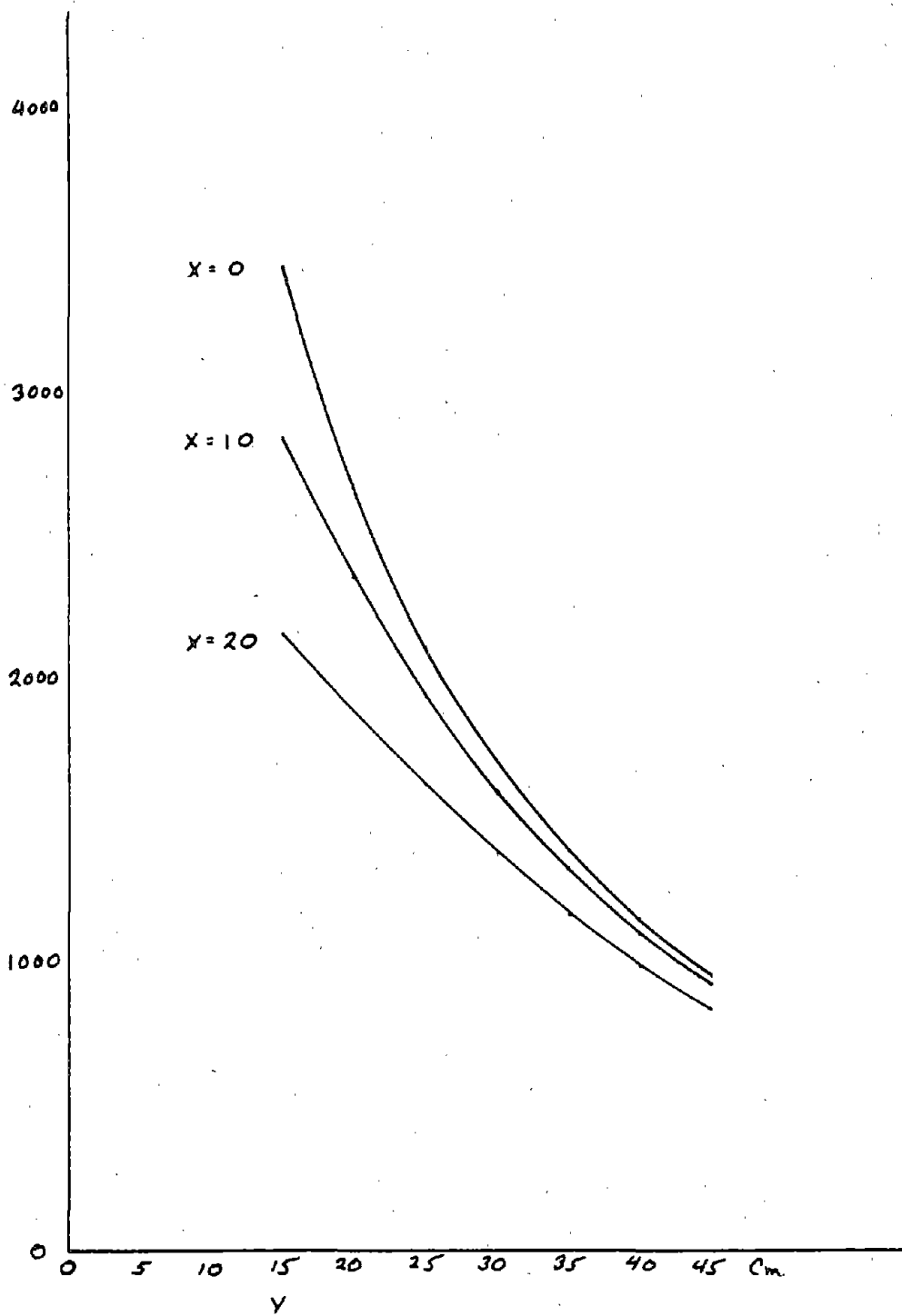


Figure 8. The amplitude in Newtons of the fundamental component of the single phase vertical force F_y acting on a single vehicle coil as a function of vertical displacement y for three lateral displacements $x = 0, 10, 20$ cm.

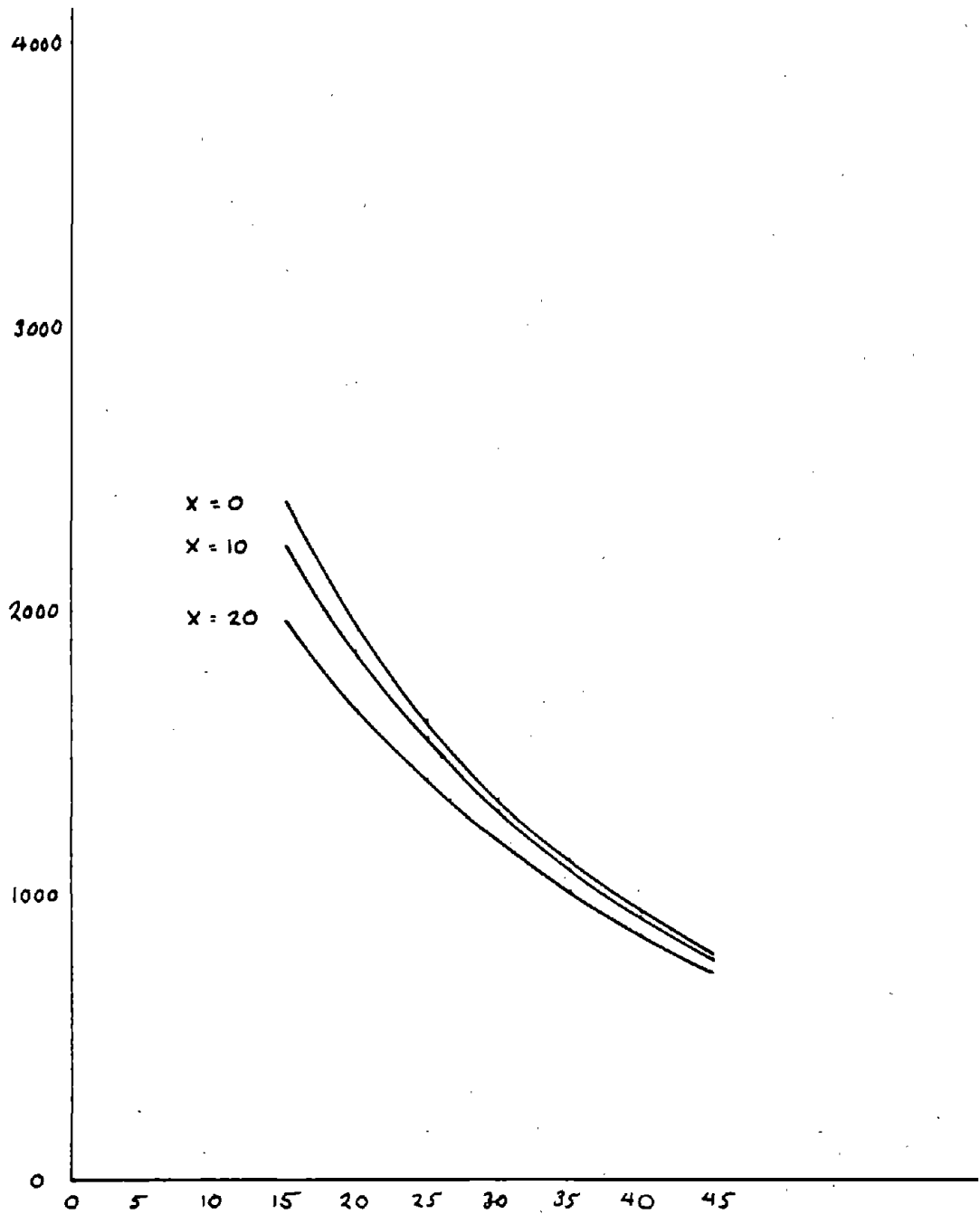


Figure 9. The amplitude in Newtons of the fundamental component of the single phase propulsion force F_z acting on a single vehicle coil as a function of vertical displacement y for three lateral displacements $x = 0, 10, 20$ cm.

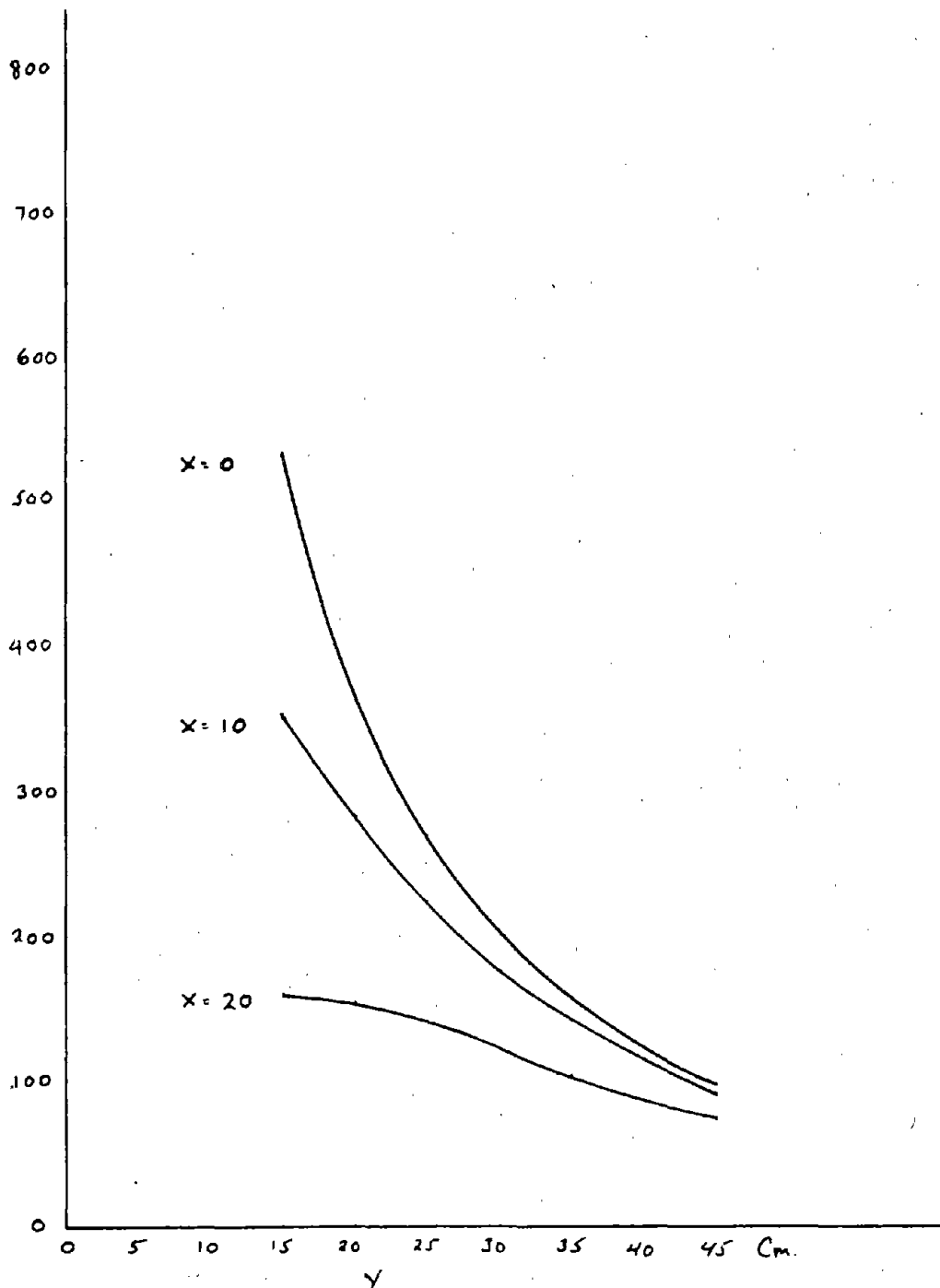


Figure 10. The amplitude in Newton-meters of the fundamental component of the single phase pitch torque T_x acting about the center of a single vehicle coil as a function of vertical displacement y for three lateral displacements $x = 0, 10, 20$ cm.

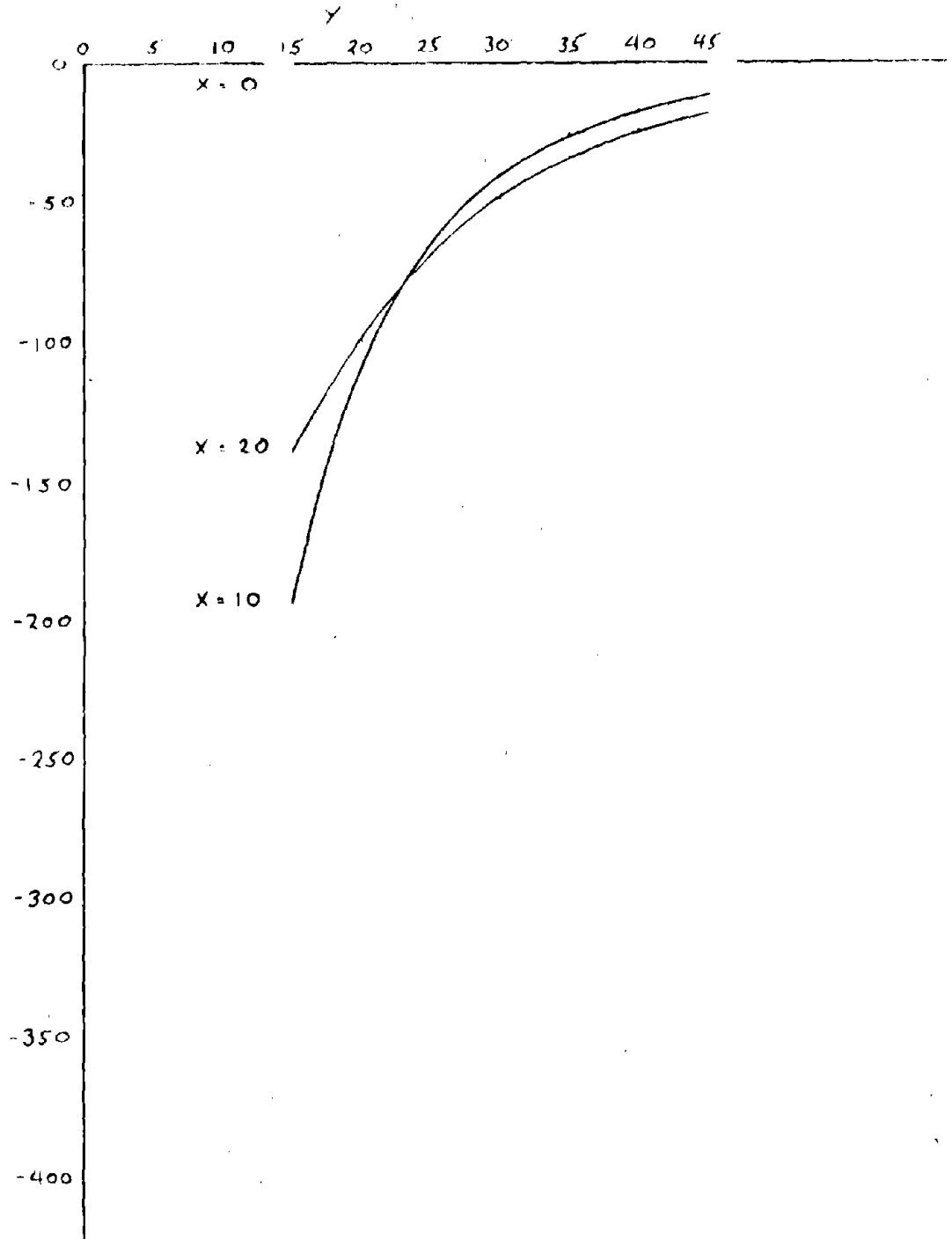


Figure 11. The amplitude in Newton-meters of the fundamental component of the single phase yaw torque T_y acting about the center of a single vehicle coil as a function of vertical displacement y for three lateral displacements $x = 0, 10, 20$ cm.

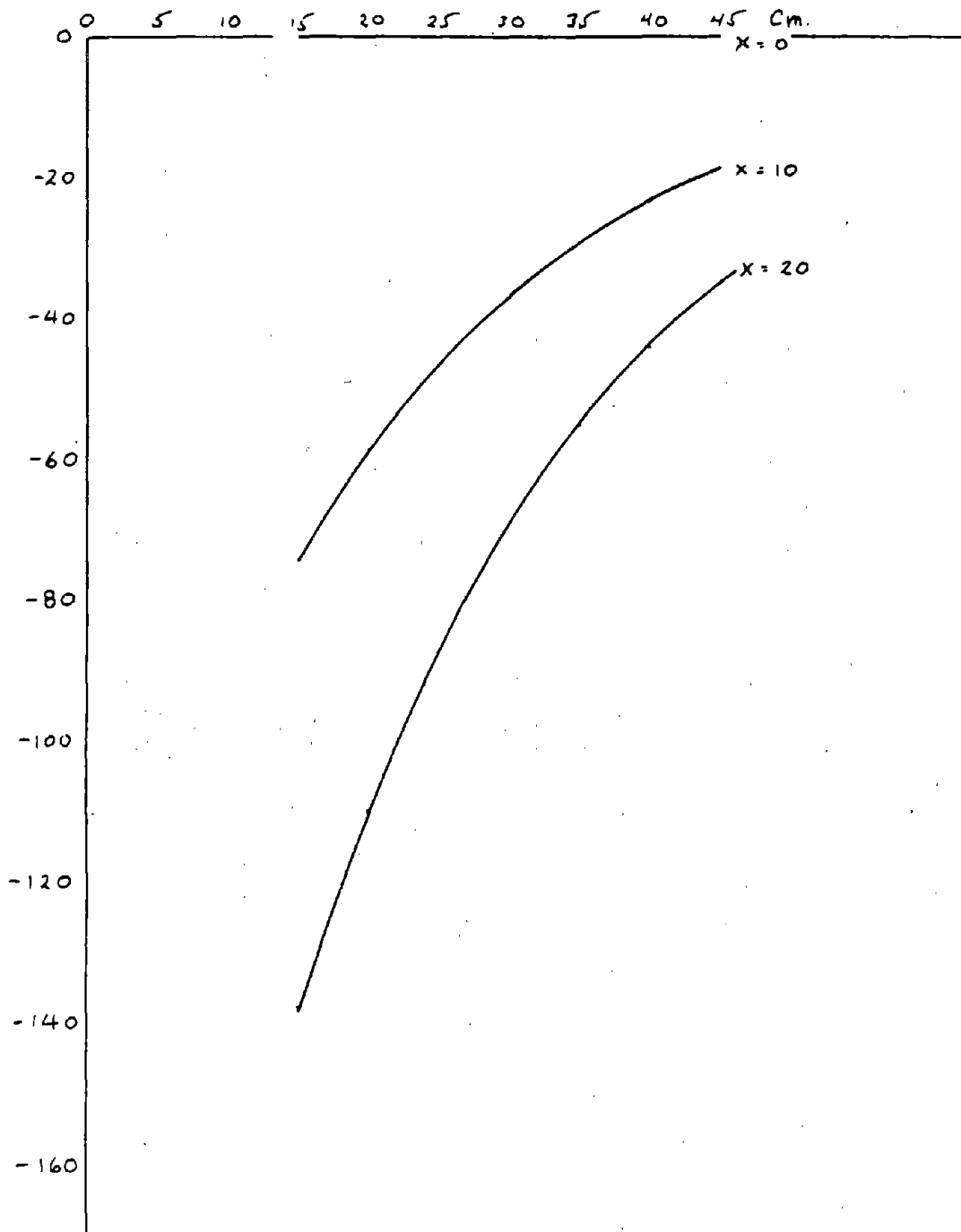


Figure 12. The amplitude in Newton-meters of the fundamental component of the single phase roll torque T_z acting about the center of a single vehicle coil as a function of vertical displacement y for three lateral displacements $x = 0, 10, 20$ cm.

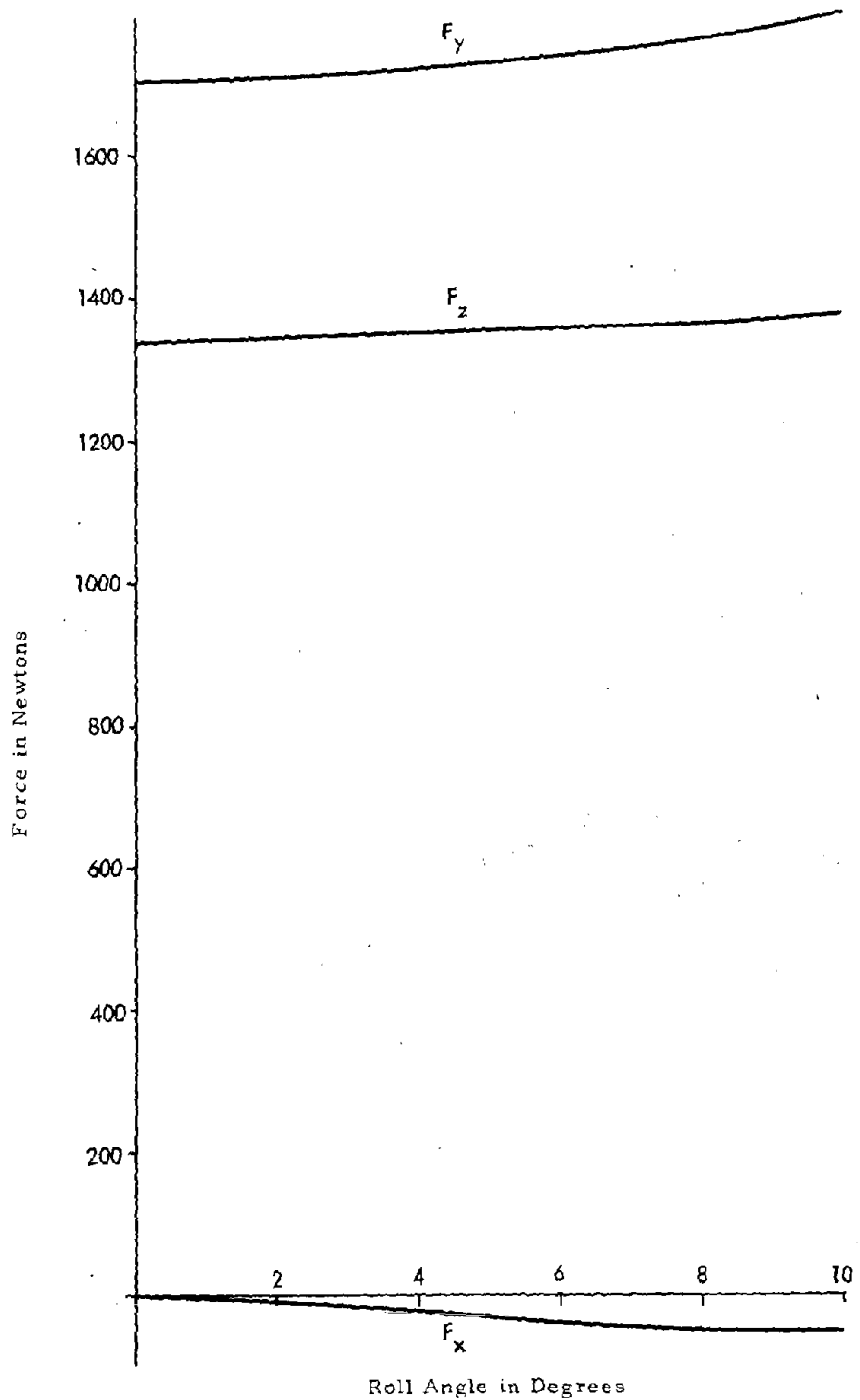


Figure 13a. The Amplitude of the Fundamental Component of the Three Single Phase Forces as a Function of Roll Displacement ($x = 0$, $y = 30$ cm)

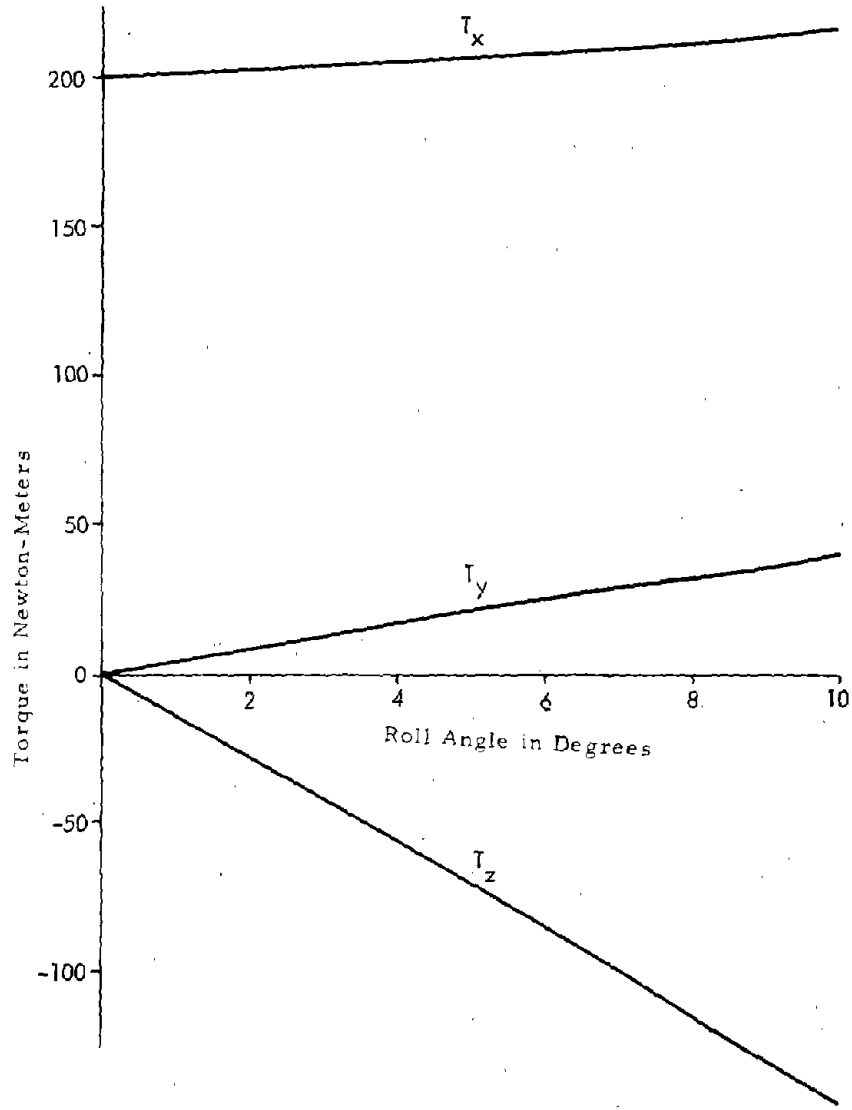


Figure 13b. The Amplitude of the Fundamental Component of Torques as a Function of Roll Displacement ($x = 0$, $y = 30$ cm)

It was found that within the range of y considered, i. e., $y = 15$ to 45 cm extremely good accuracy is obtained with the modified exponential expression. Where F_1 , T_1 , α and β are empirical constants for the gap displacement.

As a function of the lateral displacement, F_x , T_y and T_z are odd functions of x , and F_y , F_z and T_x are even function of x . It was found within the range of x considered, i. e., $x = 0, 10, 20$ cm, a two term polynomial, in the case of F_x , T_y and T_z , and a three term polynomial, in the case of F_y , F_z and T_x , give very good accuracy. Thus

$$\begin{aligned} (F_x, T_y, T_z) &= (F_{x1}, T_{y1}, T_{z1})x + (F_{x3}, T_{y3}, T_{z3})x^3 \\ (F_y, F_z, T_x) &= (F_{y0}, F_{z0}, T_{x0}) + (F_{y2}, F_{z2}, T_{x2})x^2 + \\ &\quad (F_{y4}, F_{z4}, T_{x4})x^4 \end{aligned}$$

where F_{xn} , F_{yn} , F_{zn} , T_{xn} , T_{yn} and T_{zn} are empirical constants for the lateral displacement.

Empirical force and moment expressions for other vehicle displacements can be developed in similar fashions.

5.4.2 Harmonic Contents of Forces and Moments

- a. As a function of y , higher order harmonic contents of all forces decrease as y increases. This holds at $x = 0, 10$ and 20 cm. The harmonic contents of torques are more complicated, particularly that of the yaw torque.
- b. As a function of x , higher order harmonic contents of all forces and torques, except the yaw torque, are relatively independent of x (within the range $x = 0, 10, 20$ cm and $y = 30$ cm). The general tendency is a slight increase of third harmonic content as the lateral displacement is increased.

5.4.3 Effects of Change in Coil Dimensions

In addition to the 1×1.1 coil configuration, smaller size configurations were also evaluated. Additional cases considered include 0.9×0.99 , 0.84×0.935 , 0.8×0.88 and 0.6×0.66 .

It was found that

- a. As coil dimension decreases, both the vertical force and the thrust decrease. Also the ratio of vertical force to thrust decreases.
- b. Specific thrust/vertical force with respect to the coil length and the coil areas for various scaled coils are shown in the Table 2.

Table 2. Specific Thrust and Vertical Force

	Specific Thrust		Specific Vertical Force	
	w. r. t. coil length	w. r. t coil area	w. r. t coil length	w. r. t. coil area
1 x 1.1	274	1045	477	1820
0.9 x 0.99	278	1174	455	1920
0.85 x 0.935	277	1245	437	1960
0.8 x 0.88	274	1305	423	2020
0.6 x 0.66	250	1590	345	2130

To calculate the forces and torques on the vehicle as a function of linear displacement and roll it is necessary only to calculate the forces and torques on one coil and then to multiply those figures by the number of vehicle coils. In the case of pitch and yaw each vehicle coil is located differently with respect to the field of the stator. It is therefore necessary to calculate the forces and torques on each coil and sum them in order to determine the total force in the vehicle. This would require an excessive amount of computer time. For this reason pitch and yaw calculations were performed on only two vehicle coils to allow an estimation of the effect on the entire vehicle.

The forces and torques as a function of pitch are shown in Figure 14. As is to be expected from the symmetry the lateral force F_x and the torque about the y and z axes are zero. The propulsion force F_z and the vertical force F_y are almost invariant with respect to pitch.

The torque about the x axis (pitch torque) increases from 400 Newton meter to 600 Newton meter as the pitch angle changes from 0 to 1.06 degrees.

The forces and torques as a function of yaw are shown in Figure 15 and 16. As would be expected the lateral force F_x and T_y and T_z are odd functions of yaw, vanishing for zero yaw. As shown in Figure 16 the propulsion force F_z , the vertical force F_y and the pitch torque T_x are virtually independent of yaw for angles up to 1.06.

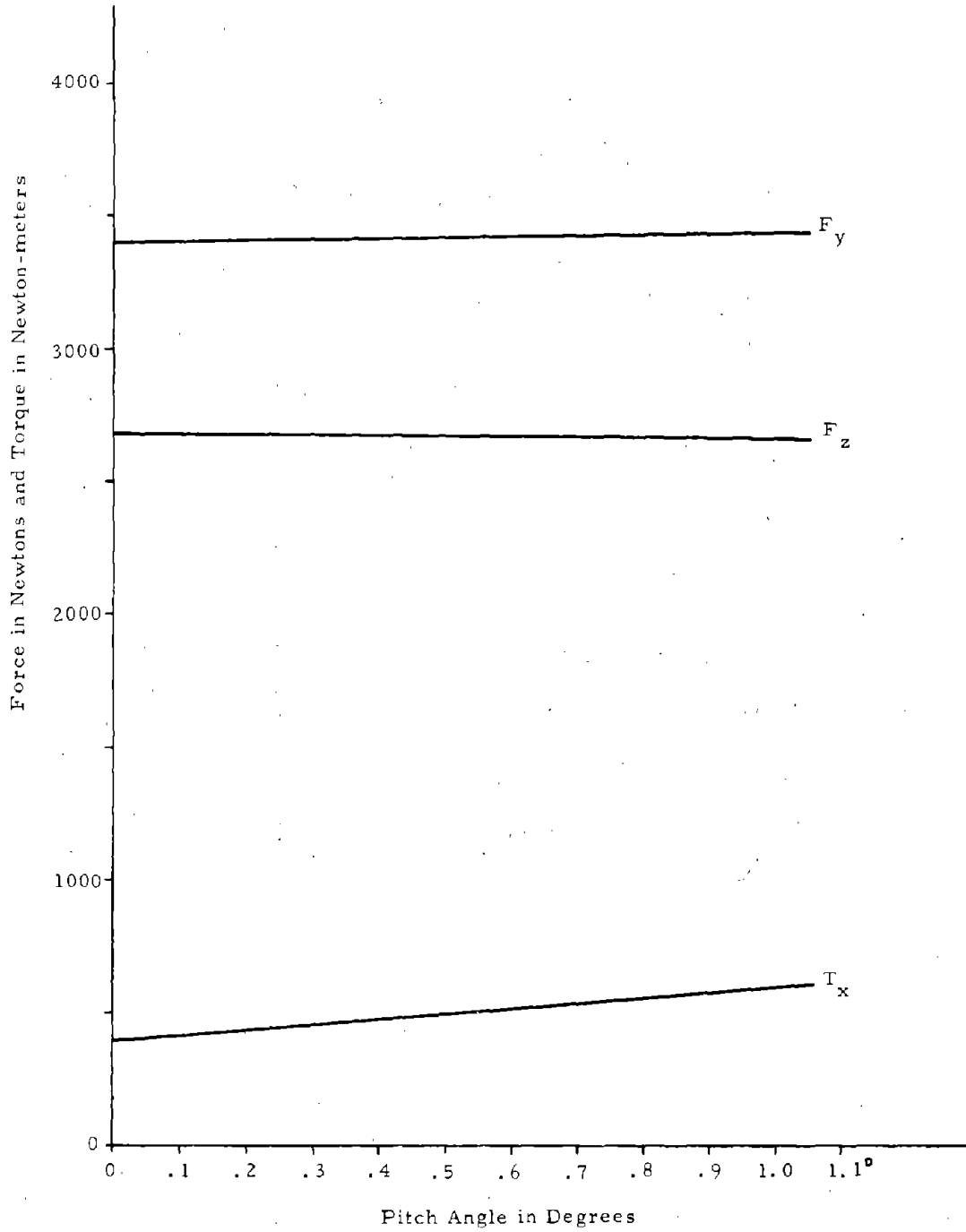


Figure 14. Amplitude of the Fundamental Component of the Single Phase Force and Torques: F_y (vertical), F_z (propulsion) and T_x (pitch) As a Function of Pitch. ($x = 0$, $h = y = 30$ cm)

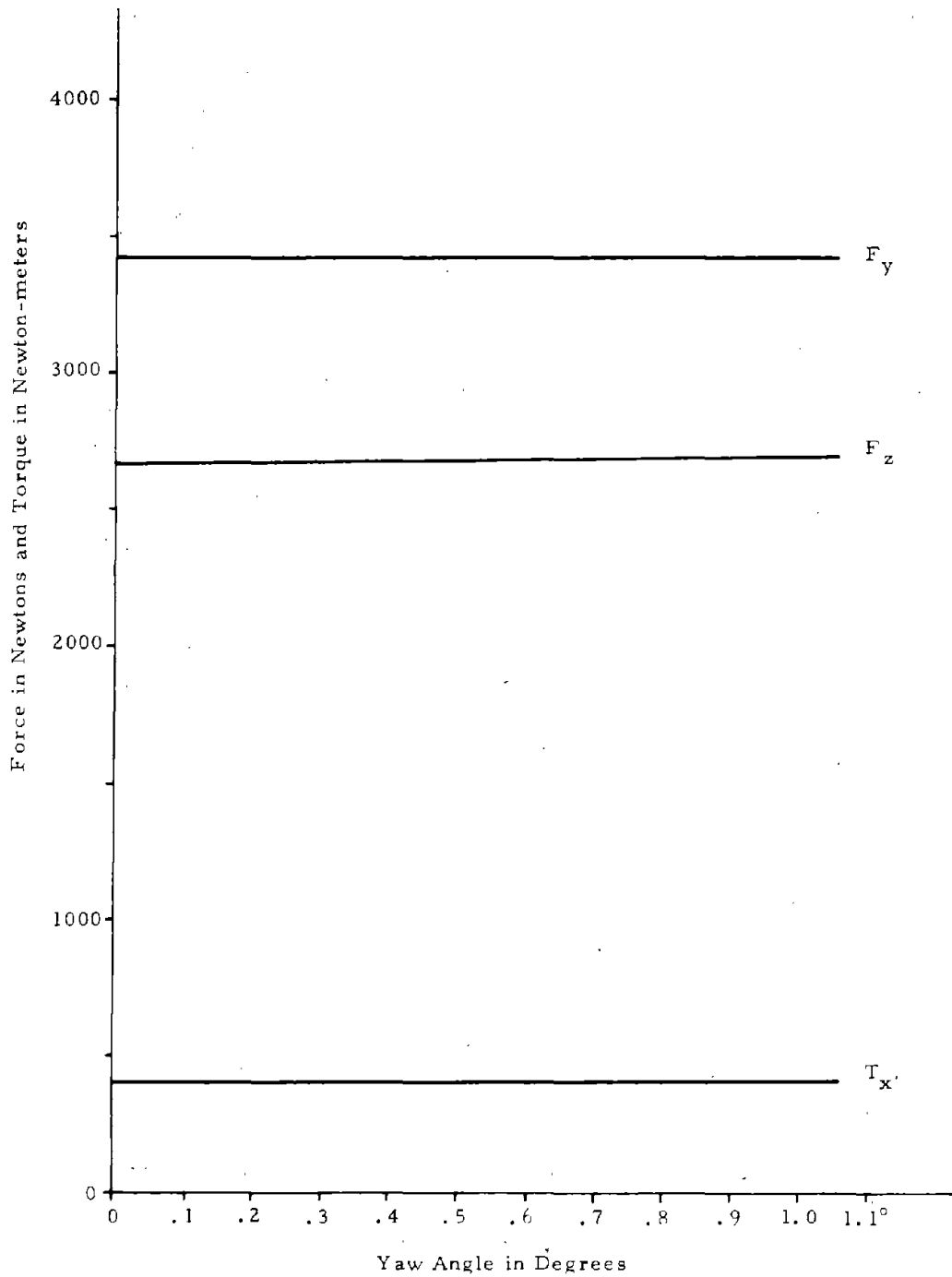


Figure 15. Amplitude of the Fundamental Component of the Single Phase Force and Torques: F_y (vertical), F_z (propulsion) and T_x (pitch) As a Function of Yaw. ($x = 0$, $h = y = 30$ cm)

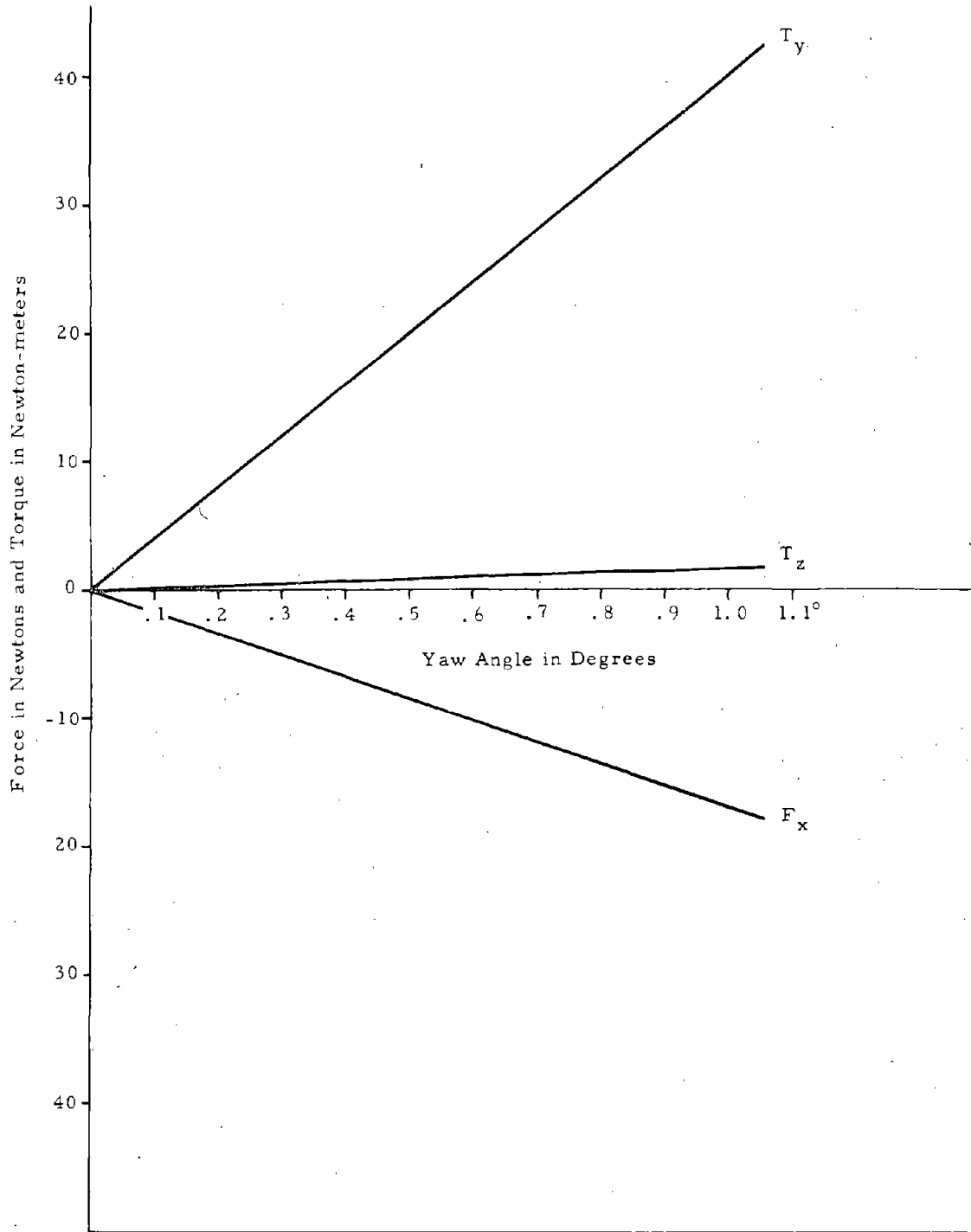


Figure 16. Amplitude of the Fundamental Component of the Single Phase Forces and Torques: F_x (lateral), T_y (yaw) and T_z (roll) As a Function of Yaw. ($x = 0$, $h = y = 30$ cm)

6. HYBRID LSM DESIGN

A typical hybrid LSM configuration is shown in Figures 1a and 1b. Functions of the hybrid LSM and their associated operational principles are described here together with its specific performance characteristics. Also documented are the evaluation of multi winding coupling and vehicle moments about the vehicle center, rather than the center of vehicle coil.

6.1 HYBRID LSM FUNCTIONS AND OPERATIONAL PRINCIPLES

As was mentioned, the specific hybrid LSM concept of interest is to achieve adequate sway and yaw control in addition to satisfying the TMLV propulsion requirement. The operational principles of these functions will now be described.

The hybrid LSM is configured to consist of two identical component motors. Vehicle magnets and winding mechanical specifications for each LSM are identical. Electrical excitation characteristics of the two guideway windings are controlled independently. The three phase winding electric controls include the winding current amplitude and the operation phase (or the slip) of each component motor.

Under a normal condition, the two component motors are operated in a symmetric mode, i. e., the winding currents are equal and their slips are set to zero. The winding currents are such as to satisfy the thrust rating. In general, there are two different thrust ratings that should be provided for any transportation system. The long term thrust rating for cruise and the short term thrust rating for acceleration. It is to be noted the LSM design concept can optimize this situation without penalizing the vehicle pay load. (Passive guideway concepts do not have this option.)

Since the winding current and its operating phase can be controlled independently, the following vehicle controls can be achieved:

- a. The yaw control of the vehicle is produced at zero slip with differential winding currents (for differential propulsive forces).
- b. The sway control of the vehicle is achieved by operating the two component motors at non-zero, anti-symmetric slips.

If we denote the winding currents as i_1 and i_2 , and the slips as s_1 and s_2 , then the total propulsion of the hybrid LSM is

$$P = i_1 p_1 (s_1) + i_2 p_2 (s_2), \quad N$$

the total sway force of the vehicle is

$$S = \pm |i_1 v_1 (s_1) - i_2 v_2 (s_2)|, \quad N$$

and the total controllable yaw moment is

$$Y = \pm |i_1 p_1 (s_1) - i_2 p_2 (s_2)| (0.82 \text{ meter}) \quad N\cdot m$$

where $p_i (s)$ and $v_i (s)$ are respectively the propulsion force and the vertical force of each component motor. Using these notations, the hybrid LSM functions can be characterized as

propulsion	$s_1 = s_2 = 0,$	$i_1 = i_2$
yaw control	$s_1 = s_2 = 0,$	$i_1 \neq i_2$
sway control	$s_1 = -s_2,$	$i_1 = i_2$

Note, from equations (11) and (12)

$$p = p_m \cos (\pi s / \lambda p)$$

$$v = v_m \sin (\pi s / \lambda p)$$

where values of p_m and v_m can be found in Section 5.

6.2 SPECIFIC HYBRID LSM DESIGN

Based on computational results presented in Section 4, a specific hybrid LSM design is discussed here. Additional optimization considerations will be outlined in Sections 6 and 7.

Using 1 meter wide by 1.1 meter long magnets as the baseline design, and using the same coil dimensions for the guideway winding, the per vehicle coil, per winding phase propulsive force is determined to be 1340 Newtons. Thus in order to obtain a short term thrust rating of 64 KN, a total of 32 magnets is required.

Therefore we envision two identical component motors, each with the 16 magnets. For this estimate, the vehicle coil current is 500 KAT and the guideway winding current is 1.5 KAT.

The short term thrust requirement can be used as a reference for establishing other vehicle dynamical requirement. Thus, the long term thrust rating of 41 KN (at the cruise) can be satisfied with a guideway winding current of 0.956 KAT which is 63.7% of the short term rating.

6.2.1 Estimate of Yaw Moment

For the yaw control, we can assume $s_1 = s_2 = s$, thus

$$Y = \pm 0.82 (\Delta i) p_m \cos (\pi s / \lambda_p) \quad \text{N-m}$$

At the zero slip, the above gives

$$Y = \pm 0.82 (\Delta i) p_m \quad \text{N-m}$$

Typical yaw moment can be given as

$$Y = \pm (0.82) \cdot (0.363) \cdot (64) = \pm 19 \quad \text{KN-m}$$

where a moment arm of 0.82 meter is used together with 64 KN propulsion force. The differential winding currents is taken to be 0.363 which the percentage difference between the long term winding current and the short term winding current. Higher yaw moment can be obtained by applying larger differential winding currents.

6.2.2 Estimate of Sway Control Force

For the sway control, we assume $i_1 = i_2 = i$ and $s_1 = -s_2$, then

$$\begin{aligned} S &= \pm i [v_1 (s) - v_2 (-s)] = \pm 2i v (s) \\ &= \pm 2i v_m \sin (\pi s / \lambda_p) \end{aligned}$$

Thus for a given vehicle guideway design, the total sway force can be controlled by applying a proper amount of winding current. At the small slip region, the above is reduced to

$$S = \pm 2i v_m (\pi s / \lambda_p)$$

where v_m is, as shown in Section 5, a function of the vehicle lateral displacement.

In order to relate the sway control force to the vehicle lateral spring constant, the following estimation is made. From Section 5, we found that the rate of change of v_m as a function of the vehicle lateral displacement is approximately

$$1.5 \times 16 \times 3820 = 0.87 \times 10^5 \text{ N/m}$$

If desired, a larger spring constant can be obtained by having more vehicle magnets. (Note that in the above calculation, 16 rather than 32 is used, because the elemental spring constant of 3820 N/m is estimated on the basis of a lateral pair of vehicle magnets).

6.3 EVALUATION OF SPECIFIC HYBRID LSM CONFIGURATION

The force and moment analyses of an elemental LSM unit were discussed in Section 5. Since the proposed hybrid LSM configuration consists of two elemental LSM units, a computation was carried out to determine the amount of coupling effect between the two units. Also the moments of the hybrid LSM are computed about the vehicle center.

Consider the geometry of the hybrid LSM as shown in Figure 1. The total LSM system consists of two guideway windings and two vehicle magnet sets. If we label the two component LSM units as a and b, we would have windings a and b, and magnet sets a and b. Based on previous analysis of the elemental LSM unit, the design information on forces and moments due to the interaction of the magnet set a (or b) and the guideway winding a (or b) have been made explicit. It is desirable to determine the interaction between the magnet set a and the guideway winding b, or vice-versa. Also, previous moment results are generated with respect to the coil center. All results discussed here are generated with respect to the vehicle center (of course, this change of moment center does not affect the result for the force calculation).

Figure 17 shows forces and moment due to the elemental LSM unit, i. e., due to the interaction of magnet set a (or b) and guideway winding a (or b), as a function of the slip. Note the change of T_x , as compared to the previous result.

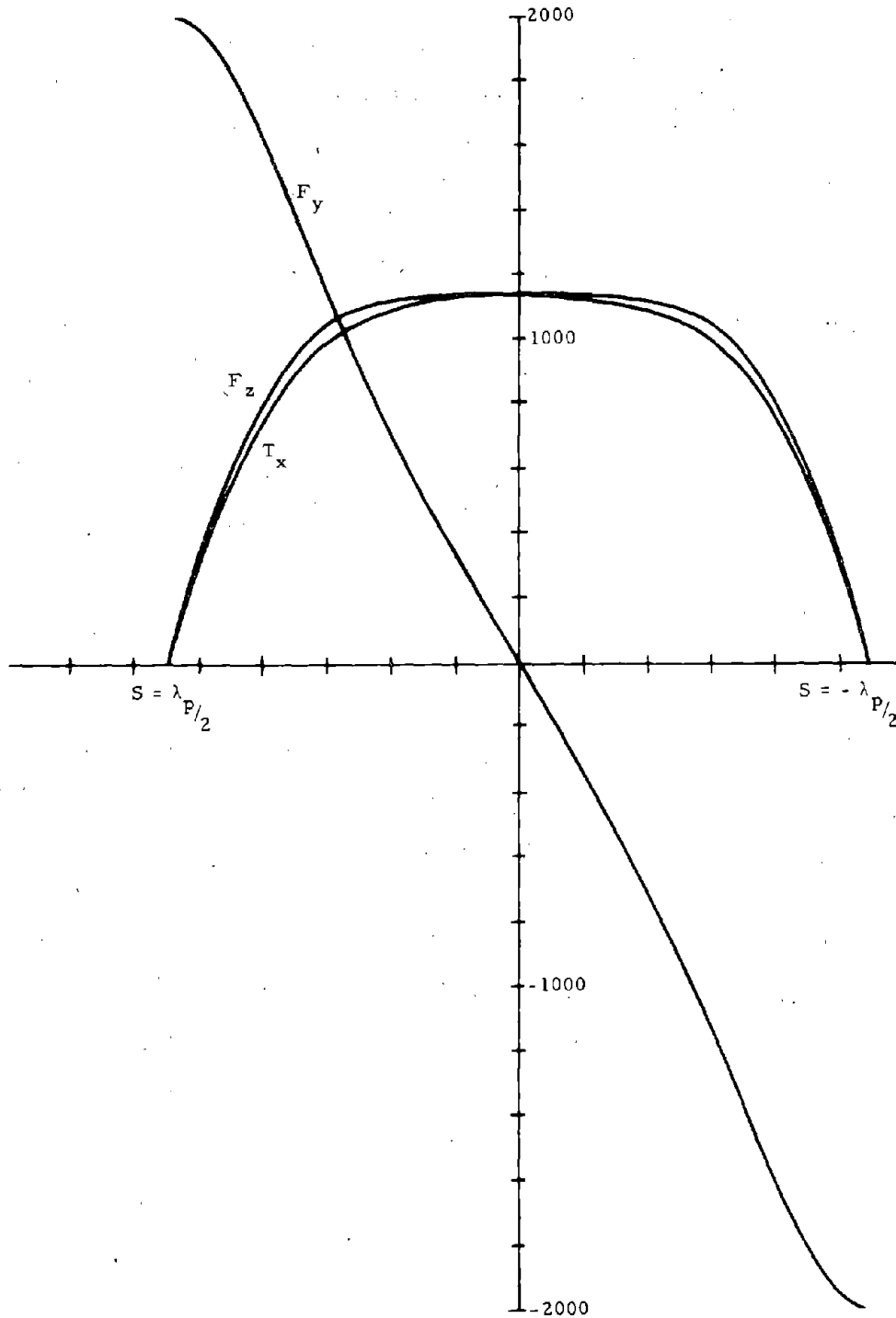


Figure 17. Single Phase Forces (Newtons) and Torque (Newton-meters) Acting on a Single Vehicle Coil (as a Function of Slip s) with Moment about the Vehicle Center of the Hybrid LSM--Computation for Elemental Unit.

Figure 18 shows forces and moment due to the mutual coupling effect, i. e., due to the interaction of magnet set a and guideway winding b (or vice-versa), as a function of the slip. Note the interaction gap distance for the elemental LSM unit is 0.3m and a moment arm of 0.82m, while for the mutual interaction, the gap is 1.34m and same moment arm. Due to the fast decay nature of the near magnet field, a weak coupling effect is expected because of a fairly large difference in gap sizes.

The following table compares the forces and moment for the above two computations.

	Elemental LSM	Mutual Interaction	Percentage
$(F_y)_{max}$	2004	47.3	2.36%
$(F_z)_{max}$	1145	42.5	3.7%
$(T_x)_{max}$	1145	38	2.52%

The above results relate to LSM force and moment when the hybrid LSM is at the normal height, i. e., 0.3 meter from the ground levitation conductor. Two additional computations were performed to evaluate effects of the moment center on various torques.

Figure 19 shows three elemental LSM torques about the vehicle center when the height of the vehicle magnet set is perturbed by 10 cm. Results for a 20 cm height perturbation are shown in Figure 20.

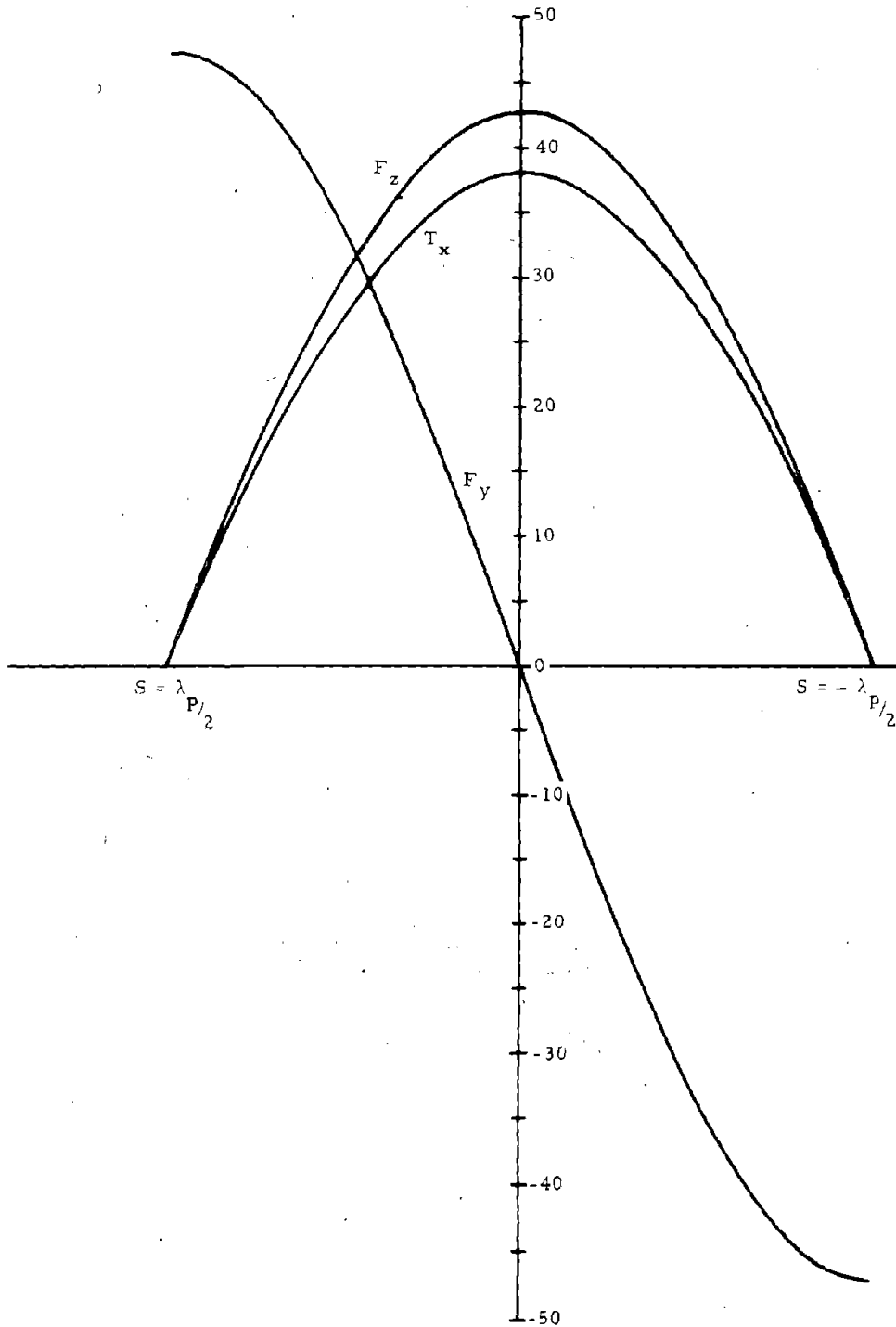


Figure 18. Single Phase Forces (Newtons) and Torque (Newton-meters) Acting on a Single Vehicle Coil (as a Function of Slip s) with Moment About the Vehicle Center of the Hybrid LSM--Mutual Interaction Computation.

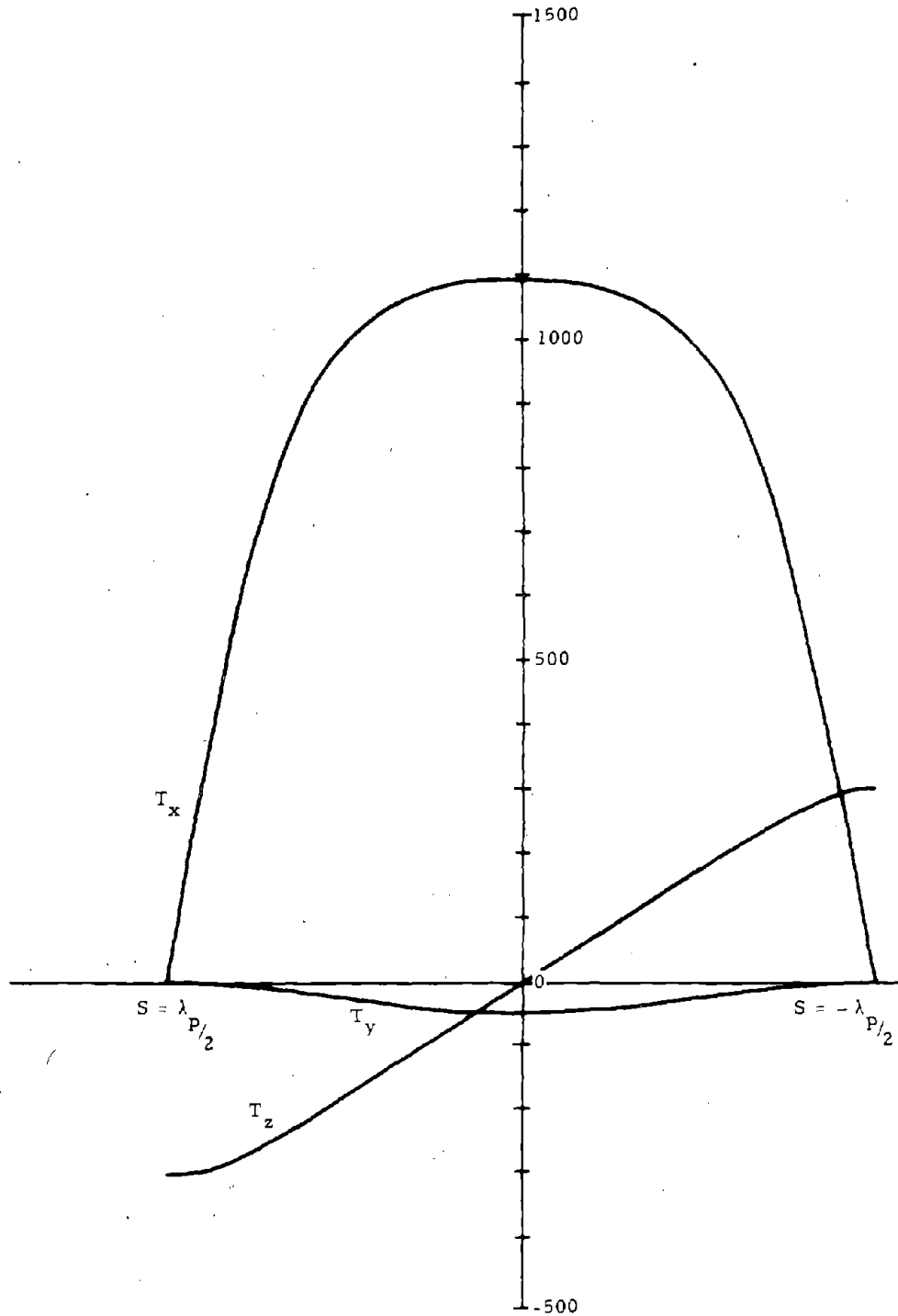


Figure 19. Single Phase Elemental LSM Torques (Newton-meters) About the Vehicle Center (as a Function of Slip s)--The Height of the Vehicle Magnet is Displaced by 10 cm.

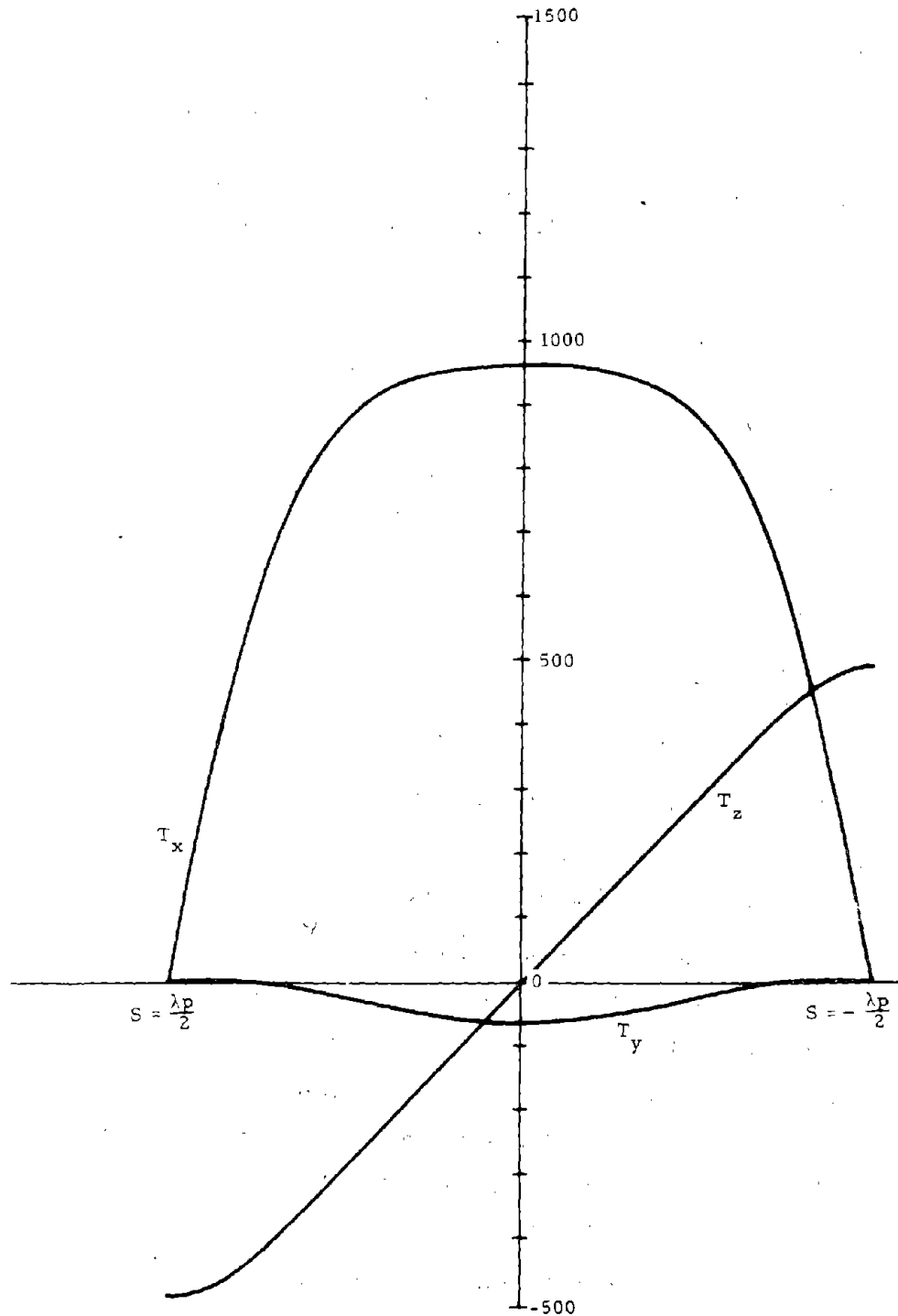


Figure 20. Single Phase Elemental LSM Torques (Newton-meters) About the Vehicle Center (as a Function of Slip s)--The Height of the Vehicle Magnet is Displaced by 20 cm.



7. ON DETAILED LSM DESIGN PROBLEMS

7.1 SELECTION OF COIL GEOMETRIES OF VEHICLE MAGNET/GUIDEWAY WINDING

Computations were performed previously (see reference 1) for coils of various geometries. They were intended for determining effects of coil geometry and dimension on the associated thrust and vertical force. Several observations are described here.

- a. Thrust and vertical force are more dependent on the coil aspect ratio than the detailed coil geometry.
- b. For all cases evaluated (more than 15 cases), the amplitude of the vertical force is always greater than that of the thrust.
- c. If we let R be the ratio of the vertical force to the thrust, then

$$R_l > R_r > R_w > 1$$

where

R_l is the ratio for long coils

R_r is the ratio for regular coils, such as circular, square and diamond

R_w is the ratio for wide coils

- d. In terms of specific thrust (with respect to the coil length), the thrust associated with a wide coil is much larger than that associated with a long coil.
- e. It might be expected that a hybrid combination of coil geometries of vehicle magnet and guideway winding should produce an optimum design. Based on our computations, this is shown to be the case. However, the improvement is only slight.

Note the above consideration concerns only the thrust and the vertical force evaluation. This is meaningful only in conjunction with other design considerations, such as the winding current density, the eddy current loss



and winding stranding, the thermal and insulation problem and the selection of pole pitch (as constrained by the frequency and the magnetic field distortion).

7.2 WEIGHT OF THE SUPERCONDUCTING MOTOR MAGNETS

Two estimates of the weight of the motor magnets, based on widely differing estimation of superconductor current density, were made. In their paper, "Design of a Full Scale Magneplane Vehicle",¹² Iwasa, Hoenig and Kolm assumed an average composite current density of 5600 A/cm² (Superconductor current density 2.5 x 10⁵ A/cm²). They propose a hollow niobium titanium multifilament, aluminum stabilized and stainless steel reinforced, composite conductor with a rectangular cross section.

The liquid helium in the system is pumped through a 1 sq cm channel in the conductors. In his paper "High density Superconducting Magnets Using Heavy Current",¹³ D. L. Atherton suggests that much higher composite current densities are possible. He describes three solenoids wound with twisted fine filamentary composite conductors which operate at 27,200, 30,500 and 42,000 A/cm². In his conductors the Cu: niobium titanium ratio is 1.35:1, 1:1, and 1.25:1.

Weight Based on the Design Approval of Iwasa et al

$$\text{Magnet Area: } 500,000 \text{ A} / 5600 \text{ A/cm}^2 = 89.3 \text{ cm}^2$$

$$\text{Conductor Length: } 2 (1.1 + 1) = 4.2 \text{ meters}$$

$$\text{Conductor Volume: } 89.3 \times 420 = 3700 \text{ cc}$$

$$\text{Volume of N}_b \text{ T}_i: 37,500 \times \frac{5600}{2.5 \times 10^5} = 840 \text{ cc}$$

$$\text{Volume of A}_e: 36,600 \text{ cc}$$

$$\text{Weight of N}_s \text{ T}_i: (840. \text{cc}) (5.6 \text{ gm/cc}) = 4.7 \text{ kg}$$

$$\text{Weight of A}_e: (36,660 \text{ cc}) (2.76 \text{ gm/cc}) = 101 \text{ Kg}$$

$$\text{Weight of Conductor: } 105.7 \text{ Kg}$$

Weight Based on the Design of Atherton

Magnet Area: $500,000 \text{ A} / 30,500 = 16.4 \text{ cm}^2$

Conductor Length: 4.2 meters

Conductor Volume: $16.4 \times 420 = 6900 \text{ cc}$

Volume of $N_b T_i$: 3450 cc

Volume of Cu: 3450 cc

Weight of $N_b T_i$: $3450 \text{ cc} \times 5.6 \text{ gm/cc} = 19.3 \text{ Kg}$

Weight of Cu: $3450 \text{ cc} \times 8.9 \text{ gm/cc} = 30.7 \text{ Kg}$

Weight of Conductor: 49 Kg

7.3 ESTIMATED WEIGHT OF THE DEWAR SYSTEM

The weight of the dewar system is based on a rule of thumb which states that the weight of the vacuum chambers, heat shields and support structure can be estimated as equal to the weight of a half-inch thick wall of stainless steel enclosing the winding. Since a similar structure would be needed for either winding, the estimate is made only for the MIT design.

I. D. of the sst. 10.6 cm

Volume = $(10.6 + 1.27) \pi 420 = 15,650 \text{ cc}$

Weight of Dewar $15.65 \text{ liter} \times 7.8 \text{ Kg/liter} = 122 \text{ Kg}$

Thus, the total magnet weights for the two systems are

227.5 Kg and 171 Kg

7.4 GUIDEWAY WINDING DESIGN

The following guidelines relative to the guideway winding design are of interest.

- a. Selection of pole pitch - a compromise between the magnetic field distortion and the amount of winding conductor.

- b. Current density in winding conductors - thermal problem is a concern, the current density typically ranges from 200 to 600 amp/cm² depending on the ventilation condition. In this respect, the linear motor should have less of a thermal problem than the rotary counterpart.
- c. Demagnetizing effect of the guideway winding current should be analyzed so as to avoid force degradation due to higher order harmonics.
- d. Machine loss models - accurate models for evaluating eddy current loss and that for determining the interaction between LSM winding and levitation conductor should be established so as to generate explicit design information.
- e. Effects of unbalanced three-phase winding current on various forces and moments should be evaluated. The dominant effect is expected to be on the third harmonic force contribution.

8. CONCLUSIONS AND RECOMMENDATIONS

As a propulsion system for tracked magnetically levitated vehicles, the LSM design stands out as a strong candidate for the ultimate Maglev system. Reasons for this conclusion are stated in Section 4. They include the large gap compatibility, the multidimensional controllability, the synchronous feature, the optimum thrust rating option, the high efficiency and high speed potentials, and the quiet operation with minimal pollution. A brief comparison of various propulsion systems is also made.

The cost of an active guideway has often been stated as a major disadvantage of the LSM design. Yet, there does not seem to exist any explicit cost data to justify the statement in a strong sense.* In fact, various preliminary analyses have indicated the cost-effectiveness of the LSM design. It is to be noted, two key factors to be stressed in the cost analysis are: (a) the high traffic density for the justification of any high speed ground transportation system,* (b) the unique feature of the LSM system for improved ride quality.*

The major part of the present study effort is on an explicit design analysis of the LSM force and moment models. Mathematical bases for various evaluations are established. They are used to develop a set of computer programs, mentioned previously. Using these computed programs, numerical results of the LSM force and moment are generated. They are also used for evaluating a specific hybrid LSM design.

A hybrid LSM system configured for the sway and yaw control in addition to the propulsion function is described. Specific design data estimated for the hybrid LSM are also discussed.

Through the studies of the LSM force and moment models and the design evaluation of the hybrid LSM design, the viability of the LSM system has thus been made more explicit. Several detailed LSM design problems have also been identified. It is deemed desirable to summarize here a set of recommendations for a further LSM study.

*As stated in earlier footnotes, the Ford/Philco analyses are in disagreement with the noted statements. We also conclude that the "unique feature" of LSM, i. e. for improved ride quality, is a substantial disadvantage since it complicates the guideway without providing tangible system benefits.

- i. Integration of LSM with levitation design.
 - i.1 Compatibility of propulsion and levitation magnets.
 - i.2 Application of stable guideway configurations.
 - i.3 Interaction of LSM winding and levitation conductors.
- ii. Generate a simulation model for control and ride quality analysis.
 - ii.1 Analytical modelling of passive levitation and active LSM forces and moments.
 - ii.2 Devise and classify multidimensional LSM controls.
 - ii.3 Simulate various LSM control characteristics.
- iii. Develop computer program for handling field distortion problems.
 - iii.1 Analyze demagnetizing effect of the guideway winding current.
 - iii.2 Optimization of vehicle magnet/guideway winding with practical constraints (cool current density, thermal rating, pole pitch, etc.).
- (iv) Select power distribution systems and perform trade-off studies.
- (v) Investigate and devise power switching designs.
- (vi) Identify sensor and instrumentation requirements.
- (vii) Cost analyses of guideway and power distribution systems.

APPENDIX I

Derivation of a Trigonometric Identity

To analyze the expression

$$G_n = \cos n \left(\kappa z - \frac{2m\pi}{3} \right) \cos \left(\omega t - \frac{2m\pi}{3} \right)$$

it is convenient to make the substitutions

$$\begin{aligned} \alpha &= \kappa z \\ \beta &= \frac{2m\pi}{3} \\ \gamma &= \omega t \end{aligned}$$

Thus,

$$G_n = \cos n (\alpha - \beta) \cos (\gamma - \beta)$$

now by trigonometric identity, we have

$$\begin{aligned} \cos n (\alpha - \beta) &= \cos n \alpha \cos n \beta + \sin n \alpha \sin n \beta \\ \cos (\gamma - \beta) &= \cos \gamma \cos \beta + \sin \gamma \sin \beta \end{aligned}$$

Therefore

$$\begin{aligned} G_n &= \cos \gamma \cos \beta \cos n \alpha \cos n \beta \\ &+ \cos \gamma \cos \beta \sin n \alpha \sin n \beta \\ &+ \sin \gamma \sin \beta \cos n \alpha \cos n \beta \\ &+ \sin \gamma \sin \beta \sin n \alpha \sin n \beta \end{aligned}$$

For the purpose of this analysis it is convenient to regroup the products as

$$\begin{aligned} G_n &= \cos \gamma \cos n \alpha (\cos \beta \cos n \beta) \\ &+ \cos \gamma \sin n \alpha (\cos \beta \sin n \beta) \\ &+ \sin \gamma \cos n \alpha (\sin \beta \cos n \beta) \\ &+ \sin \gamma \sin n \alpha (\sin \beta \sin n \beta) \end{aligned}$$

now it is easily shown by trigonometric identity that

$$\begin{aligned}\cos \beta \cos n\beta &= \frac{1}{2} (\cos (n+1)\beta + \cos (n-1)\beta) \\ \cos \beta \sin n\beta &= \frac{1}{2} (\sin (n+1)\beta - \sin (n-1)\beta) \\ \sin \beta \cos n\beta &= \frac{1}{2} (\sin (n+1)\beta + \sin (n-1)\beta) \\ \sin \beta \sin n\beta &= \frac{1}{2} (-\cos (n+1)\beta + \cos (n-1)\beta)\end{aligned}$$

and that similarly

$$\begin{aligned}\cos \gamma \cos n\alpha &= \frac{1}{2} (\cos (\gamma+n\alpha) + \cos (\gamma-n\alpha)) \\ \cos \gamma \sin n\alpha &= \frac{1}{2} (\sin (\gamma+n\alpha) - \sin (\gamma-n\alpha)) \\ \sin \gamma \cos n\alpha &= \frac{1}{2} (\sin (\gamma+n\alpha) + \sin (\gamma-n\alpha)) \\ \sin \gamma \sin n\alpha &= \frac{1}{2} (-\cos (\gamma+n\alpha) + \cos (\gamma-n\alpha))\end{aligned}$$

substituting these identities into the equation for G_n one has

$$\begin{aligned}4 G_n &= \cos (\gamma+n\alpha) \cos (n+1)\beta + \cos (\gamma+n\alpha) \cos (n-1)\beta \\ &+ \cos (\gamma-n\alpha) \cos (n+1)\beta + \cos (\gamma-n\alpha) \cos (n-1)\beta \\ &+ \sin (\gamma+n\alpha) \sin (n+1)\beta - \sin (\gamma+n\alpha) \sin (n-1)\beta \\ &- \sin (\gamma-n\alpha) \sin (n+1)\beta + \sin (\gamma-n\alpha) \sin (n-1)\beta \\ &+ \sin (\gamma+n\alpha) \sin (n+1)\beta + \sin (\gamma+n\alpha) \sin (n-1)\beta \\ &+ \sin (\gamma-n\alpha) \sin (n+1)\beta + \sin (\gamma-n\alpha) \sin (n-1)\beta \\ &+ \cos (\gamma+n\alpha) \cos (n+1)\beta - \cos (\gamma+n\alpha) \cos (n-1)\beta \\ &- \cos (\gamma-n\alpha) \cos (n+1)\beta + \cos (\gamma-n\alpha) \cos (n-1)\beta\end{aligned}$$

collecting terms and cancelling, one finds that

$$G_n = \frac{1}{2} \left[\begin{aligned} &\cos (\gamma+n\alpha) \cos (n+1)\beta + \cos (\gamma-n\alpha) \cos (n-1)\beta \\ &+ \sin (\gamma+n\alpha) \sin (n+1)\beta + \sin (\gamma-n\alpha) \sin (n-1)\beta \end{aligned} \right]$$

REFERENCES

1. "Electromagnetic propulsion for Magnetically Levitated Vehicle"
W. J. Harrold, R. S. Kasevich, C. H. Tang, N. P. Viens.
19th Annual Conference on Magnetism and Magnetic Materials,
Boston, Mass., Nov. 1973.
2. "Characteristics of Superconductive Magnetic Suspension and
Propulsion for High Speed Trains". E. Ohno, M. Iwamoto, T. Yamada,
The Central Reserach Lagoratory, Mitsubishi Electric Corporation,
Amagasaki, Hyogo, Japan.
3. "Ford Maglev Progress Report", J. R. Reitz et al, October 16
to November 15, 1972.
4. "Magneplane Linear Synchronous Motor Study - Final Report",
A. H. Greene, W. J. Harrold, R. S. Kasevich, C. H. Tang, E Weiss.
5. "Study of Magnetic Levitation and Linear Synchronous Motor
Propulsion", Canadian Maglev Group, Annual Report for 1972.
6. "Analysis of Superconducting Magnetic Levitation and Linear
Synchronous Motor Propulsion for high speed Guided Ground
Transportation", Canadian Maglev Group, Annual Report for 1973.
7. "Magnetic Levitation Linear Synchronous Motor Efficiency",
D. L. Atherton, L. E. G. Love, P. O. Prentiss, Can. J. Phys.,
vol. 50, No. 24, pp3143-6, 1972.
8. "Report on a study of the Magneplane power system and Guideway",
United Engineers and Constructors, Inc., April 1973.
9. "Electronic Control of a Linear Synchronous Motor", J. H. Schultz,
Master Thesis, MIT, September 1973.
10. "The Theory and Design of Cycloconverters", W. McMurray,
The MIT Press, 1972.
11. "The Magnetic Suspension and Guidance of High Speed Vehicles",
I. A. Alston, J. M. Clark. J. T. Hayden, High Speed Ground
Transportation Journal, vol. 7, pp215-245, 1973.

REFERENCES (Cont)

12. "Design of a full-scale Magneplane Vehicle", Y. Iwasa, M. O. Hoenig, and H. H. Kohn, IEEE Trans. on Magnetics, Vol. MAG-10, September 1974, p402.
13. "High Current Density Superconducting Magnets using Heavy Currents", D. L. Atherton, Canadian Journal of Physics, Vol. 49, 1971, pp155-156.

